

博士論文

Development of Wide-Area Measurements Based PSS Design for Improving Inter-Area Oscillation in Power Systems

(電力系統の地域間動揺を抑制する
ための広域計測データに基づいたPSS設計手法の開発)

トラン フィン ノツ
Tran Huynh Ngoc

Advisor: Professor Akihiko Yokoyama

A dissertation submitted in partial fulfillment of the requirements
of the degree of Doctor of Philosophy in the
Graduate School of Engineering, the University of Tokyo,

December 2014

TABLE OF CONTENTS

| | |
|--|-----------|
| CHAPTER 1. INTRODUCTION | 6 |
| 1.1 MOTIVATION..... | 6 |
| 1.2 LITERATURE REVIEW ON WIDE-AREA MEASUREMENTS BASED PSS FOR IMPROVING INTER-AREA MODE .. | 9 |
| 1.3 OBJECTIVES AND CONTRIBUTIONS | 11 |
| 1.4 ORGANIZATION OF THIS DISSERTATION..... | 12 |
| CHAPTER 2. POWER SYSTEM MODELING..... | 14 |
| 2.1 POWER SYSTEM COMPONENT DYNAMIC MODEL..... | 14 |
| 2.1.1 Synchronous generator model..... | 14 |
| 2.1.2 Governor model | 17 |
| 2.1.3 Exciter model..... | 21 |
| 2.1.4 Load model | 21 |
| 2.1.5 Power system stabilizer model..... | 22 |
| 2.2 LINEARIZED STATE SPACE MODEL OF POWER SYSTEM..... | 23 |
| 2.3 EIGENANALYSIS AND SMALL SIGNAL STABILITY | 29 |
| 2.3.1 Recall of eigenvalues and eigenvectors | 29 |
| 2.3.2 Modal analysis | 30 |
| CHAPTER 3. WIDE-AREA MEASUREMENTS BASED PSS DESIGN | 33 |
| 3.1 STRUCTURE OF WIDE-AREA MEASUREMENTS BASED PSS | 33 |
| 3.2 CONCEPT OF ADAPTIVE WAM BASED PSS..... | 34 |
| 3.3 WAM BASED PSS OUTPUT LOCATION | 38 |
| 3.4 PROPOSED OF WAM BASED PSS FEEDBACK SIGNAL..... | 38 |
| 3.5 TUNING METHOD FOR WAM BASED PSS | 40 |
| 3.6 PROPOSED ITERATIVE DESIGN OF WAM BASED PSS..... | 44 |
| 3.7 TIME DELAY AND MEASUREMENT ERROR..... | 45 |
| 3.7.1 Time delay | 45 |
| 3.7.2 Impact of time delay on a mode of concern..... | 46 |
| 3.7.3 Modeling time delay block for system linearization and time simulation..... | 47 |
| 3.7.4 Measurement error | 49 |
| CHAPTER 4. CASE STUDIES..... | 50 |
| 4.1 IEEE EAST 10-MACHINE SYSTEM..... | 52 |
| 4.1.1 Case 1..... | 52 |

| | | |
|--|---|-----------|
| 4.1.2 | Case 2..... | 55 |
| 4.2 | IEEJ WEST 10-MACHINE SYSTEM..... | 58 |
| 4.2.1 | Case 3..... | 58 |
| 4.2.2 | Case 4..... | 62 |
| 4.3 | TIME DELAY AND MEASUREMENT ERROR CONSIDERATION | 66 |
| 4.3.1 | Impact of delay time on controller designed without time delay consideration..... | 66 |
| 4.3.2 | Implementation of design process with time delay | 71 |
| 4.3.3 | Impact of time delay and measurement error on controller performance | 80 |
| CHAPTER 5. CONCLUSION AND FUTURE WORK | | 83 |
| LIST OF PUBLICATION | | 85 |
| REFERENCES..... | | 86 |

LIST OF FIGURES

| | |
|--|----|
| FIGURE 1.1 WIDE-AREA MONITORING AND CONTROL (WAMC) CONFIGURATION FOR A POWER SYSTEM [1]..... | 6 |
| FIGURE 1.2 AUGUST 10TH, 1996 DISTURBANCE RECORDING [2] | 7 |
| FIGURE 1.3 INFORMATION FLOW WITHIN A SELECTIVE CONTROL STRUCTURE [4] | 8 |
| | |
| FIGURE 2.1 SYNCHRONOUS MACHINE SCHEMATIC DIAGRAM | 14 |
| FIGURE 2.2 GOVERNOR MODEL (LPT=1) FOR THERMAL AND NUCLEAR POWER PLANT | 18 |
| FIGURE 2.3 GOVERNOR MODEL (LPT=4) FOR HYDRO POWER PLANT | 19 |
| FIGURE 2.4 ADJUSTMENT PRINCIPLE OF FREE-RESPOND GOVERNOR (PML>0)..... | 20 |
| FIGURE 2.5 ADJUSTMENT PRINCIPLE OF BLOCKED-OPERATION GOVERNOR (PML<0)..... | 20 |
| FIGURE 2.6 EXCITER MODEL (LAT=1) BY IEEJ RECOMMENDATION | 21 |
| FIGURE 2.7 A PSS MODEL WITH THREE PHASE COMPENSATIONS..... | 22 |
| | |
| FIGURE 3.1 STRUCTURE OF A WIDE-AREA MEASUREMENTS BASED PSS | 34 |
| FIGURE 3.2 THE CONCEPT FOR AN ADAPTIVE WAM BASED PSS..... | 36 |
| FIGURE 3.3 PSS TYPE CONTROLLER | 41 |
| FIGURE 3.4 THE EIGENVALUE OPTIMIZATION ALGORITHM | 43 |
| FIGURE 3.5 ITERATIVE DESIGN FLOWCHART | 44 |
| FIGURE 3.6 TIME DELAY EXPRESSED IN LAPLACE DOMAIN..... | 45 |
| FIGURE 3.7. IMPACT OF TIME DELAY ON A MODE | 47 |
| FIGURE 3.8. COMPARISONS BETWEEN FIRST ORDER PADE APPROXIMATION AND ACTUAL DELAY | 48 |
| FIGURE 3.9. WAM BASED PSS CONSIDERING TIME DELAY | 49 |
| | |
| FIGURE 4.1 THE IEEJ EAST 10-MACHINE SYSTEM..... | 51 |
| FIGURE 4.2 THE IEEJ WEST 10-MACHINE SYSTEM..... | 51 |
| FIGURE 4.3 THE CONTROLLER CONFIGURATION IN CASE 1 | 53 |
| FIGURE 4.4 DEVIATIONS OF ANGULAR DIFFERENCES BETWEEN MACHINES 1 AND 9 | 54 |
| FIGURE 4.5 EXCITER OUTPUT DURING FAULT SCENARIO | 54 |
| FIGURE 4.6 THE CONTROLLER CONFIGURATION IN CASE 2 | 56 |
| FIGURE 4.7 DEVIATIONS OF ANGULAR DIFFERENCES BETWEEN MACHINES 1 AND 6 | 57 |
| FIGURE 4.8 EXCITER OUTPUT DURING FAULT SCENARIO | 58 |
| FIGURE 4.9 THE CONTROLLER CONFIGURATION IN CASE 3 | 59 |
| FIGURE. 4.10 DEVIATIONS OF ANGULAR DIFFERENCES BETWEEN MACHINES 10 AND 1 | 61 |
| FIGURE. 4.11 EXCITER OUTPUT DURING FAULT SCENARIO | 62 |
| FIGURE. 4.12 THE CONTROLLER CONFIGURATION IN CASE 3 | 63 |
| FIGURE. 4.13 DEVIATIONS OF ANGULAR DIFFERENCES BETWEEN MACHINE 10 AND 1 | 65 |
| FIGURE. 4.14 EXCITER OUTPUT DURING FAULT SCENARIO | 66 |

| | |
|--|----|
| FIGURE 4.15 PROPOSED AND CONVENTIONAL FEEDBACK CONSIDERING TIME DELAY _CASE 1 | 66 |
| FIGURE 4.16 PROPOSED AND CONVENTIONAL FEEDBACK CONSIDERING TIME DELAY _CASE 2 | 67 |
| FIGURE 4.17 PROPOSED AND CONVENTIONAL FEEDBACK CONSIDERING TIME DELAY _CASE 3 | 67 |
| FIGURE 4.18 PROPOSED AND CONVENTIONAL FEEDBACK CONSIDERING TIME DELAY _CASE 4 | 68 |
| FIGURE 4.19 IMPACT OF TIME DELAY ON EAST 10-MACHINE SYSTEM_CASE 1 | 69 |
| FIGURE 4.20 IMPACT OF TIME DELAY ON EAST 10-MACHINE SYSTEM_CASE 2 | 69 |
| FIGURE 4.21 IMPACT OF TIME DELAY ON WEST 10-MACHINE SYSTEM_CASE 3 | 70 |
| FIGURE 4.22 IMPACT OF TIME DELAY ON WEST 10-MACHINE SYSTEM_CASE 4 | 70 |
| FIGURE 4.23 IMPACT OF VARIOUS TIME DELAY ON CONTROLLER PERFORMANCE - TIME DELAY SETTING =0.25s | 73 |
| FIGURE 4.24 PERFORMANCE OF CONVENTIONAL AND PROPOSED CONTROLLER WITH ACTUAL TIME DELAY T=0.15s .. | 74 |
| FIGURE 4.25 PERFORMANCE OF CONVENTIONAL AND PROPOSED CONTROLLER WITH ACTUAL TIME DELAY T=0.25s .. | 75 |
| FIGURE 4.26 PERFORMANCE OF CONVENTIONAL AND PROPOSED CONTROLLER WITH ACTUAL TIME DELAY T=0.35s .. | 75 |
| FIGURE 4.27 IMPACT OF VARIOUS TIME DELAY ON CONTROLLER PERFORMANCE - TIME DELAY SETTING =0.25s | 77 |
| FIGURE 4.28 PERFORMANCE OF CONVENTIONAL AND PROPOSED CONTROLLER WITH ACTUAL TIME DELAY T=0.15s .. | 78 |
| FIGURE 4.29 PERFORMANCE OF CONVENTIONAL AND PROPOSED CONTROLLER WITH ACTUAL TIME DELAY T=0.25s .. | 79 |
| FIGURE 4.30 PERFORMANCE OF CONVENTIONAL AND PROPOSED CONTROLLER WITH ACTUAL TIME DELAY T=0.35s .. | 79 |
| FIGURE 4.31 SYSTEM PERFORMANCE WITH TIME DELAY AND MEASUREMENT ERROR _CASE 1 | 81 |
| FIGURE 4.32 SYSTEM PERFORMANCE WITH TIME DELAY AND MEASUREMENT ERROR _CASE 2 | 81 |
| FIGURE 4.33 SYSTEM PERFORMANCE WITH TIME DELAY AND MEASUREMENT ERROR _CASE 3 | 82 |
| FIGURE 4.34 SYSTEM PERFORMANCE WITH TIME DELAY AND MEASUREMENT ERROR _CASE 4 | 82 |

LIST OF TABLES

| | |
|---|----|
| TABLE 3.1 TOTAL TIME DELAYS FOR DIFFERENCE COMMUNICATION LINK [31] | 46 |
| TABLE 4.1 INTER-AREA MODES OF THE BASE CASE 1 | 53 |
| TABLE 4.2 AFFECTED MODES BY WAM BASED PSS | 53 |
| TABLE 4.3 INTER-AREA MODES OF THE BASE CASE 2 | 56 |
| TABLE 4.4 AFFECTED MODES BY WAM BASED PSS | 56 |
| TABLE 4.5 AFFECTED MODES BY WAM BASED PSS | 60 |
| TABLE 4.6 AFFECTED MODES BY WAM BASED PSS | 60 |
| TABLE 4.7 CCT IN CORRESPONDING TO FAULTED BUSES | 61 |
| TABLE 4.8 AFFECTED MODES BY WAM BASED PSS | 64 |
| TABLE 4.9 AFFECTED MODES BY WAM BASED PSS | 64 |
| TABLE 4.10 CCT IN CORRESPONDING TO FAULTED BUSES | 65 |
| TABLE 4.11 ASSUMED DELAY TIME | 68 |
| TABLE 4.12 PSS CONFIGURATION WITH AND WITHOUT CONSIDERING TIME DELAY | 71 |
| TABLE 4.13 PSS'S PARAMETERS WITH AND WITHOUT CONSIDERING TIME DELAY | 72 |
| TABLE 4.14 EIGENVALUE RESULT WITH SETTING DT =0, ACTUAL DT=0 | 72 |
| TABLE 4.15 EIGENVALUE RESULT WITH SETTING DT =0, ACTUAL DT=0.25 | 72 |
| TABLE 4.16 EIGENVALUE RESULT WITH SETTING DT =0.25s, ACTUAL DT= 0.25s | 73 |
| TABLE 4.17 PSS CONFIGURATION WITH AND WITHOUT CONSIDERING TIME DELAY | 76 |
| TABLE 4.18 PSS'S PARAMETERS WITH AND WITHOUT CONSIDERING TIME DELAY | 76 |
| TABLE 4.19 EIGENVALUE RESULT WITH SETTING DT=0, ACTUAL DT=0 | 76 |
| TABLE 4.20 EIGENVALUE RESULT WITH SETTING DT=0, ACTUAL DT=0.25 | 76 |
| TABLE 4.21 EIGENVALUE RESULT WITH SETTING DT=0.25, ACTUAL DT=0.25 | 77 |

CHAPTER 1. INTRODUCTION

1.1 MOTIVATION

Wide - area measurements and control (WAMC)

Power energy has become more important for the world so that many efforts have been made to prevent power systems from outage scenarios. While power system size and the demands on it are increasing, the inter - connecting power system becomes more necessary. However, beside some benefits it could provide, such as increasing power system reliability, effectiveness of backup sources, some problems, especially instability problems, also need to be solved.

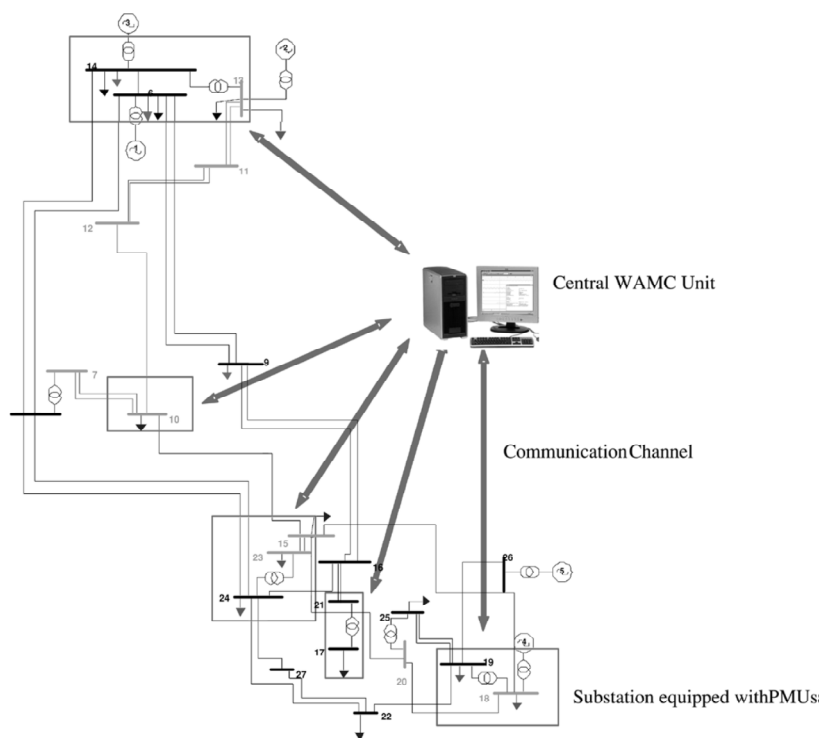


Figure 1.1 Wide-area monitoring and control (WAMC) configuration for a power system [1]

In the common power system, due to low sampling rate of Supervisory Control and Data Acquisition/Energy Management system (SCADA/EMS), it is not qualified enough to capture the dynamic of power system. Also, there is uncoordinated local actions e.g. in decentralized protection system. Meanwhile, due to the economic constrains, the power system today being operated close to its stability limits and changing the monitoring and control roles from

preventive to emergency ones. In order to observe the system dynamic, the essential measurement should match following characteristics: must be taken from different system locations, with sampling high rate and at the same time instant. A measurement device, called synchronized Phasor Measurement Unit (PMU), could possess these above features, working together with global positioning system (GPS) system [1].

Fig.1.1 demonstrates a monitoring and control system in which PMUs are connected to a control center via communication channels. The control center which embedded by stability assessments and stabilization algorithms will send the computed signals to desired controllers. Such a system is called wide area monitoring and control (WAMC) system.

Inter- area oscillation: Main causes of instability problem of inter-connected power system

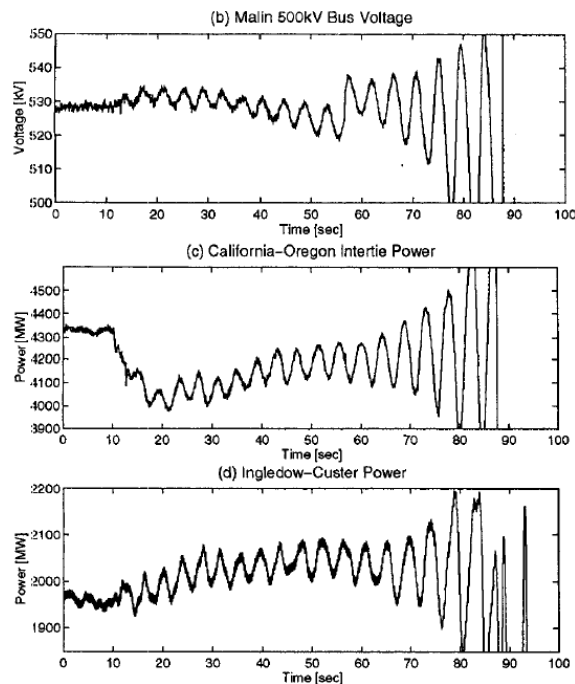


Figure 1.2 August 10th, 1996 disturbance recording [2]

For past decade, many researchers have pointed out that inter-area oscillation is the main concern in instability problems of a large scale power system. The oscillation modes, which range in 0.2Hz - 1Hz, have been detected in many networks, such as Western North America [2], Queensland system [3], Hydro - Quebec system [4], Nordic power system [5], China Southern power grid [6]. In [2], the recording behavior of power transmitted via an inter-transmission line

showed that an inter-area mode had been excited after lines and 13 generators units tripping 40s following a fault on a 500kV line.

Local and global control

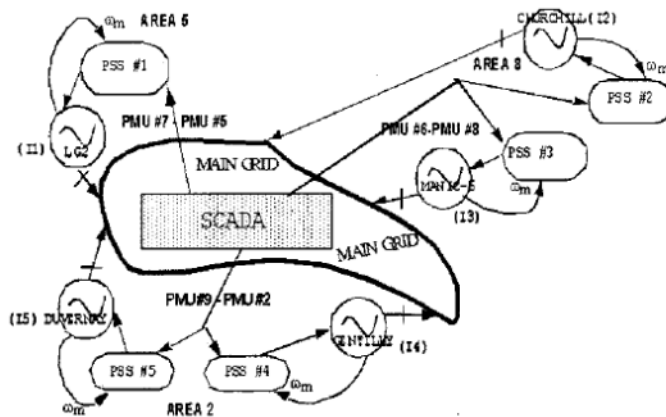


Figure 1.3 Information flow within a selective control structure [4]

Power system stabilizer (PSS) is the most cost-effective control device for improving damping of power system oscillations. Years ago, PSS has been considered as the most effective local controller which can provide good damping to instability modes in power systems. In addition, many research investigated on FACTS devices controller for enhancing power system stability. Recent years ago, especially after Western North America blackout, many researchers [4,7,8,9,10,11] have proved that a controller such as PSS or FACTS devices can provide a better behavior to an inter-connected power system if the remote signals (from other than its own area) are used as the input signals. In the other hand, the inter-area oscillation can be well damped if global signals are used for a reasonable coordination controller. In this dissertation, such a PSS is called wide-area measurements based PSS.

For example, fig.1.3 shows the structure of a control system in which the remote signals, "the pilot frequency of area#x- pilot frequency of area#y", are used as global input signals for the PSSs, besides the local input signal ω_m .

1.2 LITERATURE REVIEW ON WIDE-AREA MEASUREMENTS BASED PSS FOR IMPROVING INTER-AREA MODE

Before the research direction of WAM based PSS is suggested, there was also research on using local PSS for improving inter-area oscillations. But the main function of local PSS is damping out local oscillation so that the effectiveness of using local PSS to improve inter-area oscillation is not high. In a heavily condition, local PSS even can not improve inter-area oscillation any more [8]. Another research direction is coordinating of some local PSS to enhance inter-area oscillation. However, the tuning process corresponding with this coordinating is very complicated. Therefore, research on design of WAM based PSS for improving inter-area oscillation has become more popular in recent years.

Designing a wide-area measurement based PSS for improving inter-area oscillation concerning to several issues:

- (1) Identifying the inter - area modes
- (2) Observer and controller placement or output and feedback signals selecting
- (3) Tuning controller's parameters
- (4) Dealing with the time delay introduced by wide - area data transmission

The issue of identifying the system dynamic and inter-area mode can be solved by numerical algorithms using PMU data. There were some analysis tools for identifying the system dynamic were discussed: parametric mode estimation, parametric ring-down analysis using Prony method, spectral and correlation analysis using Fourier transforms [12], and Kalman filtering [13,14,15].

This dissertation does not deal with power system identification techniques. Instead, we assume that PMU and SCADA/EMS system is good enough to capture the system dynamic. Also, eigenanalysis technique is used to extract poor-damping inter-area oscillations. Eigenanalysis has been well-established for analyzing the inter-area modes characteristics [16]. With several attractive capabilities such as identifying individual mode and mode shapes, providing information about sensitivities to parameter changes, eigenanalysis is frequently applied to study inter-area oscillations in multi-machine systems.

Output and feedback signals selecting are importance steps of design of WAM based PSS. Generator speed deviations ($\Delta\omega$) [4,8], voltage angle shift [17] and active power [18] are

common used as input for WAM based PSS. Generator speed deviation is also the most common input signal for local control, although, when selecting this signal, torsional oscillations need to be considered [19]. For longitudinal power system, inter-area active power is a suitable input signal for improving inter-area oscillation, because it has a high observability for the oscillation. However, in common power systems, corridors of power oscillations are not easy to be determined.

The most common way to select input signal is using observability measurement of signals for the mode of concern. So far, there is not any research pointing out which type of signals is the most adequate for the WAM based PSS.

The output signal of WAM based PSS is conventionally placed at voltage reference input of machine's exciter, based on controllability measurement for the mode of concern [4,8,17].

This dissertation has nothing to do to improve the method of output signal placement, but proposes a new method for feedback signal selection, based on residue function which can be calculated in eigenanalysis.

There are many methods established for tuning PSS's parameter which can be used in WAM based PSS design. Most of them such as pole placement method, residue based method [18], H_∞ [20], and linear matrix inequality technique [8] are toward to a robustness PSS which is suitable for a range of system conditions. Besides, Y. Sekinen and A. Yokoyama have firstly proposed an eigenvalue control method for design of an adaptive local PSS [21]. This adaptive PSS is changed its parameters once the system is changed.

Based on idea of paper [21], this dissertation proposed a concept of adaptive WAM based PSS which change its configuration, that is its input and output, and its parameters subjected to the system change. Because that an adaptive controller does not keep the same parameters for various operating point of power system, it is not necessary to consider a robustness tuning method for design the PSS. Instead, a combination method between residue based method and eigenvalue control method is adopted to tune the controller's parameters.

To deal with time delay introduced by signal transmission, Pade Approximation [22] are used for modeling time delay function. In this dissertation, impact of time delay on the designed controller is investigated, and design framework considering time delay is also adopted.

1.3 OBJECTIVES AND CONTRIBUTIONS

The work reported in this dissertation, is conducted keeping the following objectives:

- ❖ To design a multi-input single-output(MISO) WAM based adaptive PSS for damping out inter-area modes
- ❖ To propose a new method of feedback signal selection for the MISO WAM based PSS
- ❖ To proposed an iterative design combining proposed feedback selection and eigenvalue control

Assumptions: PMU and SCADA/EMS system can identify power system dynamic well

So far, for adaptive PSS, there is only idea of changing controller's parameters subjected to system change. This dissertation proposes a concept of adaptive WAM based PSS which change both configuration and parameters subjected to system change. The advantage of changing both configuration and parameters is to reduce number of required controllers while providing good damping to inter-area oscillations. The work reported in this dissertation shows that for a test system, only one adaptive WAM based PSS can enhance inter-area oscillations, instead of using each controller for each inter-area oscillation.

This dissertation also proposes a new method of feedback signal selection for the MISO WAM based PSS. This method is based on a systematic framework, and it is appropriate to not only adaptive controllers, but also robustness controllers. The difference between this method and conventional method is that it considers observability of feedback signal for not only the mode of concern, but also other modes. For instance, using weighting factor added to each measurement, the method can maximize observability of feedback signal to the mode of concern, while minimizing that to others.

In coordination with the new method of feedback selection, this dissertation proposes an algorithm of iterative design for choosing the best parameters of controller, once tuning method for the controller is fixed. This iterative design is general, regardless to type of parameter tuning method. It can be used with any method of parameter tuning which is mentioned in the review section.

1.4 ORGANIZATION OF THIS DISSERTATION

This dissertation consists of five chapters:

Chapter 1. Introduction

Chapter 1 makes an introduction and talks about objectives and contributions of the dissertation. This chapter also provide a literature review on the field of wide-area measurements based PSS for improving inter-area oscillations.

Chapter 2. Power system modeling

Chapter 2 describes the dynamic models of power system component used in this dissertation, including generator, exciter, governor and load models. The PSS form controller's model is also described in this chapter. The generator is modeled by a 6-order model. The model LTA=1 recommended by IEEJ is used for exciters. Model LPT=1 and LPT=4 recommended by IEEJ are used for governors of thermal and hydro power plant, respectively. Load model in this dissertation is the constant impedance static load model.

Chapter 2 also gives a recall of eigenanalysis of the linearized power system. It recalls how to linearize a power system dynamic model around an equilibrium point. This linearization technique will be applied for Matlab programming on test cases in chapter 4. Definitions of eigenvalues, eigenvector are also explained. The standard multi modal decomposition and participation factor, matrix are described. Based on the standard multi modal decomposition of the given linearized power system, definitions of observability, controllability matrixes and residues value of controller output-input are also recalled.

Chapter 3. Wide-area measurements based PSS design

Chapter 3 describes a systematic procedure of design wide-area measurements based PSS for inter-area oscillations. There are 8 steps of design: 1) Forming the dynamic system; 2) Linearizing the dynamic system, calculating eigenvalues and identifying the inter-area modes; 3) Locating the controller output; 4) Selecting the feedback signal ; 5) Tuning controller parameters; 6) Iteratively design that is repeat step 4) and 5) until best result obtained; 7) Considering impact of time delay and measurement errors; 8) Calculating eigenvalues and time domain simulating of the close-loop system to evaluate the proposed design strategy.

The comparative strength of the proposed feedback for each system operation point is evaluated by eigenvalue result and time domain simulation test. Advantage of iterative design is also shown in this chapter. Besides, practical issues like time delays, measurement errors are considered and discussed. Total time delay of the input and output signal introduced by signal transmission is assumed by 0.15, 0.25

and 0.35s. For the actual $\Delta\omega$ which is measured to be take part in the feedback signal $Y_{fb} = [a_1 \ a_2][\Delta\omega_{a1} \ \Delta\omega_{a2}]^T$, a measurement error of $\pm 5\%$ is assumed, and in each test case, 4 combinations of measurement errors are considered.

Chapter 4 . Case studies

Chapter 4 describes four design examples on IEEJ East 10-machine and IEEJ West 10-machine systems. In each case, the design result such as output signal location, input signal selection and parameter tuning are presented. Eigenvalue results and time domain simulations are used to evaluate the goodness of the proposed strategy design.

In the East system, two operating points which has different dominant inter-area modes has been tested. The result shows that the controller configuration and controller parameters are different from each case. It is also seen that the proposed feedback is slightly better than the conventional feedback in the East system case. The impact of time delay on system performance is not a bad impact, and the impact of measurement error is insignificant.

In the West system, because of the characteristics of the system, two operating points which has the same dominant inter-area modes has been tested. The controller configuration is not changed, but the parameters. Both the proposed feedback and iterative design have shown their goodness more significant than the East case. The impact of time delay on system performance is not good, but acceptable, and the impact of measurement error is insignificant.

Chapter 5. Conclusions and future works

Chapter 5 make an conclusion based on the result of this research. Besides, some several issues for the future work are listed.

CHAPTER 2. POWER SYSTEM MODELING

2.1 POWER SYSTEM COMPONENT DYNAMIC MODEL

2.1.1 Synchronous generator model

Synchronous generators play as the main source of electric energy in power systems. One of stability problems in power system is to keep the synchronism between interconnected synchronous generators [23]. Hence, in order to study power system stability, it is necessary to understand generator characteristics and its accurate modeling for dynamic performance. This dissertation considers a six-order model for synchronous generators, as described in [24].

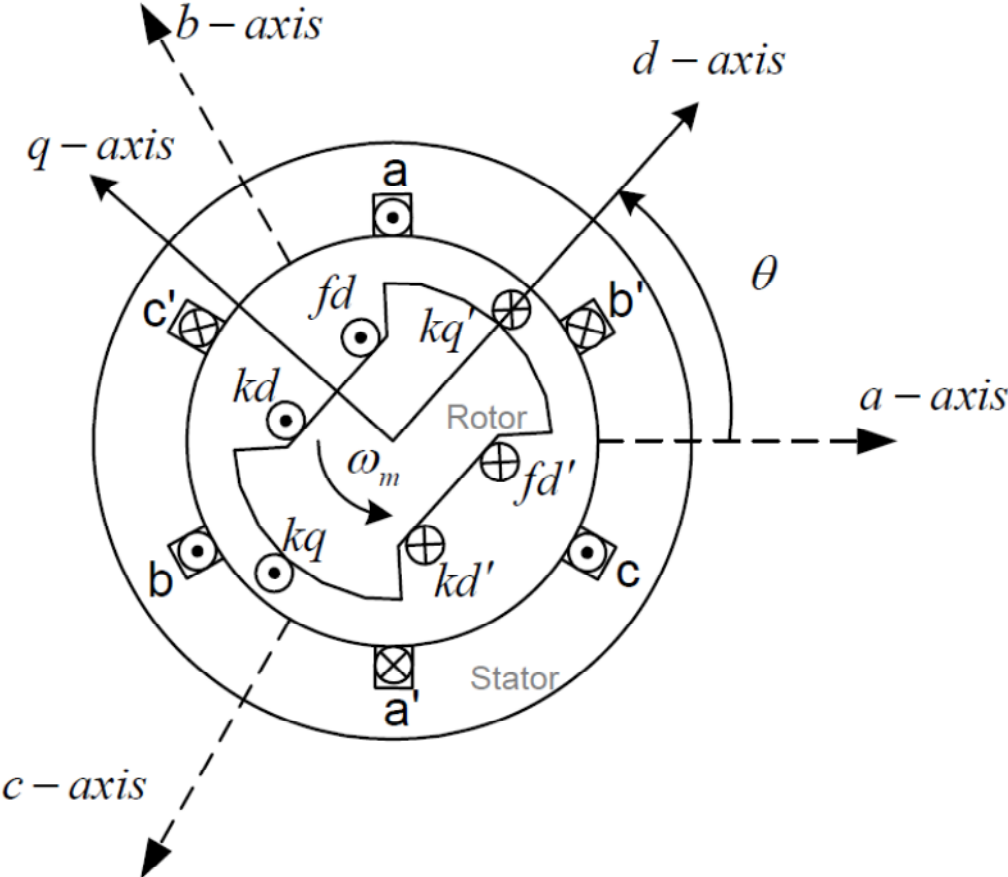


Figure 2.1 Synchronous machine schematic diagram

As shown in figure 2.1, rotor quantities are presented in a rotating direct-quadrature coordinate frame while stator quantities are presented in three AC phases a , b , c . To simplify the analysis of three-phase synchronous machines, a direct-quadrature-zero (d-q-o) transformation

was firstly proposed in 1929 by Robert H. Park. By transformation of three phase stator and rotor quantities into a single rotating reference frame, it can eliminate the effect of time varying inductances. The transformation depends on the difference in phase $\delta - \theta$, between the terminal voltage and the internal rotor angle.

With Park transformation, the dynamic equations of the synchronous generator for the six-order model can be written as:

$$\dot{\delta}(t) = \omega_{base}(\omega(t) - 1) \quad (2.1)$$

$$\dot{\omega}(t) = \frac{1}{2H} \left[\frac{1}{\omega(t)} P_m(t) - \frac{1}{\omega(t)} P_e(t) - D(\omega(t) - 1) \right] \quad (2.2)$$

$$\dot{e}'_q(t) = \frac{1}{T'_{d0}} \left[e_f(t) + \frac{(L_d - L'_d)(L'_d - L''_d)}{(L'_d - L_l)^2} K_d e''_q(t) - \left\{ 1 + \frac{(L_d - L'_d)(L'_d - L''_d)}{(L'_d - L_l)^2} \right\} e'_q(t) - \omega(t) \frac{(L_d - L'_d)(L'_d - L''_d)}{L'_d - L_l} i_d(t) \right] \quad (2.3)$$

$$\dot{e}''_q(t) = \frac{1}{T''_{d0} K_d} \{ K_d e''_q(t) - e'_q(t) + \omega(t)(L'_d - L_l) i_d(t) \} \quad (2.4)$$

$$\dot{e}'_d(t) = \frac{1}{T'_{q0}} \left[-\frac{(L_q - L'_q)(L'_q - L''_q)}{(L'_q - L_l)^2} K_q e''_d(t) - \left\{ 1 + \frac{(L_q - L'_q)(L'_q - L''_q)}{(L'_q - L_l)^2} \right\} e'_d(t) - \omega(t) \frac{(L_q - L'_q)(L'_q - L''_q)}{L'_q - L_l} i_q(t) \right] \quad (2.5)$$

$$\dot{e}''_d(t) = \frac{1}{T''_{q0} K_q} \{ K_q e''_d(t) - e'_d(t) + \omega(t)(L'_q - L_l) i_q(t) \} \quad (2.6)$$

where
$$K_d = 1 + \frac{(L_d - L'_d)(L'_d - L_l)}{(L'_d - L''_d)(L_d - L_l)}; \quad K_q = \frac{(L_d - L'_d)(L'_d - L_l)}{(L'_d - L''_d)(L_d - L_l)}$$

- δ generator's rotor angle in rad
- ω generator frequency in p.u
- H generator inertia constant in sec.
- P_m generator input mechanical power in p.u
- P_e generator output electrical power in p.u
- D damping coefficient in p.u

| | |
|----------------------|---|
| T'_{d0}, T'_{q0} | direct and quadrature axis transient open circuit time constants |
| T''_{d0}, T''_{q0} | direct and quadrature axis sub-transient open circuit time constants |
| e_f | exciter output in p.u |
| L_l | stator inductance relating to leakage flux in p.u |
| L_d, L'_d, L''_d | standard synchronous, transient and sub transient inductances on direct axis in p.u |
| L_q, L'_q, L''_q | standard synchronous, transient and sub transient inductances on quadrature axis in p.u |
| $i(t)$ | terminal bus current |
| $i_d(t), i_q(t)$ | internal Park transformed components of terminal bus current $i(t)$ |

The relation between the external bus quantities and the internal machine transformed quantities can be stated as:

$$e_{gd}(t) = K_q \frac{L'_q - L''_q}{L'_q - L_q} e''_d(t) + \frac{L''_q - L_l}{L_q - L_l} e'_d(t) \quad (2.7)$$

$$e_{gq}(t) = K_q \frac{L'_d - L''_d}{L'_d - L_d} e''_q(t) + \frac{L''_d - L_l}{L_d - L_l} e'_q(t) \quad (2.8)$$

$$v_d(t) = e_{gd}(t) + \omega_0 L'_q i_q(t) - R i_d(t) \quad (2.9)$$

$$v_q(t) = e_{gq}(t) - \omega_0 L''_d i_d(t) - R i_q(t) \quad (2.10)$$

$$P_e(t) = v_d(t) i_d(t) + v_q(t) i_q(t) \quad (2.11)$$

$$Q_e(t) = v_d(t) i_d(t) - v_q(t) i_q(t) \quad (2.12)$$

| | | |
|-------|------------------|---|
| where | $e_g(t)$ | internal voltage behind sub-transient reactance |
| | $v(t)$ | terminal bus voltage |
| | e_{gd}, e_{gq} | internal Park transformed components of $e_g(t)$ |
| | $v_d(t), v_q(t)$ | internal Park transformed components of terminal bus voltage $v(t)$ |
| | $P_e(t), Q_e(t)$ | generator real and reactive power |

Let

$$E_{gd} = e_{gd}(t); E_{gq} = e_{gq}(t); V_d = v_d(t); V_q = v_q(t); I_d = i_d(t); I_q = i_q(t)$$

Therefore,

$$\dot{E}_g = E_{gd} + jE_{gq}; \dot{V} = V_d + jV_q; \dot{I} = I_d + jI_q$$

Then (2.9)-(2.12) can be rewritten as follows:

$$V_d = E_{gd} + \omega_0 L_q'' I_q - R I_d \quad (2.13)$$

$$V_q = E_{gq} - \omega_0 L_d'' I_d - R I_q \quad (2.14)$$

$$P_e = V_d I_d + V_q I_q \quad (2.15)$$

$$Q_e = V_d I_d - V_q I_q \quad (2.17)$$

Relation between phase components and Park's transformed components of bus voltage:

$$V_d = V \sin(\delta - \theta) \quad (2.18)$$

$$V_q = V \cos(\delta - \theta) \quad (2.19)$$

Substituting (2.18) and (2.19) into (2.13)-(2.17), then we have the relation between the external bus quantities and the internal machine transformed quantities as follows:

$$K_q \frac{L_q' - L_q''}{L_q' - L_q} e_d'' + \frac{L_q' - L_l}{L_q' - L_l} e_d' - V \sin(\delta - \theta) + \omega_0 L_q'' I_q - R I_d = 0 \quad (2.18)$$

$$K_d \frac{L_d' - L_d''}{L_d' - L_d} e_q'' + \frac{L_d' - L_l}{L_d' - L_l} e_q' - V \cos(\delta - \theta) - \omega_0 L_d'' I_d - R I_q = 0 \quad (2.19)$$

$$P_e = V \sin(\delta - \theta) I_d + V \cos(\delta - \theta) I_q \quad (2.20)$$

$$Q_e = V \sin(\delta - \theta) I_d - V \cos(\delta - \theta) I_q \quad (2.21)$$

2.1.2 Governor model

Governor is equipped with generator's turbine for keeping generator's frequency in an acceptable range. Its function is to adjust input mechanical torque subjected to frequency deviation. In this dissertation, IEEJ East and West 10-machine systems are used as test systems, therefore governor models presented in this dissertation are ones recommended by IEEJ [25].

There are two models of Governors for Thermal and Hydro Power Plants which are shown in figures 2.2 and 2.3, respectively.

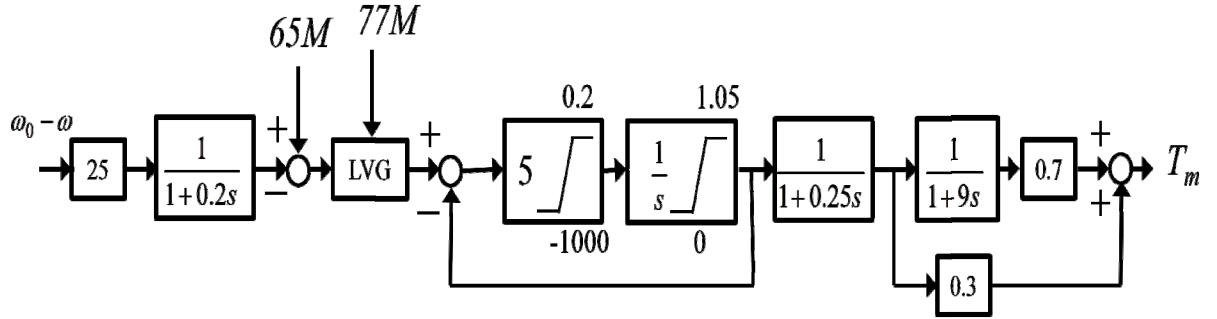


Figure 2.2 Governor model (LPT=1) for Thermal and Nuclear Power Plant

Difference equations of governor model in figure 2.2:

$$\dot{x}_{1Gov} = 25(\omega_0 - \omega) - 5x_{1Gov} \quad (2.22)$$

$$\dot{x}_{2Gov} = 5 \min\{77M, 65M - 5x_{1Gov}\} - 5x_{2Gov} \quad (2.23)$$

$$-1000 \leq \dot{x}_{2Gov} \leq 0.2$$

$$0 \leq x_{2Gov} \leq 1.05 \text{ p.u}$$

$$\dot{x}_{3Gov} = x_{2Gov} - 4x_{3Gov} \quad (2.24)$$

$$\dot{x}_{4Gov} = 4x_{3Gov} - (1/9)x_{4Gov} \quad (2.25)$$

$$T_m = 1.2x_{3Gov} + (0.7/9)x_{4Gov} \quad (2.26)$$

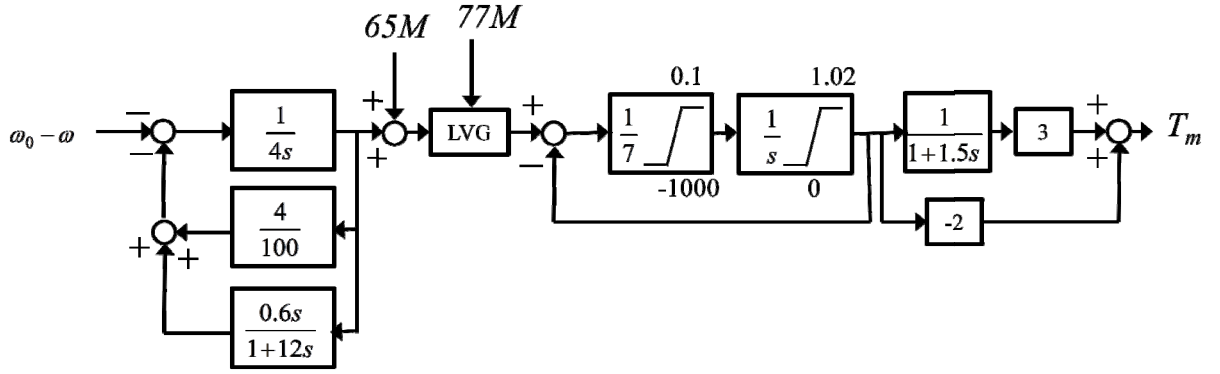


Figure 2.3 Governor model (LPT=4) for Hydro Power Plant

Difference equations of governor model in figure 2.3:

$$\dot{x}_{1Gov} = -(\omega_0 - \omega) - 0.0225x_{1Gov} + \left(\frac{1}{240}\right)x_{2Gov} \quad (2.27)$$

$$\dot{x}_{2Gov} = 0.25x_{1Gov} - \left(\frac{1}{12}\right)x_{2Gov} \quad (2.28)$$

$$\dot{x}_{3Gov} = \left(\frac{1}{7}\right) (\min[77M, 65M + 0.25x_{1Gov}] - x_{3Gov}) \quad (2.29)$$

$$-1000 \leq \dot{x}_{3Gov} \leq 0.1$$

$$0 \leq x_{3Gov} \leq 1.02 \text{ p.u}$$

$$\dot{x}_{4Gov} = x_{3Gov} - (2/3)x_{4Gov} \quad (2.30)$$

$$T_m = -2x_{3Gov} + 2x_{4Gov} \quad (2.31)$$

In figures 2.2 and 2.3, 65M and 77M are turbine load reference and turbine load limiter, respectively. Their values depend on reserve function of each power plant, as described in figures 2.4 and 2.5. Fig. 2.4 describes adjustment principle of spinning reserve governor which is allowed to adjust turbine output for supporting frequency control. Fig. 2.5 describes principle of non-spinning reserve governor which is not allowed to change turbine output.

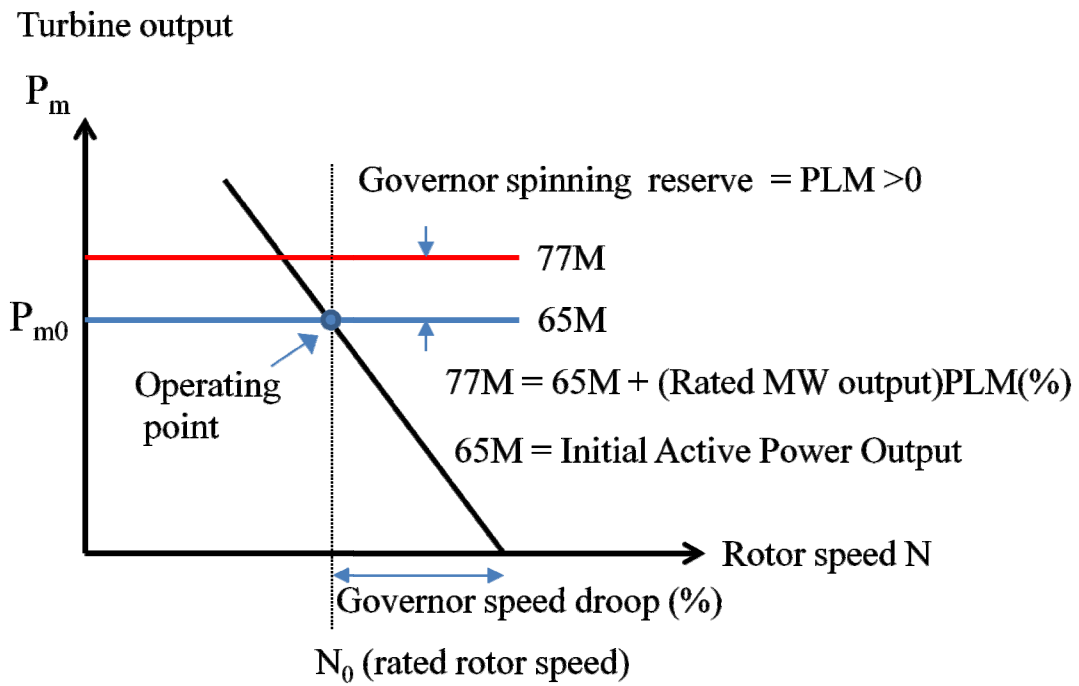


Figure 2.4 Adjustment principle of free-response governor ($PLM > 0$)

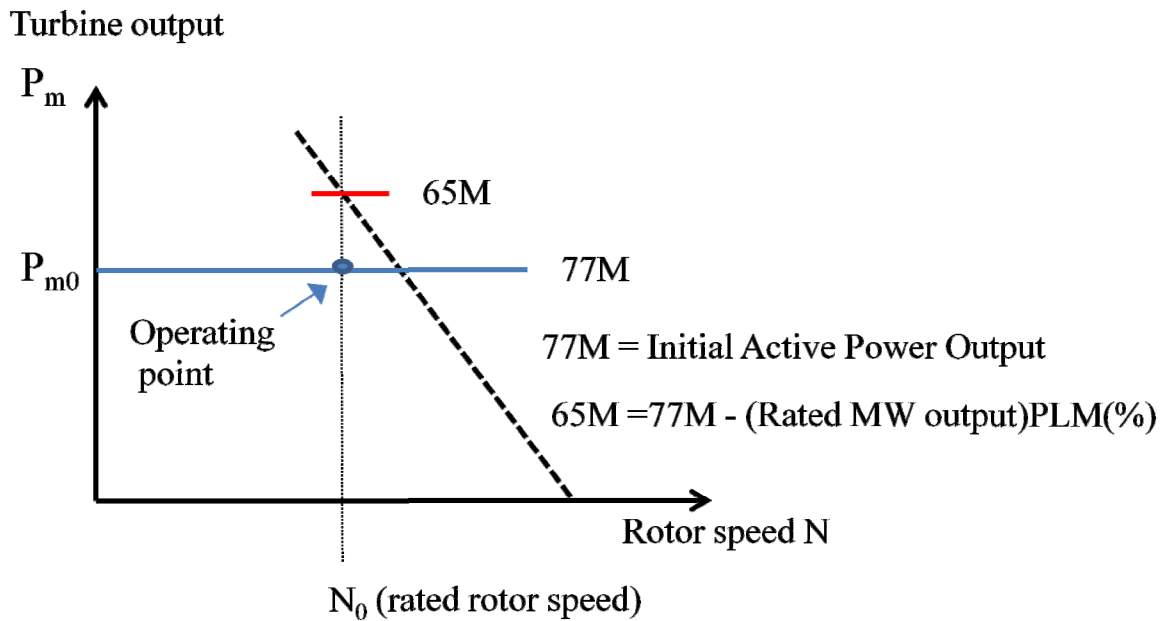


Figure 2.5 Adjustment principle of blocked-operation governor ($PLM < 0$)

2.1.3 Exciter model

Function of exciter (AVR) is to regulate machine's terminal voltage by adjusting field circuit current. Similar to governor model, this dissertation also use 3-order exciter model recommended by IEEJ, as shown in fig. 2.6. The input u in this model is for PSS output, and also presented as input u in DAE model presented in the section of linearized space state model.

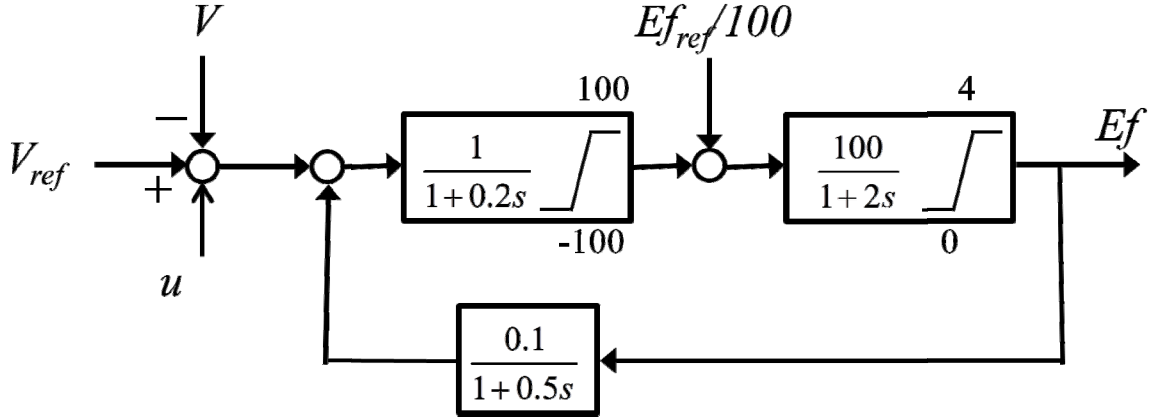


Figure 2.6 Exciter model (LAT=1) by IEEJ recommendation

Difference equations of exciter model in figure 2.4:

$$\dot{x}_{1AVR} = -5x_1 - 10x_2 + 0.4x_3 + V_{ref} - V + u \quad (2.32)$$

$$-20 \leq x_1 \leq 20$$

$$\dot{x}_{2AVR} = 5x_1 - 0.5x_2 + 0.01E_{f_{ref}} \quad (2.33)$$

$$0 \leq Ef = 50x_2 \leq 4 \text{ p.u}$$

$$\dot{x}_{3AVR} = 50x_2 - 2x_3 \quad (2.34)$$

2.1.4 Load model

In stability studies for transmission system, load demand can be aggregated into lump-sum load without affecting much on study results. Load models can be divided into two broad categories: static loads and dynamic loads. Constant power, constant current and constant impedance load models are used to model the static loads. Constant power load model has its

real and reactive powers have no relation to the voltage magnitude, but has constant MVA load. Constant current load model has its real and reactive power is directly proportional to the voltage magnitude. Constant impedance load model has its real and reactive power is proportional to the square of the voltage magnitude. This dissertation does not study the impact of loads on controller performance, therefore the constant impedance static load model is used. Load formula is as follows:

$$P_L = P_0 \left(\frac{V}{V_0}\right)^2 \quad (2.35)$$

$$Q_L = Q_0 \left(\frac{V}{V_0}\right)^2 \quad (2.36)$$

where P_0, Q_0, V_0 are initial active power, reactive power and voltage at load bus, respectively.

2.1.5 Power system stabilizer model

A PSS generates stabilizing signals to control machine's excitation and in this way it can provide damping to the generator rotor oscillation. Feedback signals of a PSS can be shaft speed, terminal frequency or power which has a large observability for the concern oscillation.

A local PSS must produce a component of electrical torque in phase with the rotor speed deviations, in order to provide damping to local oscillation. It normally has one or two phase compensations. In this dissertation, for the WAM based PSS, a PSS form controller with three phase compensation is used as illustrated in fig. 2.7.

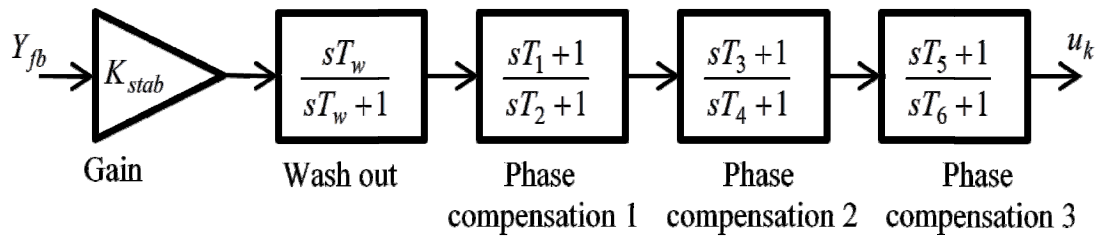


Figure 2.7 A PSS model with three phase compensations

The first block of PSS in fig. 2.7 is the gain block. The amount of damping introduced by the PSS is proportional to the stabilizer gain K_{stab} . Subsequently, the gain should be selected as large as possible to provide maximum damping. Unfortunately, it is often limited to ensure overall system stability, because PSS may destabilize other modes while provide damping to the concern oscillation.

The second is signal washout block. With the time constant T_w high enough, its function is as a high-pass filter preventing the steady state changes to modify the terminal voltages. By the wash out block, the PSS is allowed to respond only to changes in speed. The phase compensation blocks provide the appreciate phase lead characteristic to compensate for the phase lag between the exciter input and the generator electrical (air-gap) torque. The phase compensations should provide compensation over an entire frequency range of interest which is 0.1 to 2.0 Hz. In some literatures [19], it is recommended that some under-compensation is desirable. Also, it is recommended that the number of compensation blocks can be 1, 2 or 3, and each phase compensation block should not provide more than 60 degree of lead/lag phase. Therefore, in order to ensure that the PSS form controller can sufficiently provide compensation phase, a three-compensation-blocks PSS form controller has been chosen. The differential equations stating a PSS shown in fig.2.7 are:

$$\dot{x}_{1PSS} = -\frac{1}{T_w}x_{1PSS} + Y_{fb}K_{stab} \quad (2.37)$$

$$\dot{x}_{2PSS} = -\frac{1}{T_w}x_{1PSS} - \frac{1}{T_2}x_{2PSS} + Y_{fb}K_{stab} \quad (2.38)$$

$$\dot{x}_{3PSS} = -\frac{T_1}{T_w T_2}x_{1PSS} + \frac{T_2 - T_1}{T_2^2}x_{2PSS} - \frac{1}{T_4}x_{3PSS} + Y_{fb}K_{stab} \quad (2.39)$$

$$\dot{x}_{4PSS} = -\frac{T_1 T_3}{T_w T_2 T_4}x_{1PSS} + \frac{T_2 - T_1}{T_2^2} \frac{T_3}{T_4}x_{2PSS} + \frac{T_4 - T_3}{T_4^2}x_{3PSS} - \frac{1}{T_6}x_{4PSS} + Y_{fb}K_{stab} \quad (2.40)$$

2.2 LINEARIZED STATE SPACE MODEL OF POWER SYSTEM

This subsection presents linearized state space model of power system which is needed to study both steady-state and voltage stabilities. As shown in section 2.1, power system behavior is nonlinear and difficult to be investigated. However, at an equilibrium point of power system, its behavior can be approximately reflected by its linearized state space model, in existence of small disturbances. Because the power system model is large in size and complex in behavior, it is not easy to analysis with nonlinear technique. Instead, its linearized state space model is usually used in design of controller so that linear technique can be useful for solving controller parameters.

Power system equations consist of differential equations which are shown in section 2.1 and algebraic equations. From previous subsection, the differential equations of a synchronous

thermal generator along with the associated regulating devices, which are AVR and Governor, can be stated as:

$$\dot{\delta}(t) = \omega_{base}(\omega(t) - 1) \quad (2.41)$$

$$\dot{\omega}(t) = \frac{1}{2H} \left[\frac{1}{\omega(t)} P_m(t) - \frac{1}{\omega(t)} P_e(t) - D(\omega(t) - 1) \right] \quad (2.42)$$

$$\begin{aligned} \dot{e}'_q(t) = \frac{1}{T'_{d0}} \left[e_f(t) + \frac{(L_d - L'_d)(L'_d - L''_d)}{(L'_d - L_l)^2} K_d e''_q(t) - \left\{ 1 + \frac{(L_d - L'_d)(L'_d - L''_d)}{(L'_d - L_l)^2} \right\} e'_q(t) - \right. \\ \left. \omega(t) \frac{(L_d - L'_d)(L'_d - L''_d)}{L'_d - L_l} i_d(t) \right] \end{aligned} \quad (2.43)$$

$$\dot{e}''_q(t) = \frac{1}{T''_{d0} K_d} \{ K_d e''_q(t) - e'_q(t) + \omega(t)(L'_d - L_l) i_d(t) \} \quad (2.44)$$

$$\begin{aligned} \dot{e}'_d(t) = \frac{1}{T'_{q0}} \left[-\frac{(L_q - L'_q)(L'_q - L''_q)}{(L'_q - L_l)^2} K_q e''_d(t) - \left\{ 1 + \frac{(L_q - L'_q)(L'_q - L''_q)}{(L'_q - L_l)^2} \right\} e'_d(t) - \right. \\ \left. \omega(t) \frac{(L_q - L'_q)(L'_q - L''_q)}{L'_q - L_l} i_q(t) \right] \end{aligned} \quad (2.45)$$

$$\dot{e}''_d(t) = \frac{1}{T''_{q0} K_q} \{ K_q e''_d(t) - e'_d(t) + \omega(t)(L'_q - L_l) i_q(t) \} \quad (2.46)$$

$$\dot{x}_{1Gov} = 25(\omega_0 - \omega) - 5x_{1Gov} \quad (2.47)$$

$$\dot{x}_{2Gov} = 5 \min\{77M, 65M - 5x_{1Gov}\} - 5x_{2Gov} \quad (2.48)$$

$$-1000 \leq \dot{x}_{2Gov} \leq 0.2$$

$$0 \leq x_{2Gov} \leq 1.05 \text{ p.u}$$

$$\dot{x}_{3Gov} = x_{2Gov} - 4x_{3Gov} \quad (2.49)$$

$$\dot{x}_{4Gov} = 4x_{3Gov} - (1/9)x_{4Gov} \quad (2.50)$$

$$\dot{x}_{1AVR} = -5x_1 - 10x_2 + 0.4x_3 + V_{ref} - V + u \quad (2.51)$$

$$-20 \leq x_1 \leq 20$$

$$\dot{x}_{2AVR} = 5x_1 - 0.5x_2 + 0.01E f_{ref} \quad (2.52)$$

$$0 \leq Ef = 50x_2 \leq 4 \text{ p.u}$$

$$\dot{x}_{3AVR} = 50x_2 - 2x_3 \quad (2.53)$$

Similarly, we also have the difference equations for a synchronous hydro generator along with the associated regulating devices as follows:

$$\dot{\delta}(t) = \omega_{base}(\omega(t) - 1) \quad (2.54)$$

$$\dot{\omega}(t) = \frac{1}{2H} \left[\frac{1}{\omega(t)} P_m(t) - \frac{1}{\omega(t)} P_e(t) - D(\omega(t) - 1) \right] \quad (2.55)$$

$$\begin{aligned} \dot{e}'_q(t) = \frac{1}{T'_{d0}} \left[e_f(t) + \frac{(L_d - L'_d)(L'_d - L''_d)}{(L'_d - L_l)^2} K_d e''_q(t) - \left\{ 1 + \frac{(L_d - L'_d)(L'_d - L''_d)}{(L'_d - L_l)^2} \right\} e'_q(t) - \right. \\ \left. \omega(t) \frac{(L_d - L'_d)(L'_d - L''_d)}{L'_d - L_l} i_d(t) \right] \end{aligned} \quad (2.56)$$

$$\dot{e}''_q(t) = \frac{1}{T''_{d0} K_d} \{ K_d e''_q(t) - e'_q(t) + \omega(t)(L'_d - L_l) i_d(t) \} \quad (2.57)$$

$$\begin{aligned} \dot{e}'_d(t) = \frac{1}{T'_{q0}} \left[-\frac{(L_q - L'_q)(L'_q - L''_q)}{(L'_q - L_l)^2} K_q e''_d(t) - \left\{ 1 + \frac{(L_q - L'_q)(L'_q - L''_q)}{(L'_q - L_l)^2} \right\} e'_d(t) - \right. \\ \left. \omega(t) \frac{(L_q - L'_q)(L'_q - L''_q)}{L'_q - L_l} i_q(t) \right] \end{aligned} \quad (2.58)$$

$$\dot{e}''_d(t) = \frac{1}{T''_{q0} K_q} \{ K_q e''_d(t) - e'_d(t) + \omega(t)(L'_q - L_l) i_q(t) \} \quad (2.59)$$

$$\dot{x}_{1Gov} = -(\omega_0 - \omega) - 0.0225x_{1Gov} + \left(\frac{1}{240} \right) x_{2Gov} \quad (2.60)$$

$$\dot{x}_{2Gov} = 0.25x_{1Gov} - \left(\frac{1}{12} \right) x_{2Gov} \quad (2.61)$$

$$\dot{x}_{3Gov} = \left(\frac{1}{7} \right) (\min[77M, 65M + 0.25x_{1Gov}] - x_{3Gov}) \quad (2.62)$$

$$-1000 \leq \dot{x}_{3Gov} \leq 0.1$$

$$0 \leq x_{3Gov} \leq 1.02 \text{ p.u}$$

$$\dot{x}_{4Gov} = x_{3Gov} - (2/3)x_{4Gov} \quad (2.63)$$

$$\dot{x}_{1AVR} = -5x_1 - 10x_2 + 0.4x_3 + V_{ref} - V + u \quad (2.64)$$

$$-20 \leq x_1 \leq 20$$

$$\dot{x}_{2AVR} = 5x_1 - 0.5x_2 + 0.01Ef_{ref} \quad (2.65)$$

$$0 \leq Ef = 50x_2 \leq 4 \text{ p.u}$$

$$\dot{x}_{3AVR} = 50x_2 - 2x_3 \quad (2.66)$$

In two thirteen-order models above, the dynamic states are:

$$x_{di} = [\delta \quad \omega \quad e'_q \quad e''_q \quad e'_d \quad e''_d \quad x_{1Gov} \quad x_{2Gov} \quad x_{3Gov} \quad x_{4Gov} \quad x_{1AVR} \quad x_{2AVR} \quad x_{3AVR}]$$

In the design framework, the controller input to the system is located at AVR. Then the control inputs for the power system are:

$$u = [u_1 \quad u_2 \quad \dots \quad u_n]$$

where n is the number of generators at which the controller output can be located.

For algebraic equations, there are stator algebraic equations and network equations. Stator algebraic equations have been derived by (2.18), (2.19), hereby we recall them for the i -th machine:

$$K_{qi} \frac{L'_{qi} - L''_{qi}}{L'_{qi} - L''_{qi}} e''_{di} + \frac{L''_{qi} - L_{li}}{L'_{qi} - L_{li}} e'_{di} - V_i \sin(\delta_i - \theta_i) + \omega_0 L''_{qi} I_{qi} - R_i I_{di} = 0 \quad (2.67)$$

$$K_{qi} \frac{L'_{di} - L''_{di}}{L'_{di} - L''_{di}} e''_{qi} + \frac{L''_{di} - L_{li}}{L'_{di} - L_{li}} e'_{qi} - V_i \cos(\delta_i - \theta_i) - \omega_0 L''_{di} I_{di} - R_i I_{qi} = 0 \quad (2.68)$$

or

$$\begin{bmatrix} I_{di} \\ I_{qi} \end{bmatrix} = \begin{bmatrix} R_i & -\omega_0 L''_{qi} \\ \omega_0 L''_{di} & R_i \end{bmatrix}^{-1} \begin{bmatrix} K_{qi} \frac{L'_{qi} - L''_{qi}}{L'_{qi} - L''_{qi}} e''_{di} + \frac{L''_{qi} - L_{li}}{L'_{qi} - L_{li}} e'_{di} - V_i \sin(\delta_i - \theta_i) \\ K_{qi} \frac{L'_{di} - L''_{di}}{L'_{di} - L''_{di}} e''_{qi} + \frac{L''_{di} - L_{li}}{L'_{di} - L_{li}} e'_{qi} - V_i \cos(\delta_i - \theta_i) \end{bmatrix} \quad (2.69)$$

The network equations, which are the power flow equations for buses, are described as follows:

$$P_{ei}(x_{di}, I_{di-qi}, x_{ai}) - P_{Li} - P_i(x_a) = 0 \quad (2.70)$$

$$Q_{ei}(x_{di}, I_{di-qi}, x_{ai}) - Q_{Li} - Q_i(x_a) = 0 \quad (2.71)$$

where x_a are bus voltage magnitudes and phase angles, P_{ei}, Q_{ei} are generator active and reactive power derived by (2.20) and (2.21) for the machine at i -th bus. P_{Li}, Q_{Li} are active and reactive load at i -th bus, and $P_i(x_d, x_a), Q_i(x_d, x_a)$ are active and reactive power injections at i -th bus.

From (2.41)-(2.66) and (2.69)-(2.71), we have nonlinear model in power balance form of power system as follows:

$$\dot{x}_d = f_0(x_d, I_{d-q}, x_a, u) \quad (2.72)$$

$$I_{d-q} = h_0(x_d, x_a) \quad (2.73)$$

$$0 = g_0(x_d, I_{d-q}, x_a) \quad (2.74)$$

By substituting I_{d-q} from (2.69) into (2.72) and (2.74), we get:

$$\begin{cases} \dot{x}_d = f_1(x_d, x_a, u) \\ 0 = g_1(x_d, x_a) \end{cases} \quad (2.75)$$

Equation (2.75) is defined as the Differential Algebraic Equation (DAE) model of the power system dynamics [19].

If output signal of power system is considered, the full dynamic behavior of power system can be stated by equations:

$$\dot{x}_d = f_1(x_d, x_a, u) \quad (2.76)$$

$$0 = g_1(x_d, x_a) \quad (2.77)$$

$$y = h(x_d, x_a, u) \quad (2.78)$$

where y is the vector of output variables. Equation (276.) shows the system dynamic of the power system, equation (2.77) is actually the power flows equations and equation (2.78) shows relation between output variable and state and input variables.

Considering an equilibrium point which is stable, relation between initial value of state, algebraic, input and output variables are as follows:

$$0 = f_1(x_{0d}, x_{0a}, u_0) \quad (2.79)$$

$$0 = g_1(x_d, x_a) \quad (2.80)$$

$$y_0 = h(x_{0d}, x_{0a}, u_0) \quad (2.81)$$

Suppose a small input disturbance Δu perturbs the system and cause small deviation of state, algebraic and output variables, $\Delta x_d, \Delta x_a$ and Δy , respectively. That is:

$$x_d = x_{0d} + \Delta x_d \quad (2.82)$$

$$x_a = x_{0a} + \Delta x_a \quad (2.83)$$

$$y = y_0 + \Delta y \quad (2.84)$$

By partial differentiation of the nonlinear functions f_i, g_i and h , we have:

$$\Delta \dot{x}_d = A_1 \Delta x_d + A_2 \Delta x_a + B \Delta u \quad (2.85)$$

$$0 = A_3 \Delta x_d + A_4 \Delta x_a \quad (2.86)$$

$$\Delta y = C_1 \Delta x_d + C_2 \Delta x_a + D \Delta u \quad (2.87)$$

where the Jacobian matrixes are:

$$A_1 = \frac{\partial f_1}{\partial x_d}; \quad A_2 = \frac{\partial f_1}{\partial x_a}; \quad B_1 = \frac{\partial f_1}{\partial u}; \quad A_3 = \frac{\partial g_1}{\partial x_d}; \quad A_4 = \frac{\partial g_1}{\partial x_a};$$

$$C_1 = \frac{\partial h}{\partial x_d}; \quad C_2 = \frac{\partial h}{\partial x_a}; \quad D_1 = \frac{\partial h}{\partial u};$$

Assuming that A_4 is invertible, from (2.86) the algebraic variables can be described by:

$$\Delta x_a = -A_4^{-1} A_3 \Delta x_d \quad (2.88)$$

Substituting (2.88) into (2.85) and (2.87), we have:

$$\Delta \dot{x}_d = (A_1 + A_2 A_4^{-1} A_3) \Delta x_d + B_1 \Delta u \quad (2.89)$$

$$\Delta y = (C_1 + C_2 A_4^{-1} A_3) \Delta x_d + D \Delta u \quad (2.90)$$

or

$$\Delta \dot{x}_d = A \Delta x_d + B \Delta u \quad (2.91)$$

$$\Delta y = C \Delta x_d + D \Delta u \quad (2.92)$$

where $A = A_1 + A_2 A_4^{-1} A_3$ and $C = C_1 + C_2 A_4^{-1} A_3$

Neglecting deviation symbol Δ and dynamic symbol d for conciseness, we have:

$$\begin{aligned}\dot{x} &= Ax + Bu \\ y &= Cx + Du\end{aligned}\tag{2.93}$$

Equation (2.93) is called the ordinary differential equations (ODE). It is the general form of linearized state space model of power systems. In equation (2.93), matrix A is state matrix, B is input matrix, C is output matrix and D is feed forward matrix.

2.3 EIGENANALYSIS AND SMALL SIGNAL STABILITY

Based on the ordinary differential equations of power systems, the small signal stability of power system can be analyzed [19].

2.3.1 Recall of eigenvalues and eigenvectors

Suppose there exists an invertible matrix V such that:

$$A = V \Lambda V^{-1}\tag{2.94}$$

where $\Lambda = \begin{bmatrix} \lambda_1 & 0 & 0 \\ 0 & \ddots & 0 \\ 0 & 0 & \lambda_n \end{bmatrix}$ is an diagonal matrix.

From (2.94), we have a characteristic equation of state matrix A is:

$$\det(A - \lambda I) = (\lambda - \lambda_1)(\lambda - \lambda_2)(\lambda - \lambda_3) \dots (\lambda - \lambda_n) = 0$$

The solutions of the above equation is called eigenvalue of matrix A , $\lambda_i, i = 1, 2 \dots n$

Let

$$V = [v_1 \quad v_2 \quad \dots \quad v_n], v_i \text{ is } n \times 1 \text{ vector}$$

From $A = V \Lambda V^{-1} \Rightarrow AV = V \Lambda$

Then, we have

$$Av_i = \lambda_i v_i$$

v_i is defined as right eigenvector of matrix A .

Similarly, from $A = V \Lambda V^{-1} \Rightarrow V^{-1}A = \Lambda V^{-1}$

Let

$$V^{-1} = \begin{bmatrix} w_1 \\ \vdots \\ w_n \end{bmatrix}, w_i \text{ is } 1 \times n \text{ vector}$$

Then, we have

$$w_i A = w_i \lambda_i$$

w_i is defined as left eigenvector of matrix A .

2.3.2 Modal analysis

Consider a linear time invariant (LTI) system $\dot{x} = Ax$, the state response can be described by:

$$x(t) = e^{At}x(0) = \sum_1^n e^{\lambda_i t} v_i (w_i x(0)) = \sum_1^n k_i e^{\lambda_i t} v_i \quad (2.95)$$

where $k_i = w_i x(0)$.

Equation (2.95) is expressed in more explicit form:

$$\begin{bmatrix} x_1(t) \\ x_2(t) \\ \vdots \\ x_n(t) \end{bmatrix} = k_1 e^{\lambda_1 t} \begin{bmatrix} v_{1,1} \\ v_{2,1} \\ \vdots \\ v_{n,1} \end{bmatrix} + k_2 e^{\lambda_2 t} \begin{bmatrix} v_{1,2} \\ v_{2,2} \\ \vdots \\ v_{n,2} \end{bmatrix} + \dots + k_n e^{\lambda_n t} \begin{bmatrix} v_{1,n} \\ v_{2,n} \\ \vdots \\ v_{n,n} \end{bmatrix} \quad (2.96)$$

$$\text{or } x_i(t) = k_1 e^{\lambda_1 t} v_{i,1} + k_2 e^{\lambda_2 t} v_{i,2} + \dots + k_n e^{\lambda_n t} v_{i,n} \quad (2.97)$$

where $v_{i,j}$ is the j -th element of vector v_i . In the other hand, $v_{i,j} = V_{ji}$.

Based on equation (2.6), we have some definitions:

λ_i : the i -th mode of oscillations

$k_i = w_i x(0)$: the magnitude of the excitation of i -th mode due to the initial condition

$v_{i,j}$ (or V_{ji}) : the distribution of the j -th mode on the i -th state

If $\lambda_i \in R^+$: The i -th mode is aperiodic unstable.

If $\lambda_i \in R^-$: The i -th mode is non-oscillatory, over-damped mode.

If $\lambda_i \in \mathcal{C}$, assume that $\lambda_i = \sigma_i \pm j\omega_i$, then σ_i is decrement factor, ω_i is the damped frequency in rad/s, and $\zeta_i = \frac{\sigma_i}{\sqrt{\sigma_i^2 + \omega_i^2}}$ is the damped ratio of the i-th mode.

In equation (2.96), if modes other than 1-th mode are neglected, $w_i v_i$ measures how large dynamic state $x(t)$ is excited by 1-th mode, in comparison to other dynamic states. Subsequently, $k_j v_{i,j}$ measures how large the dynamic state $x_i(t)$ excited by j-th mode. Because $k_j = w_j x(0)$, $k_j v_{i,j} = w_j v_{i,j} x(0)$. If initial deviation of dynamic states other than $x_i(t)$ are zeros, $k_j v_{i,j} = w_j v_{i,j} x(0) = w_{j,i} v_{i,j} x_i(0)$. Therefore, $p_{ij} = w_{j,i} v_{i,j}$ is defined as participation factor which gives the measure of participation of dynamic state $x_i(t)$ in j-th mode.

Subsequently, a matrix P , called participation matrix, is define as follows:

$$P = [p_1 \ p_2 \ \dots \ p_n] \quad (2.98)$$

$$p_i = \begin{bmatrix} p_{1i} \\ p_{2i} \\ \vdots \\ p_{ni} \end{bmatrix} = \begin{bmatrix} v_{1,i} w_{i,1} \\ v_{2,i} w_{i,2} \\ \vdots \\ v_{n,i} w_{i,n} \end{bmatrix}$$

Based on participation factor, dynamic states playing important role in a mode can be realized. Hence, calculating participation factors of an inter-area oscillation mode can help to realize which groups of machines (or area) oscillate against to other.

In equation (2.96), there is couple relation between modes, mean any state can be affected by more than one mode. In order to decouple complex relation between modes, in some engineering areas, modal coordinate can be change to obtain a simplification of the modal system. One of modal coordinate changes has been described in [19]. This coordinate changes is used for a standard multi-modal decomposition which can transform dynamic states variable into standard state variables. By the standard multi-modal decomposition, coupling relations between modes are eliminated so that each standard state variable just have relation with only one mode.

Using standard multi-modal decomposition, we have:

$$\begin{aligned} \dot{z} &= \Lambda z + V^{-1} B u = \Lambda z + B^z u \\ y &= C V z = C^z z \end{aligned} \quad (2.99)$$

where

$$z = V^{-1}x$$

$$A = V\Lambda V^{-1}$$

z is column vector of transformed state variables for modes of matrix A , V is matrix of right eigenvectors of A , V^{-1} is matrix of left eigenvectors of A and Λ is diagonal matrix of eigenvalues of A .

In (2.99), there is no coupling effect between transformed state variables. Consider a transformed state variable z_d ,

$$\dot{z}_d = \lambda_d z_d + B_d^{zT} u \quad (2.100)$$

The row vector B_d^{zT} shows how inputs u can affect to a mode d . B_{dk}^z indicates the controllability of input u_k for mode d .

Similarly, the column vector C_d^z shows how much measurements y can observe mode d , and C_{jd}^z shows the observability of measurement y_j for mode d .

If there is a controller of which output and input signals are located at u_k and y_j , respectively, the eigenvalue shift on mode d by this controller can be estimated as follows:

$$\Delta\lambda_d \sim B_{dk}^z C_{jd}^z F(s)|_{s=\lambda_d} \quad (2.101)$$

where $F(s)$ is the transfer function of the controller.

Let $R_{u_k y_j d} = B_{dk}^z C_{jd}^z$, is the residue of a mode d which gives the measure of that mode's sensitivity to a feedback between the output y_j and input u_k .

Then, (2.101) can be rewritten as:

$$\Delta\lambda_d \sim R_{u_k y_j d} F(s)|_{s=\lambda_d} \quad (2.102)$$

CHAPTER 3. WIDE-AREA MEASUREMENTS BASED PSS DESIGN

3.1 STRUCTURE OF WIDE-AREA MEASUREMENTS BASED PSS

In general, two approaches of design damping controllers which are the decentralized approach and the centralized approach are considered. With the decentralized approach, only local measurements are used, therefore communication links are not installed. But, it is proved that only decentralized control may not provide good damping to inter-area oscillations for enhancing system stability in heavily operating condition [8]. On the other hand, centralized approach can utilize more data and provide better observations of inter-area modes. Therefore, it could be a promised solution for enhancing inter-area modes. In literature [4,7,8], it is found that if remote signals can be used for the PSS or FACTS devices, the system stability can be enhanced with respect to inter-area oscillations. A wide-area measurement based PSS is actually a centralized controller in PSS form which can use some telecommunication link to either receive the feedback signals from PMUs or to deliver stabilizing signals to V_{ref} port of machine's AVR. Structure of a wide-area based PSS can be described in fig. 3.1. In most recent research, it is suggested that some wide-area PSS are used in a power system to improve the damping of inter-area oscillations in which each wide-area controller is responds to each inter-area oscillation.

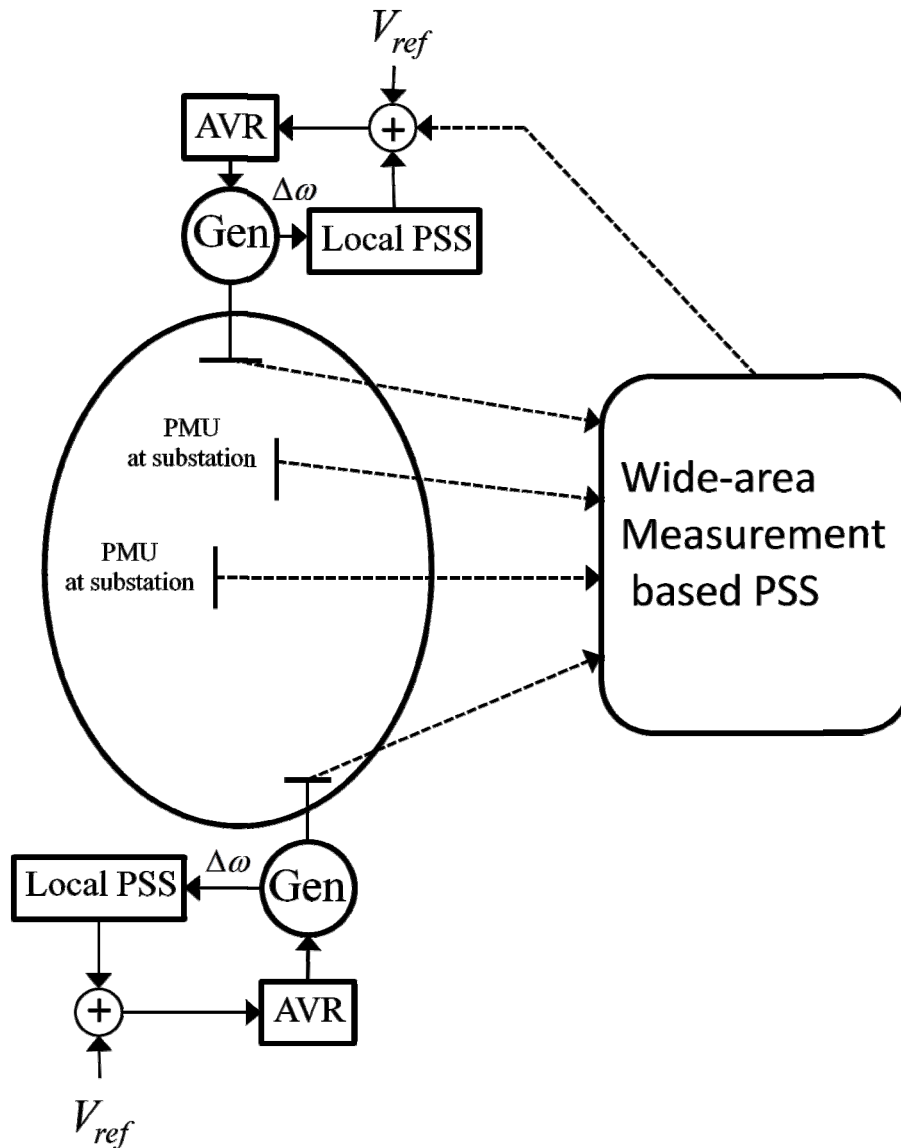


Figure 3.1 Structure of a wide-area measurements based PSS

3.2 CONCEPT OF ADAPTIVE WAM BASED PSS

As mentioned in previous section, there have been many papers investigating on design of PSS using wide-area measurements for damping out inter-area oscillation modes. However, most of the papers focused on the design of a robustness controller which provides damping to a dominant inter-area mode in several scenarios of the power systems. The designed controller configuration and parameters are fixed during the operation of the power systems.

In order to monitor the system dynamics, the synchronized Phasor Measurement Unit (PMU) has been developed to collect measurements from different locations at a high sampling rate and at the same time instant. Therefore, there have also been many researches on monitoring the dynamics of the power system or identifying the main characteristics of the system using PMUs [5, 26]. It is possible that the system dynamics can be identified based on some analytical tools on PMU data.

Assuming the above advantages of PMU data, this dissertation proposes a design strategy of damping the most dominant inter-area mode based on a concept of an adaptive controller for improving system stability. The controller is a multi-input single-output (MISO) one with PSS form. Instead of design of each robustness controller for each inter-area mode, this concept suggests to adaptively change both controller configuration, that is input and output locations of the controller, and control parameters depending on the system operating condition change [27].

The proposed concept is depicted in fig 3.2. It is said that at each period of time or when the system is manually changed, the system linearization should be done following the system identification. Then the controller's inputs and output will be reconfigured subjecting to the most dominant inter-are mode of the current operating point. After that, controller parameters will also be tuned to improve damping of the mode of concern.

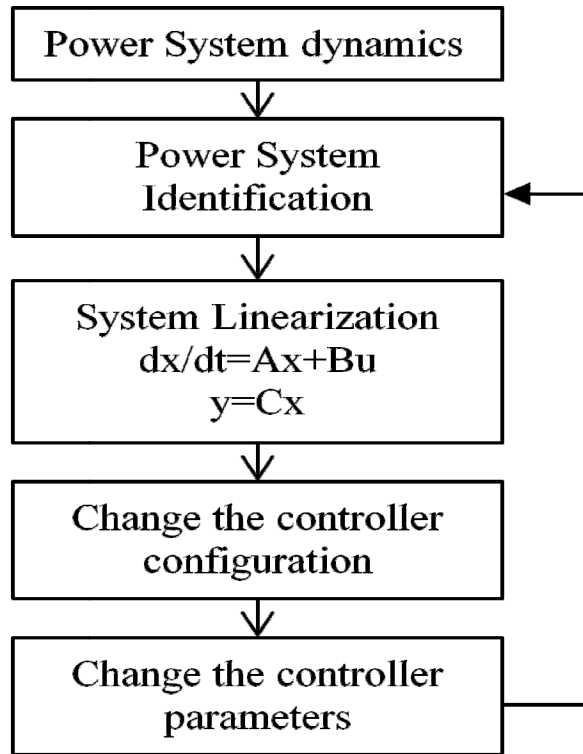


Figure 3.2 The concept for an adaptive WAM based PSS

In the dissertation, the last three steps of this concept are explained, and are applied for some operating points of the IEEJ East 10-machine and IEEJ West 10-machine system. System identification is another issue which is out of scope of this dissertation.

In this dissertation, the general procedure of design of WAM based PSS is as follows:

1) The full-order nonlinear model of the test system will be built using Matlab program. All synchronous generators are modeled using 6-order dynamic model along with Gov, AVR, PSS model which are described in chapter 2.

2) Linearized state space model of the test system at an operating point, as shown in chapter 2, is calculated using Matlab program. The calculation of eigenvalues and eigenvectors are performed. Information of mode frequencies, damped ratio and participation factor will be used to classify local modes and inter-area modes. The most dominant inter-area mode is also identified.

3) Controller output is selected. The output signal of WAM based PSS is located by controllability measurement [4,8,17], which is a conventional method.

4) Controller input signals are selected. The measurements for the controller are selected by a proposed method by this dissertation based on residue calculation. The calculated feedback signal has the maximum residue for the mode of concern and minimum residue for other modes.

5) The controller parameters are tuned using a combination method of residue based approach and eigenvalue control. The residue based approach is used for initialize parameters and eigenvalue control is used for tuning parameter focusing on the mode of concern.

6) An iterative design is proposed by this dissertation will be apply so that procedure 4) and 5) will be iteratively calculated until optimal parameters for the controller are obtained. This proposed iterative design is along with the proposed method of feedback signal in procedure 4), and regardless to the method of parameter tuning in procedure 5). That mean it can be applied with any method of parameter tuning.

7) Impacts of time delay introduced by transmission and measurement error are considered. The controller configuration and parameters are designed with and without time delay consideration.

8) Eigenvalues of the closed-loop system are calculated and time domain simulations are performed by Matlab program to verify the effectiveness of the designed strategy. Impacts of time delay and measurement error on eigenvalue result and time domain simulation are evaluated.

3.3 WAM BASED PSS OUTPUT LOCATION

After the system identification, the linearization around the system operating point will be performed. In the dissertation, the PSS output location u_k is selected among V_{ref} input of machines's exciters.

At each operating point of the system, considering a mode d which is the dominant inter-area mode to be damped out, the WAM based PSS output will be located at u_k which have the maximum controllability for mode d , i.e. B_{dk}^z is the maximum element of B_d^{zT} . By this output location, the WAM based PSS is able to control the dominant inter-area mode as much as possible.

3.4 PROPOSED OF WAM BASED PSS FEEDBACK SIGNAL

With selected location of PSS output at u_k which have the maximum controllability for mode d , the controller can have a large impact on mode d . However, it also has impacts on other modes and the controller design has to care of other modes for overall system stability.

This dissertation focuses on damping out the dominant inter-area mode using multiple feedback signals, so that a method for feedback signal selection is proposed to maximize the impact of controller on mode of concern while minimizing that on others. The proposed method does not focus on improving local modes which can be improved by the local PSS controllers.

Assume a signal has the following form,

$$Y_{fb} = [a_1 \ a_2 \ \dots \ a_m][y_1 \ y_2 \ \dots \ y_m]^T = ay^T, (a_i \in R) \quad (3.1)$$

is the feedback signal for the WAM based PSS located at u_k . Consequently, observability of Y_{fb} for any mode i is aC_i^z .

Then, for each mode i , the residue $R_{u_k Y_{fb} i}$ which give the measure of that mode's sensitivity to a feedback between the feedback signal Y_{fb} and input u_k is calculated as follows:

$$\begin{aligned} R_{u_k Y_{fb} i} &= aC_i^z B_{ik}^z \\ &= aR_{u_k i} \end{aligned} \quad (3.2)$$

where $R_{u_k i}$ is the complex column vector of residue which gives the measure of i^{th} -mode's sensitivity to a feedback between the output y and input u_k .

In order to maximize the impact of controller (u_k, Y_{fb}) on mode of concern (mode d) while minimize that on others, we try to maximize $|R_{u_k Y_{fb} d}|^2$ while minimizing $\sum_{i \neq d} |R_{u_k Y_{fb} i}|^2$

$$\begin{aligned}
|R_{u_k Y_{fb} d}|^2 &= |aR_{u_k d}|^2 = |aR_{u_k d \text{real}} + jaR_{u_k d \text{imag}}|^2 \\
&= aR_{u_k d \text{real}} R_{u_k d \text{real}}^T a^T + aR_{u_k d \text{imag}} R_{u_k d \text{imag}}^T a^T \\
&= a(R_{u_k d \text{real}} R_{u_k d \text{real}}^T + R_{u_k d \text{imag}} R_{u_k d \text{imag}}^T) a^T \\
&= aH_{kd} a^T = aQ a^T
\end{aligned} \tag{3.3}$$

$$\begin{aligned}
\sum_{i \neq d} |R_{u_k Y_{fb} i}|^2 &= \sum_{i \neq d} aH_{ki} a^T = a(\sum_{i \neq d} H_{ki}) a^T \\
&= aP a^T
\end{aligned} \tag{3.4}$$

We will solve the problem of maximizing $\frac{aQa^T}{aPa^T}$ (3.5)

Noted that matrix P and Q in (3.5) are positive definite, due to their formulation shown in (3.3) and (3.4)

This problem is quite familiar in some optimization books [28]. Hereby we recall its solution.

Notice that if a_* is a solution of the above problem, then so is ta_* , with t is any real number. Therefore, to avoid the multiple solutions, this problem can be transformed to an optimal problem as follows:

Maximizing $f(a) = aQa^T$ (3.6)

subject to: $aPa^T = 1$ or $g(a) = 1 - aPa^T = 0$

with P and Q are positive definite matrixes

This optimal problem can be solved using Lagrange method.

Let $L(a, \lambda) = f(a) + \lambda g(a) = aQa^T + \lambda(1 - aPa^T)$

If a_* is a solution of (3.6) then:

$$\frac{dL}{da_*} = 2Qa_* - 2\lambda_* Pa_* = 0 \tag{3.7}$$

$$\frac{dL}{d\lambda} = 1 - a_* Pa_*^T = 0 \tag{3.8}$$

Pre-multiplying (3.7) by P^{-1} , we obtain

$$P^{-1}Qa_* = \lambda_*a_* \quad (3.9)$$

Equation (3.9) shows that λ_* and a_* are eigenvalue and eigenvector of $P^{-1}Q$, respectively. Then, we have:

$$f(a_*) = a_* Qa_*^T = \lambda_*a_* Pa_*^T = \lambda_*$$

Hence, the eigenvector a_* corresponding to maximum eigenvalue is the solution of (3.5).

3.5 TUNING METHOD FOR WAM BASED PSS

With Y_{fb} formed from measurements y using weighting vector a_* , the impacts of the controller on the modes which are not concerned are minimized. Then, the design work can pay attention on the dominant inter-area mode.

The parameter tuning process, which is eigenvalue optimization process, includes two steps of initialization and optimization as follows:

Initialization

T_1, T_2 will be initialized by residue based tuning for mode of concern. In this step, T_w is chosen by 10, K_{stab} is chosen by a small value such as 0.5.

The change in eigenvalues of mode of concern by WAM based PSS (u_k, Y_{fb}) is as follows:

$$\Delta\lambda_d = \lambda_d^{PSS} - \lambda_d \sim R_{u_k Y_{fb} d} F(s)|_{s=\lambda_d} \quad (3.10)$$

In order to shift the dominant eigenvalue λ_d to the left-hand side in the complex plane as much as possible, $\Delta\lambda_d$ should be a negative real number. Therefore, the PSS phase compensation should be designed so that

$$\begin{aligned} \angle F(s)|_{s=\lambda_d} + \angle R_{u_k Y_{fb} d} &= 180^\circ, \text{ or} \\ \angle F(s)|_{s=\lambda_d} &= 180^\circ - \angle R_{u_k Y_{fb} d} = \theta \end{aligned} \quad (3.11)$$

Consider a PSS with three of phase compensation blocks shown in Fig. 3.3. This PSS form controller has been mentioned in chapter 2.

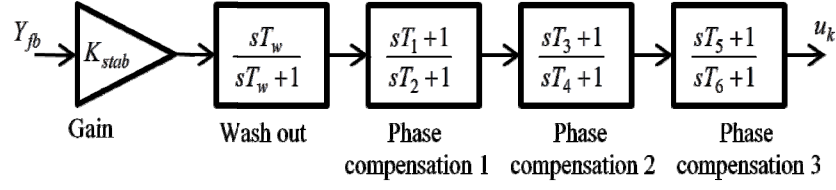


Figure 3.3 PSS type controller

For simplicity, phase compensation parameters are chosen equally: $T_1=T_3=T_5$; $T_2=T_4=T_6$. Then the initial PSS parameters are calculated as follows:

$$\varphi = \frac{T_1}{T_2} = \frac{T_3}{T_4} = \frac{T_5}{T_6} = \frac{1 - \sin(\theta/3)}{1 + \sin(\theta/3)} \quad (3.12)$$

$$T_2 = T_4 = T_6 = \frac{1}{\omega_k \sqrt{\varphi}}; T_1 = T_3 = T_5 = \varphi T_2 \quad (3.13)$$

where ω_k is the frequency of mode k .

Optimization

An eigenvalue optimization algorithm has been proposed by Sekine Y. and Yokoyama A. for a concept of eigenvalue control scheme [21]. This paper just focuses on damping the most dominant inter-area mode, therefore the following optimization problem and algorithm are adopted.

Minimizing the real part of mode of concern

$$\text{Min}_{T_1, T_2, T_w, K_{stab}} \text{Re}(\lambda_d) \quad (3.14)$$

such that

$$\begin{aligned} & \text{Maximizing } \text{Min}(\zeta_i, \zeta_d) \\ & \text{and } \begin{cases} 0.01 = T_{min} < T_1, T_2 < T_{max} = 2 \\ 2 = T_{wmin} < T_w < T_{wmax} = 15 \\ 0.5 = K_{min} < K_{stab} < K_{max} = 80 \\ \text{Re}(\lambda_i) < \alpha_{limit}, \forall \text{ mode } \lambda_i \end{cases} \end{aligned}$$

The algorithm divides modes other than mode of concern into three groups: modes which are destabilized much (λ_i) by the tuning process, modes are insignificantly destabilized (λ_t) by the tuning process, and modes are stabilized (λ_k) by the tuning process. Only damping ratios of the first group are considered in the tuning process. The second group damping will not be care of, even when their damping ratios are smaller than that of the mode of concern, because of their small sensitivity to the controller parameters. The third group is improved by the tuning process so that their damping ratio will not be considered.

The optimization problem (3.14) is solved by an iterative algorithm in Fig. 3.4. To calculate the sensitivity of the eigenvalue λ_d with respect to a parameter q , this paper use the formula which has been proved by L.Rouco [29],

$$\frac{\partial \lambda_d}{\partial q} = R_{u_k Y_{fb} d} \left. \frac{\partial F(s, q)}{\partial q} \right|_{s=\lambda_d} \quad (3.15)$$

where $R_{u_k Y_{fb} d}$ is the residue which give the measure of d^{th} -mode's sensitivity to a feedback between the feedback signal Y_{fb} and input u_k in the open-loop system, and $\frac{\partial F(s, q)}{\partial q}$ is the partial derivative of the PSS's transfer function with respect to the parameter q .

The tuning algorithm allow only one parameter (among parameters T_1, T_2, T_w, K_{stab}) is updated at each iteration. This parameter is the one to which the mode of concern's real part has the maximum sensitivity. This condition is to ensure that the tuning process can improved the mode of concern with minimum change of parameter.

The criterion " $(\frac{\Delta \zeta_{ik}}{\zeta_{io}} < -0.05 \text{ and } \zeta_{ik} < \zeta_{dk})$ " means that if there is any mode is reduced ratio damping by the controller over 5% relatively and this ratio damping is smaller than mode of concern's ratio damping, the tuning process will be terminated. But if this ratio damping is still larger than mode of concern's ratio damping, it will not terminate the tuning process. By this criterion, the tuning process will not care about modes are not affected much by the controller or modes affected by the controller but still have more damping than the mode of concern.

The updating of a parameter will be skipped at an iteration if (i)The eigenvalue sensitivity with respect to it change the sign from the previous updating; (ii)The updated one violates the limitation. The tuning process will be stopped if all parameters are skipped from updating or any real part of system mode violates the limitation.

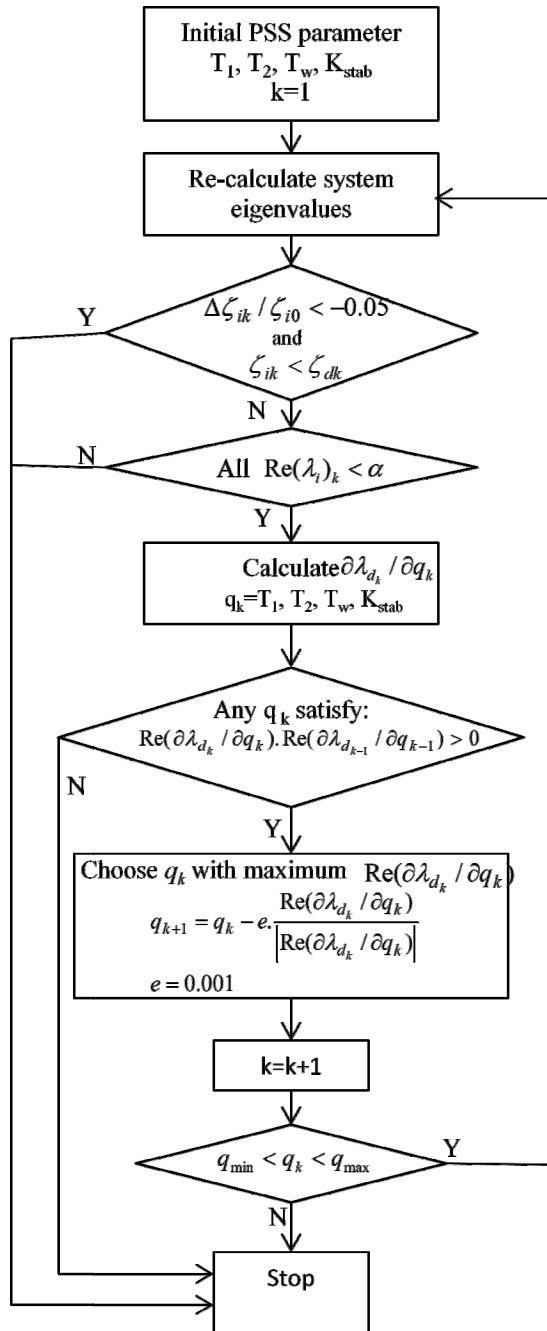


Figure 3.4 The eigenvalue optimization algorithm

3.6 PROPOSED ITERATIVE DESIGN OF WAM BASED PSS

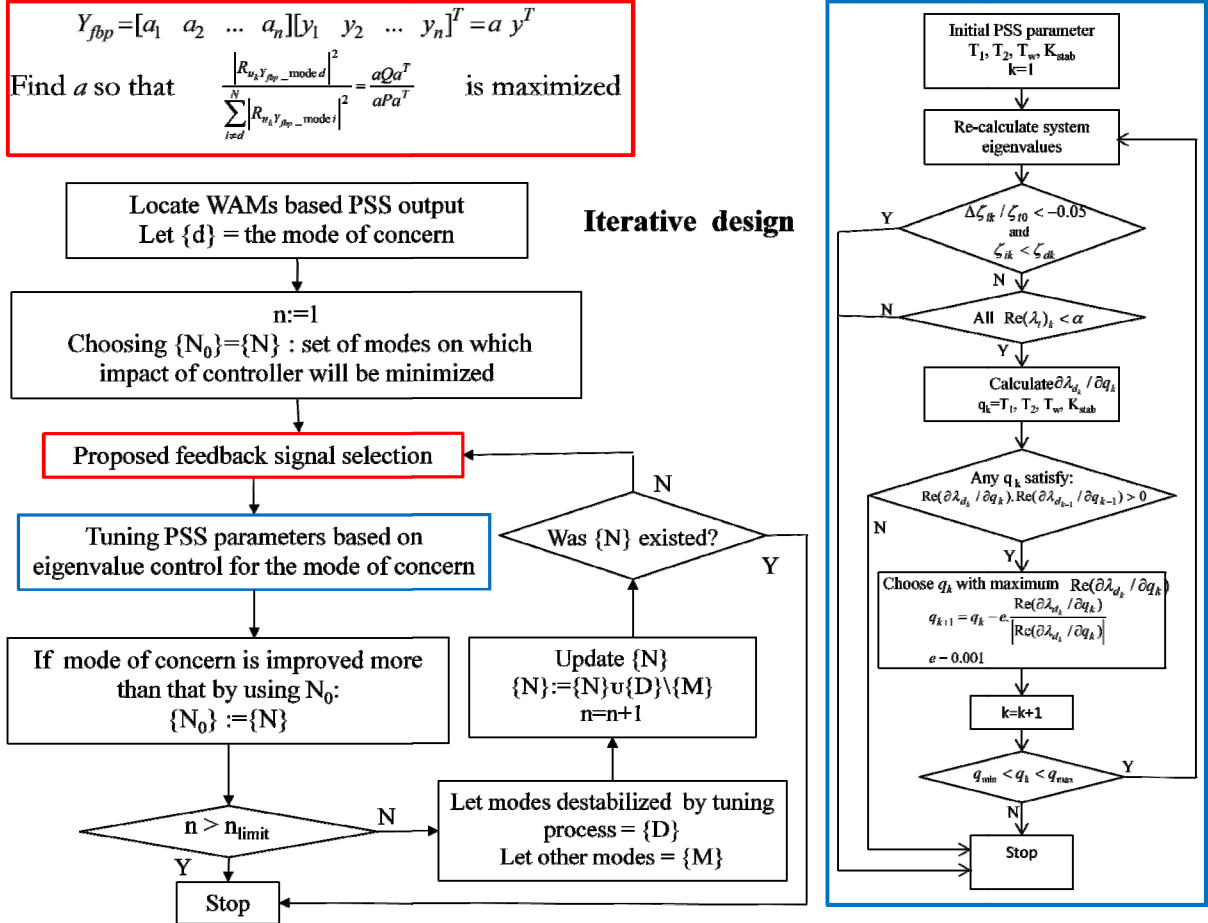


Figure 3.5 Iterative design flowchart

Section 3.4 has proposed a method of feedback signal selection which maximize the impact of controller (u_k, Y_{fb}) on mode of concern (mode d) while minimize that on others. Then, the eigenvalue optimization presented in subsection 3.5 can focus on the mode of concern. However, in the tuning process for improving the mode of concern, not all other modes are destabilized. There are also some modes are modifier by the eigenvalue control. Let $\{N\}$ is set of modes on which impact of controller (u_k, Y_{fb}) is minimized. In the flowchart in fig. 3.5, a proposed iterative design is described for choosing appropriate modes in $\{N\}$. The iterative method is a combination between feedback signal selection in 3.4 and eigenvalue control algorithm in 3.5.

In the initial step, the P matrix in the problem (3.5) is just calculated from only modes for which relative participation factor of measurements is larger than 1% or relative participation

factor of any AVR's state variables at the selected controller output is larger than 1% . Other modes for which relative participation factors of that are smaller than 1% are not affected much from controller output or cannot be observed well by measurements, therefore they are neglected in P.

At each iteration, {N} will be updated by adding modes which are destabilized and removing modes which are modified by the tuning process. {N} will be recorded as the temporary solution if mode of concern is improved better than the last temporary solution. The algorithm will be terminated if the number of iteration is over a pre-defined number, or if {N} is found to be the same with that in previous iteration.

3.7 TIME DELAY AND MEASUREMENT ERROR

3.7.1 Time delay

In wide - area damping control system, time delay are caused by [30]:

- Measurement processing, transmission, and synchronization (T_{in})
- Control signal calculation and transmission (T_{out})

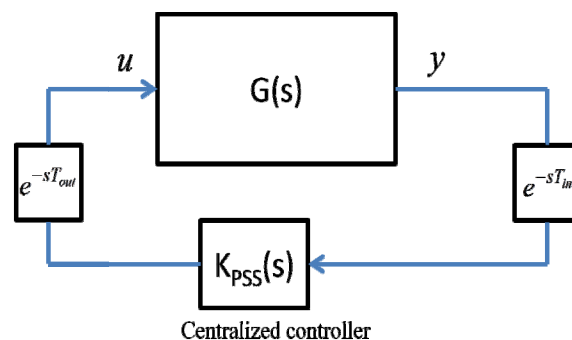


Figure 3.6 Time delay expressed in Laplace domain

Time delay T_{in} in wide - area damping control system can be divided into two parts: fixed delay and propagation delay [31].

Fixed delay:

- Due to PMU processing, DFT, multiplexing and data processing and synchronization: ~ 75(ms)

Propagation delay:

- Due to function of the communication links and physical separation: Range from 20ms (in case of fiber-optic cables) to 200ms (in case of low earth orbiting satellite)

Table 3.1 show the minimum total time delay for different communication links, from the instant of data measured by PMUs to the instant that control signals u arrive at control location. In this research, control location is V_{ref} input of AVR of selected generator.

Table 3.1 Total time delays for difference communication link [31]

| Communication link | Total time delay (ms) |
|--------------------|-----------------------|
| Fiber-optic cables | 100-150 |
| Microwave links | 100-150 |
| Power line (PLC) | 150-350 |
| Telephone lines | 200-300 |
| Satelite link | 500-700 |

If fiber-optic cables are used for communication links, T_{in} and T_{out} can be estimated in range of [100-200]ms and [50-150]ms, respectively.

3.7.2 Impact of time delay on a mode of concern

When time delay is not considered, the effectiveness of centralized PSS on the mode of concern (mode d) can be shown by:

$$\Delta\lambda_d \sim R_{uyd} K_{PSS}(\lambda_d) \quad (3.16)$$

where R_{uyd} is the residue of controller input-output for mode d

When T_{in} and T_{out} are considered, the change of the mode of concern becomes:

$$\begin{aligned} \Delta\lambda_d^{delay} &\sim R_{uyd} e^{-\lambda_d T_{in}} K_{PSS}(\lambda_d) e^{-\lambda_d T_{out}} \\ &= e^{-\lambda_d (T_{in} + T_{out})} \Delta\lambda_d = e^{-\lambda_d T} \Delta\lambda_d \end{aligned} \quad (3.17)$$

Let $\lambda_d = \alpha_d \pm i\beta_d$,

$$\Delta\lambda_d^{delay} \sim e^{-\alpha_d T} e^{\mp i\beta_d T} \Delta\lambda_d \quad (3.18)$$

Due to the characteristic of inter-area oscillation and delay time:

$$\begin{cases} -0.5 < \alpha < 0 \\ 1 < \beta < 6.28 \\ T_{\text{ave}} \sim 0.25\text{s} \end{cases} \Rightarrow \begin{cases} 1 < e^{-\alpha T} = k < 1.2 \\ -89.9^\circ < -\beta T < -8.6^\circ \end{cases}$$

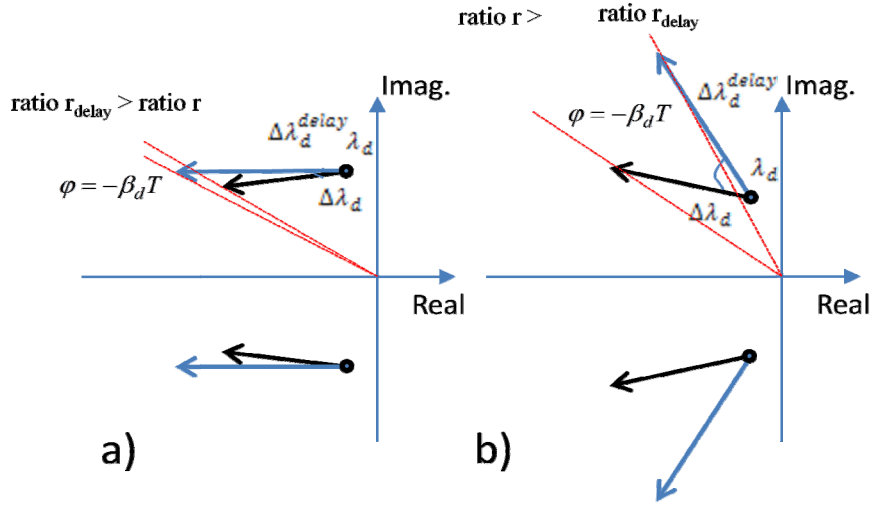


Figure 3.7. Impact of time delay on a mode

With mode's frequency in the range of $[0.2 ; 1]$ Hz, the imagine part β_d of inter-area mode is in range of $[1.26-6.28]$. Let assume a delay time $T=0.25\text{s}$, then the phase shift $-\beta_d T$ is in range of $[-89.9; -8.6]^\circ$.

Fig. 3.7 shows that adding time delay may increase mode's frequency. With stable modes, time delay may help to shift its real part more to the left hand side.

If mode's frequency had been decreased by no-time-delay designed controller, adding time delay may improve mode's damping as shown in fig. 3.7a. Otherwise, mode's damping will be decreased, as shown in fig. 3.7b.

3.7.3 Modeling time delay block for system linearization and time simulation

Time delay expressed in exponential form can be replaced by first order Pade Approximation [22]:

$$e^{-sT} \approx \frac{1-0.5Ts}{1+0.5Ts} \quad (3.19)$$

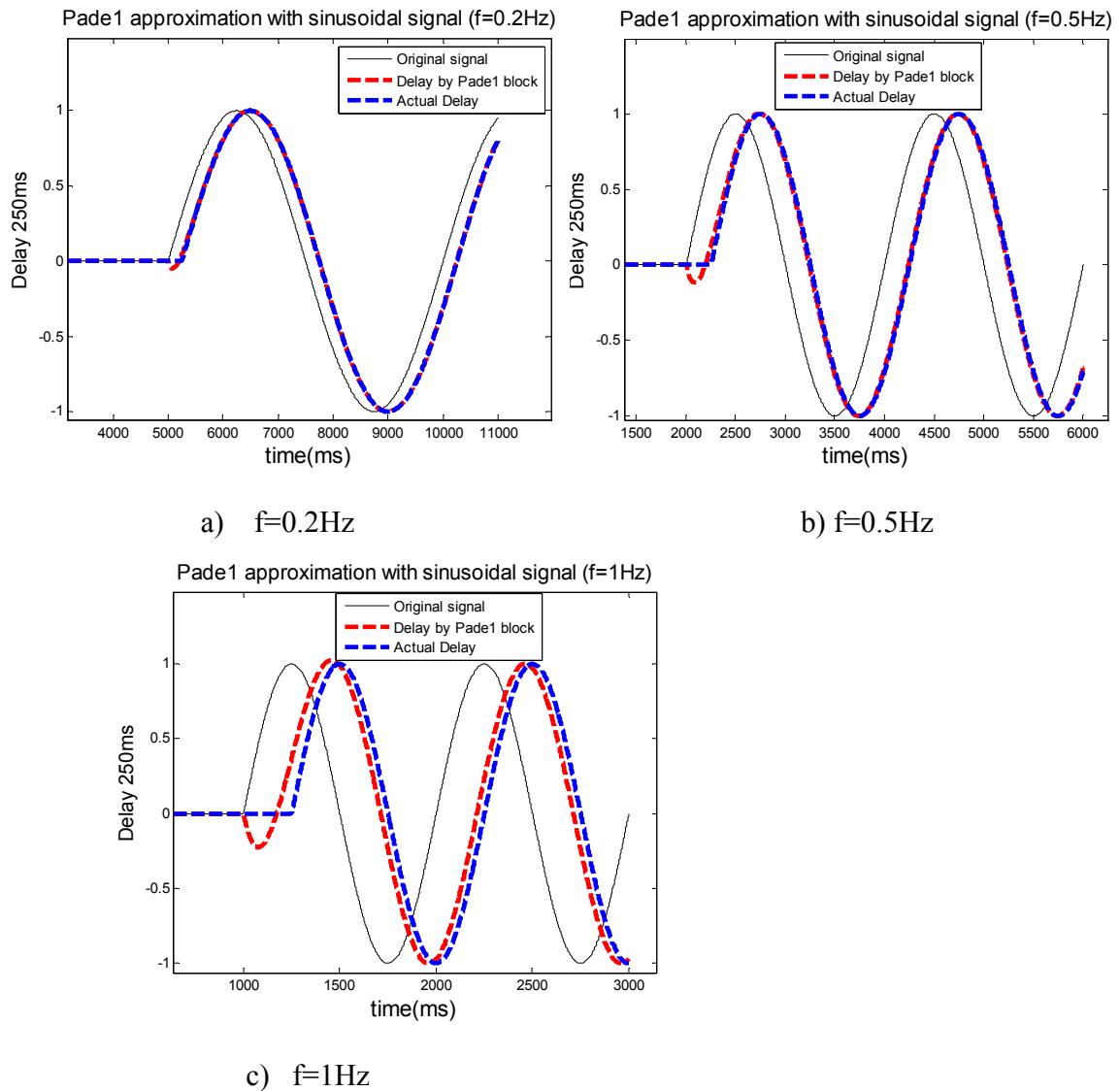


Figure 3.8. Comparisons between first order Pade Approximation and actual delay

In fig. 3.8, comparisons between first order Pade Approximation and actual delay are shown for sinusoidal signal with frequency in range of $[0.2 - 1]\text{Hz}$. It can be seen that the first order Pade Approximation is suitable to model time delay block to deal with inter-area oscillation.

Therefore, model of WAM based PSS considering time delay can be showed as follows:

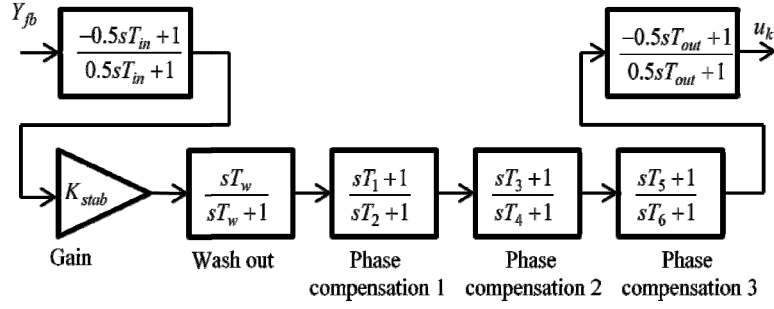


Figure 3.9. WAM based PSS considering time delay

3.7.4 Measurement error

In order to verify the robustness of the design strategy under measurements error, the dissertation also considers the system performance with a measurement error value of $\pm 5\%$.

With an assumed $\pm 5\%$ measurement error, and because the feedback signal Y_{fb} is formed by two measurements in each operating point, there are 4 critical cases of Y_{fb} should be considered to check the system performance under measurement error.

The feedback signal without measurement error: $Y_{fb} = [a_1 \ a_2][\Delta\omega_{a1} \ \Delta\omega_{a2}]^T$

Four critical cases of the feedback signal with measurement error:

$$Y_{fb} = [a_1 \ a_2][1.05 * \Delta\omega_{a1} \ 1.05 * \Delta\omega_{a2}]^T \quad , \quad Y_{fb} = [a_1 \ a_2][0.95 * \Delta\omega_{a1} \ 0.95 * \Delta\omega_{a2}]^T \quad ,$$

$$Y_{fb} = [a_1 \ a_2][1.05 * \Delta\omega_{a1} \ 0.95 * \Delta\omega_{a2}]^T \quad \text{and} \quad Y_{fb} = [a_1 \ a_2][0.95 * \Delta\omega_{a1} \ 1.05 * \Delta\omega_{a2}]^T \quad ;$$

CHAPTER 4. CASE STUDIES

The design work in chapter 3 is implemented for the IEEJ East 10-machine and West 10-machine systems [25] of which single-line diagram is shown in Figures. 4.1 and 4.2, respectively. To consider the appropriation of adaptive concept, two operating points are tested. In this research, how to form effective feedback signal from available measurements for each operating point is focused on, and the rotor angle speed deviations $\Delta\omega$ of all machines are considered as available measurements. Evaluating effectiveness of different types of measurement signals is out of scope of this research.

By the proposed method of feedback selection, the Y_{fb} can be formed from different number of participated measurements. To evaluate the effectiveness of the formed Y_{fb} , the objective function of the problem (3.5), $\frac{a^T Q a}{a^T P a}$, is used as a feedback index. For the applicable purpose, this research considers only two measurements participating in the feedback signal.

In each system operating point, the dominant inter-area mode will be selected as a mode of concern, followed by controller output location and optimal weighting feedback selection. The time domain simulation result is also presented for each case to show the effectiveness of the adaptive controller.

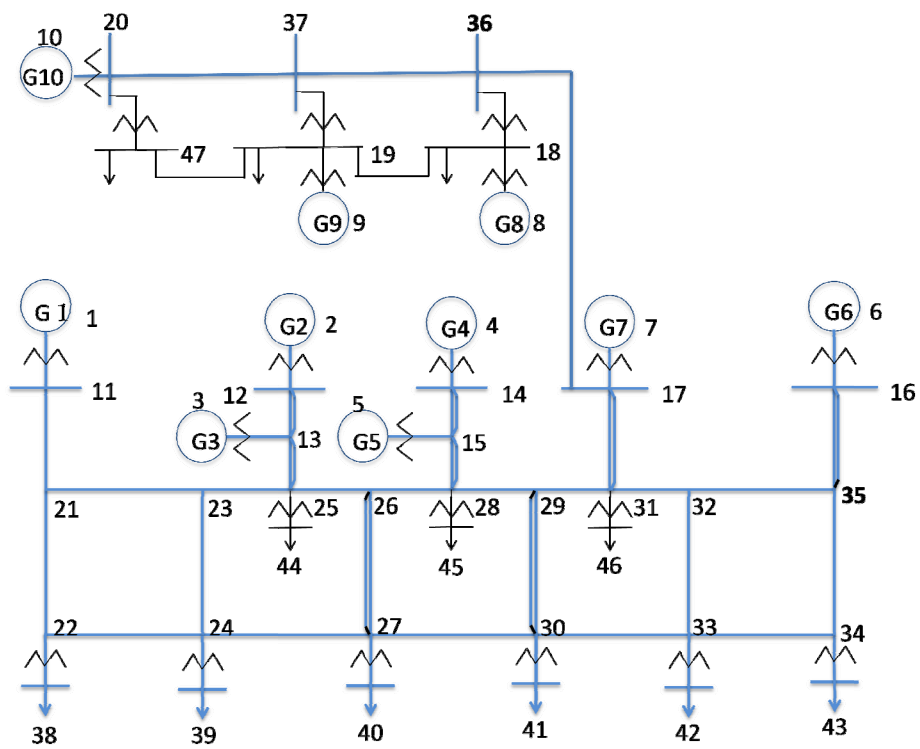


Figure 4.1 The IEEJ East 10-machine system

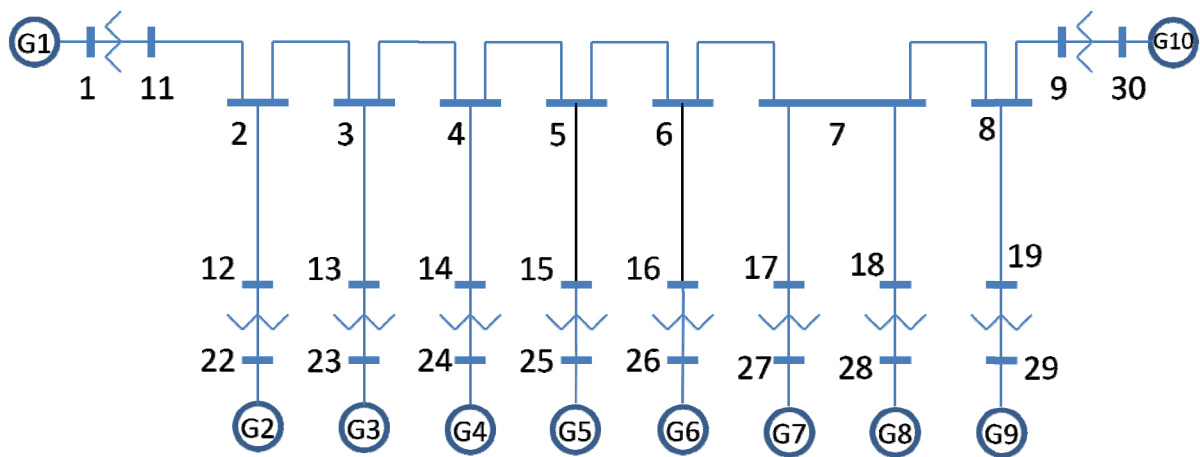


Figure 4.2 The IEEJ West 10-machine system

4.1 IEEJ EAST 10-MACHINE SYSTEM

4.1.1 Case 1

The system operating point considered in this case is made by adjusting the day time operating point of the IEEJ East 10-machine system. In order to make the inter-area oscillation between Tohoku and Tokyo Metropolitan area become dominant, all the load in Tokyo, from load 38 to load 46 are reduced by 10%, while each generator's active power in Tohoku area is reduced by 900MW. The setting values of voltage magnitudes of all machines are reduced by 0.015 so that the operating voltages are in limitation.

The inter-area modes of the system without WAM based PSS, which will be called the base case 1, are shown in Table 4.1.

Mode of concern: The mode of concern is inter-area mode between Tohoku area and Tokyo Metropolitan, mode 2 in Table 4.1.

Controller location: The maximum controllability for the inter-area mode 2 is corresponding to u_9 . Then, the location for the WAM based PSS output is at AVR 's input of machine G_9 .

Feedback signal selection and parameters tuning

In case that Y_{fb} is formed from only 2 measurements, the Y_{fb} corresponding to $[\Delta\omega_9, \Delta\omega_1]$ have the maximum value of the feedback index. The best $\{N\}$ is found to be the initial $\{N\}$. The proposed feedback selection has resulted in the weighting vector (normalized) for feedback signals as follows:

$$Y_{fb} = [0.75902 \quad -0.65107][\Delta\omega_9 \quad \Delta\omega_1]^T$$

The controller configuration is shown in fig. 4.3. With $\alpha_{limit} = -0.08$ and $K_{max} = 80$, the resulted PSS parameters are:

$$T_1 = 0.01; T_2 = 0.48; T_w = 15; K_{stab} = 80$$

Table 4.2 depicts the inter-area modes with the WAM based PSS. The damping ratio of the mode of concern is increase to 5.5%, from the original value of 2.3%. For all remaining modes of the system, it was observed that they are modified insignificantly due to the optimization tuning process for the mode of concern. In this case, the proposed feedback signal show the same result to the conventional one which is $Y_{fb} = [\sqrt{0.5} \quad -\sqrt{0.5}][\Delta\omega_9 \quad \Delta\omega_1]^T$.

Time domain simulation

To evaluate the effectiveness of the designed controller in transient stability, a temporary fault is applied at bus 36, that is located on transmission line between Tokyo Metropolitan and Tohoku area, for 0.07s. Figures 4.4 and 4.5 depict the performance of the system with and without controller during the fault.

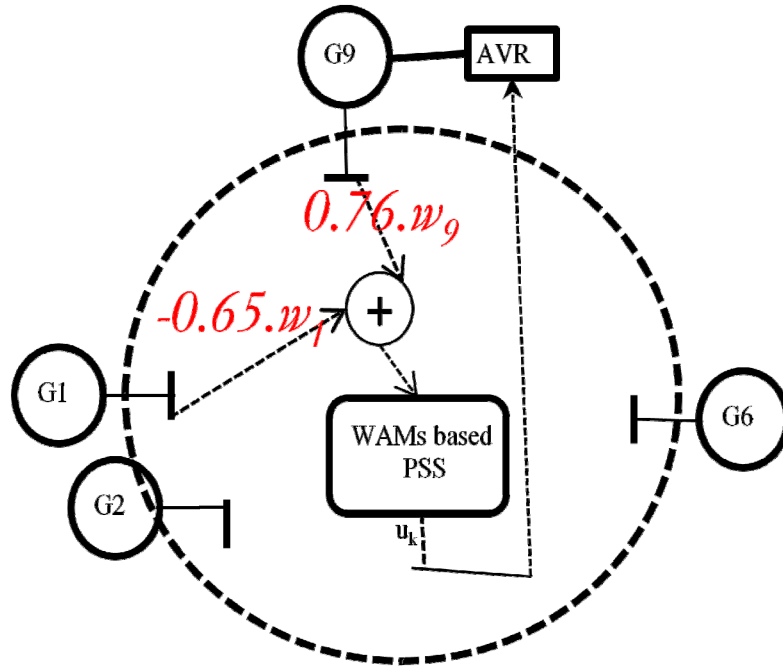


Figure 4.3 The controller configuration in case 1

Table 4.1 Inter-area Modes of the Base Case 1

| Modes | Real | Imag. | Freq. | Ratio | Dominant Participation |
|-------|--------|-------------|-------|-------|------------------------------------|
| 1 | -0.167 | ± 4.435 | 0.706 | 0.038 | $G_6 \langle G_{1,2}$ |
| 2 | -0.071 | ± 3.084 | 0.491 | 0.023 | $G_{1,2,3,4,5} \langle G_{8,9,10}$ |

Table 4.2 Affected Modes by WAM based PSS

| Case 1 | Without Controller | | With WAM PSS | | Dominant Participation |
|--------|--------------------|-------------------------------|---------------|-------------------------------|------------------------------------|
| | Real | Imag. | Real | Imag. | |
| 1 | -0.167 | ± 4.435 | -0.165 | ± 4.436 | $G_6 \langle G_{1,2}$ |
| 2 | -0.071 | ± 3.084 | -0.164 | ± 2.962 | $G_{1,2,3,4,5} \langle G_{8,9,10}$ |

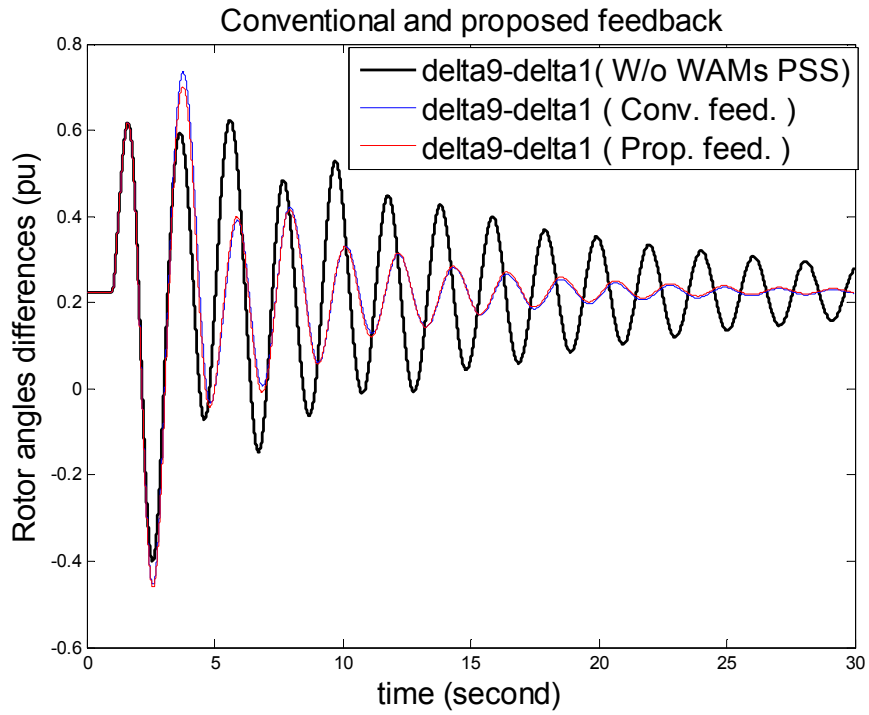


Figure 4.4 Deviations of angular differences between machines 1 and 9

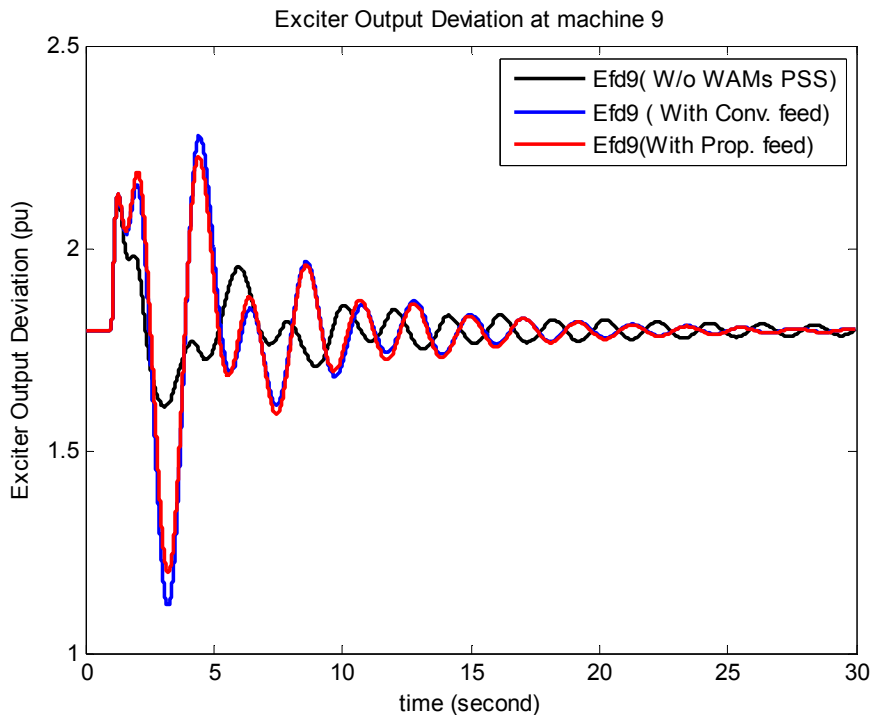


Figure 4.5 Exciter output during fault scenario

It can be seen from Figures 4.4 that the WAM based PSS has improved the mode of concern significantly. Due to a high K_{stab} , the first swing by controller performance is a little bit higher than that with out controller. In this case, the proposed and conventional feedback show similar effectiveness, as same as the eigenvalue result.

4.1.2 Case 2

The system operating point considered in case 2 is the day time operating point of the IEEJ East 10-machine system. The inter-area modes of the system without PSS in case 2 are shown in Table 4.3.

Mode of concern: The mode of concern is mode 1 in Table 4.3, the inter-area mode between groups of machine (G1, G2) and G6.

Controller location: The maximum controllability for the inter-area mode 1 in Table 3 is corresponding to u_6 . Then, the location for the WAM based PSS output is at AVR's input of machine G₆.

Feedback signal selection and parameters tuning

The Y_{fb} corresponding to $[\Delta\omega_6, \Delta\omega_1]$ shows that it has the same value of the feedback index to that corresponding to $[\Delta\omega_6, \Delta\omega_2]$. The best $\{N\}$ is found to be the initial $\{N\}$. The optimal weighting feedback selection process has resulted in the weighting vector (normalized) for feedback signal as follows:

$$Y_{fb} = [0.77017 \quad -0.63784][\Delta\omega_6 \quad \Delta\omega_1]^T$$

The controller configuration is shown in fig. 4.6. With $\alpha_{limit} = -0.08$ and $K_{max} = 100$, the resulted PSS parameters are:

$$T_1 = 0.01; T_2 = 0.325; T_w = 15; K_{stab} = 100$$

Table 4.4 depicts modes which are affected by WAM based PSS with the proposed feedback signal, in comparison with conventional feedback signal $Y_{fb} = [\sqrt{0.5} \quad -\sqrt{0.5}][\Delta\omega_6 \quad \Delta\omega_1]^T$.

The damping ratio of mode of concern is increased to 8.1% from the original damping of 3.3% by the proposed controller. Other modes which are not listed in table 4.4 are not affected

much by the controller. Beside the mode of concern, another inter-area mode, mode 2 in Table 4, is also improved by the tuning process. Mode 3 in Tables 4.4 is destabilized by the controller with either conventional or proposed feedback signal. However, with proposed feedback signal, the controller can shift the mode of concern to the left-hand side of the complex plane further than that with conventional feedback signal.

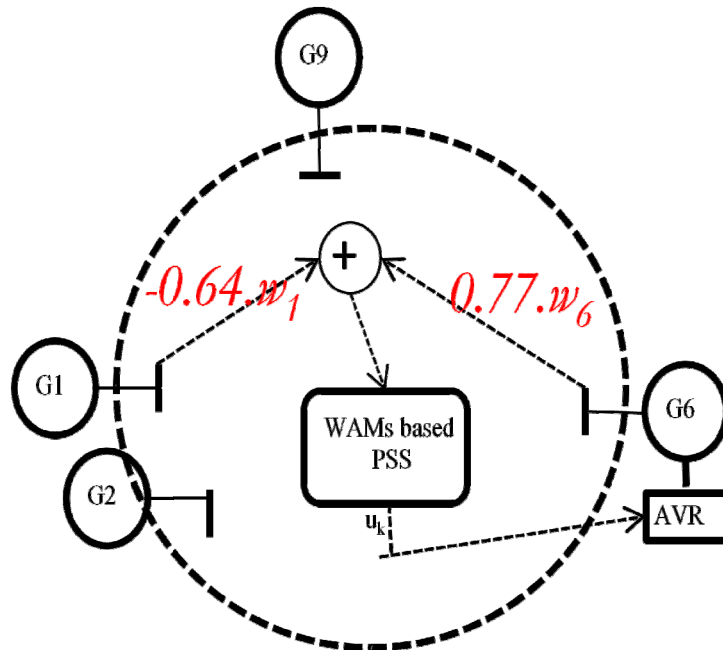


Figure 4.6 The controller configuration in case 2

Table 4.3 Inter-area Modes of the Base Case 2

| Modes | Real | Imag. | Freq. | Ratio | Dominant |
|-------|--------|-------------|-------|-------|-------------------------------------|
| 1 | -0.142 | ± 4.259 | 0.678 | 0.033 | $G_6 \diamond G_{1,2}$ |
| 2 | -0.199 | ± 2.310 | 0.368 | 0.086 | $G_{1,2,3,4,5} \diamond G_{8,9,10}$ |

Table 4.4 Affected Modes by WAM based PSS

| Case 2 | Without controller | | Controller with conventional feedback, $K_{stab}=80$ | | Controller with proposed feedback, $K_{stab}=100$ | |
|--------|--------------------|-------------------------------|--|-------------------------------|---|-------------------------------|
| | Real | Imag. | Real | Imag. | Real | Imag. |
| 1 | -0.142 | ± 4.259 | -0.273 | ± 4.096 | -0.328 | ± 4.034 |
| 2 | -0.199 | ± 2.310 | -0.236 | ± 2.419 | -0.259 | ± 2.421 |
| 3 | -0.193 | ± 1.664 | -0.101 | ± 1.640 | -0.135 | ± 1.670 |

Time domain simulation

The time domain simulation results when a temporary fault applied at bus 35 for 0.07s, in cases that feedback signal formed by $[\Delta\omega_6, \Delta\omega_1]$, are compared in Fig. 4.7. The figure shows that the performance of the controller with the proposed feedback signal is slightly better than that with the conventional feedback signal, in corresponding with the eigenvalue result shown in Tables 4.4. It can be seen that the destabilization of mode 3 in Table 4 does not affect to the time domain simulation results. The reason is that mode 3 is not an inter-area oscillation mode and that it involves to all machine.

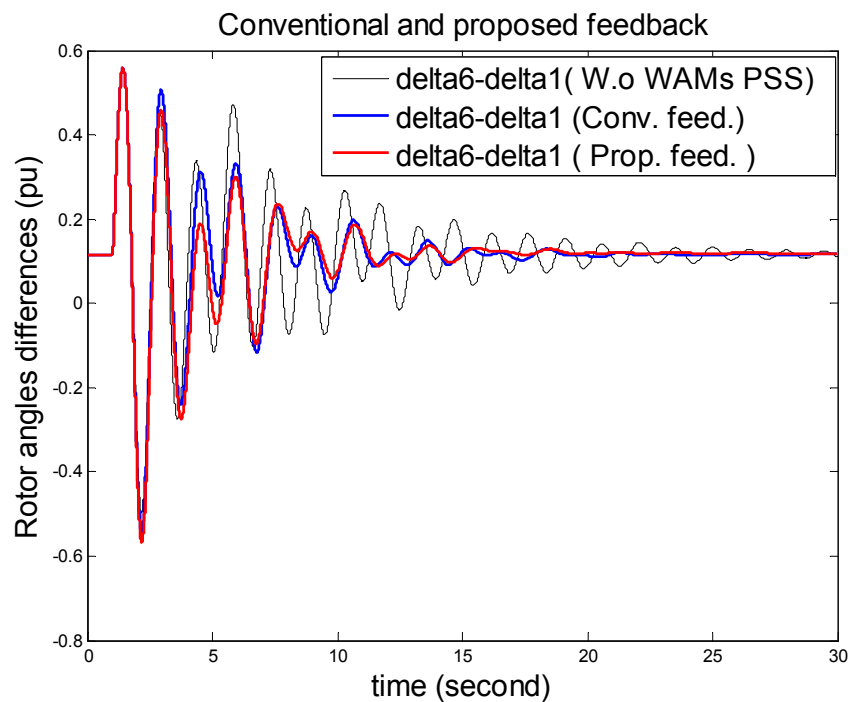


Figure 4.7 Deviations of angular differences between machines 1 and 6

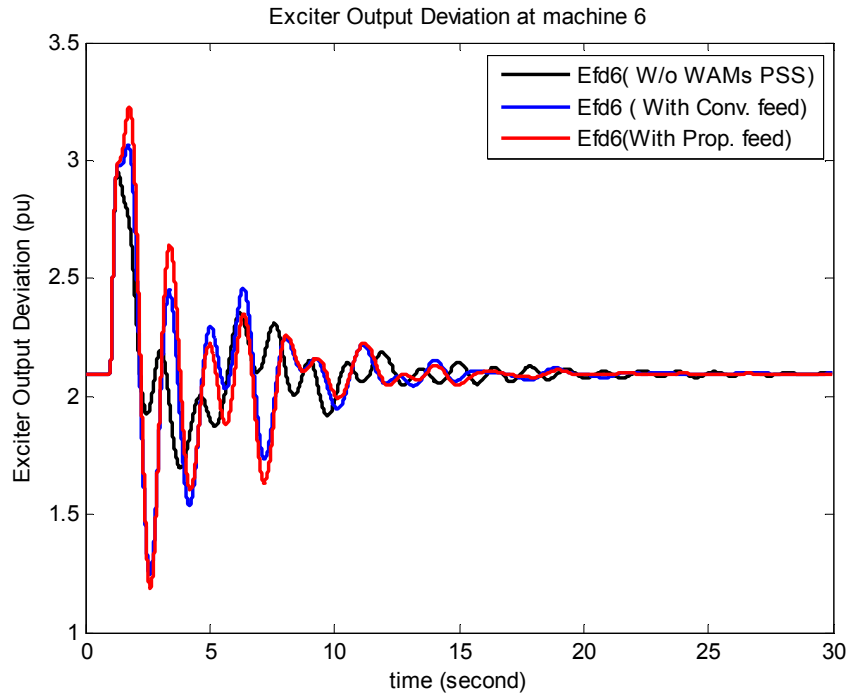


Figure 4.8 Exciter output during fault scenario

Fig. 4.8 depicts the exciter output of machine 6 with and with out WAM based PSS during fault scenario. It can be seen that the adjustment of exciter with the proposed feedback WAM based PSS is slightly better than that with the conventional one, and both of adjustments are more than that without WAM based PSS.

4.2 IEEJ WEST 10-MACHINE SYSTEM

4.2.1 Case 3

The system operating point considered in case 3 is the day time operating point of the IEEJ West 10-machine system. The inter-area modes of the system without PSS in case 3 are shown in Table 4.5.

Mode of concern: The mode of concern is mode 1 in Table 4.5, the inter-area mode between groups of machines (G10, G9, G7, G8, G6) and (G1, G2).

Controller location: The maximum controllability for the inter-area mode 1 in Table 4.5 is corresponding to u_{10} . Then, the location for the WAM based PSS output is at AVR's input of machine G₁₀.

Feedback signal selection and parameters tuning

The Y_{fb} corresponding to $[\Delta\omega_{10}, \Delta\omega_1]$ shows that it has the maximum value of the feedback index. The best $\{N\}$ is found to be $\{N_0\}$. The optimal weighting feedback selection process has resulted in the weighting vector (normalized) for feedback signal as follows:

$$\{N_0\} = \{2, 5, 6, 7\}; Y_{fb} = [0.583 \quad -0.812][\Delta\omega_{10} \quad \Delta\omega_1]^T$$

Initial parameters: $T_1=1.053$; $T_2=0.198$; $T_w=10$; $K_{stab}=0.001$;

Tuned parameters: $T_1=2$; $T_2=0.250$; $T_w=15$; $K_{stab}=0.17$;

The controller configuration is shown in the following figure.

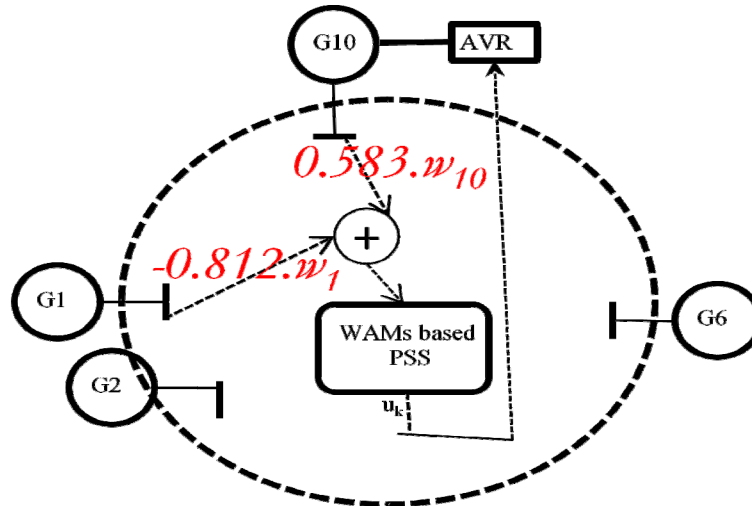


Figure 4.9 The controller configuration in case 3

To evaluate the proposed feedback signal, the above iterative method is also done with conventional feedback.

Conventional feedback:

$$Y_{fb} = [0.707 \quad -0.707][\Delta\omega_{10} \quad \Delta\omega_1]^T$$

Initial parameters: $T_1=1.054$; $T_2=0.198$; $T_w=10$; $K_{stab}=0.001$;

Tuned parameters: $T_1=2$; $T_2=0.238$; $T_w=15$; $K_{stab}=0.081$;

Table 4.5 Affected Modes by WAM based PSS

| Modes | Without WAM PSS | | WAM PSS - Conventional | | Dominant Participation (>10%) |
|-------|-----------------|----------|------------------------|----------|-------------------------------|
| | Eig.Real | Eig.Imag | Eig.Real | Eig.Imag | |
| 1 | -0.073 | ±2.189 | -0.162 | ±2.143 | G10,G9,G7,G8,G6>G1,G2 |
| 2 | -0.104 | ±1.203 | -0.090 | ±1.194 | G1, G2, G3...G9,G10 |
| 3 | -0.187 | ±4.928 | -0.238 | ±4.980 | G7,G8>G4,G10,G3,G5 |
| 4 | -0.149 | ±3.672 | -0.238 | ±3.700 | G10,G9,>G5,G6,G4 |
| 6 | -0.262 | ±6.515 | -0.259 | ±6.542 | G4>G6 |

Table 4.6 Affected Modes by WAM based PSS

| Modes | WAM PSS -Initial | | WAM PSS-Final | | Dominant Participation (>10%) |
|-------|------------------|----------|---------------|----------|-------------------------------|
| | Eig.Real | Eig.Imag | Eig.Real | Eig.Imag | |
| 1 | -0.173 | ±2.144 | -0.340 | ±2.170 | G10,G9,G7,G8,G6>G1,G2 |
| 2 | -0.096 | ±1.190 | -0.098 | ±1.178 | G1, G2, G3...G9,G10 |
| 3 | -0.238 | ±4.990 | -0.289 | ±5.044 | G7,G8>G4,G10,G3,G5 |
| 4 | -0.229 | ±3.707 | -0.279 | ±3.723 | G10,G9,>G5,G6,G4 |
| 6 | -0.257 | ±6.544 | -0.251 | ±6.569 | G4>G6 |

By proposed method, the eigenvalue of mode of concern is improved from -0.073 ± 2.189 to -0.340 ± 2.170 . The mode 's damping ratio is increased as more than three times, from 0.033 to 0.11. Besides, other inter-area modes, mode 3 and 4, are also improved. Their damping ratio are up to 1.5 times. Other modes are not affected significantly by the controller.

Tables 4.5 and 4.6 also show the goodness of the iterative design. It can be seen that the proposed feedback without iterative design (initial iteration) can improve the mode of concern better than that by the conventional feedback. However, the iterative design of which flowchart depicted in Fig. 3.5 can lead to a much better result.

Hence, the proposed feedback signal in combination with eigenvalue control and iterative design can damp out inter-area modes, especially the dominant inter-area mode without affecting other modes much.

Time domain simulation

Table 4.7 CCT in corresponding to faulted buses

| Faulted bus (FB) | 2 | 5 | 7 | 8 |
|-------------------------|-------|-------|-------|-------|
| CCT (s) without WAM PSS | 0.030 | 0.065 | 0.035 | 0.054 |
| CCT (s) with WAM PSS | 0.038 | 0.130 | 0.043 | 0.063 |

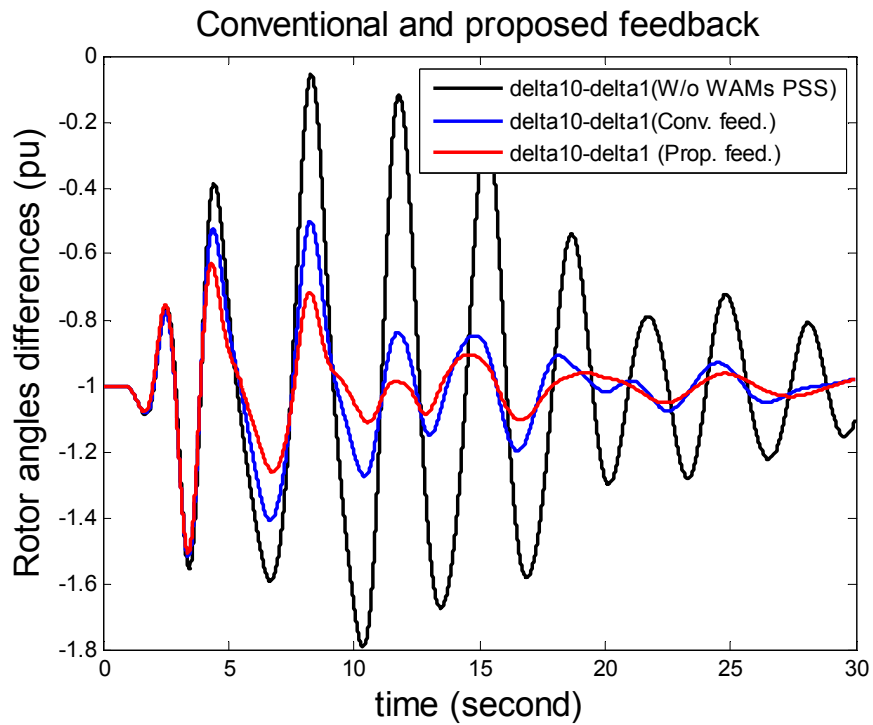


Figure. 4.10 Deviations of angular differences between machines 10 and 1

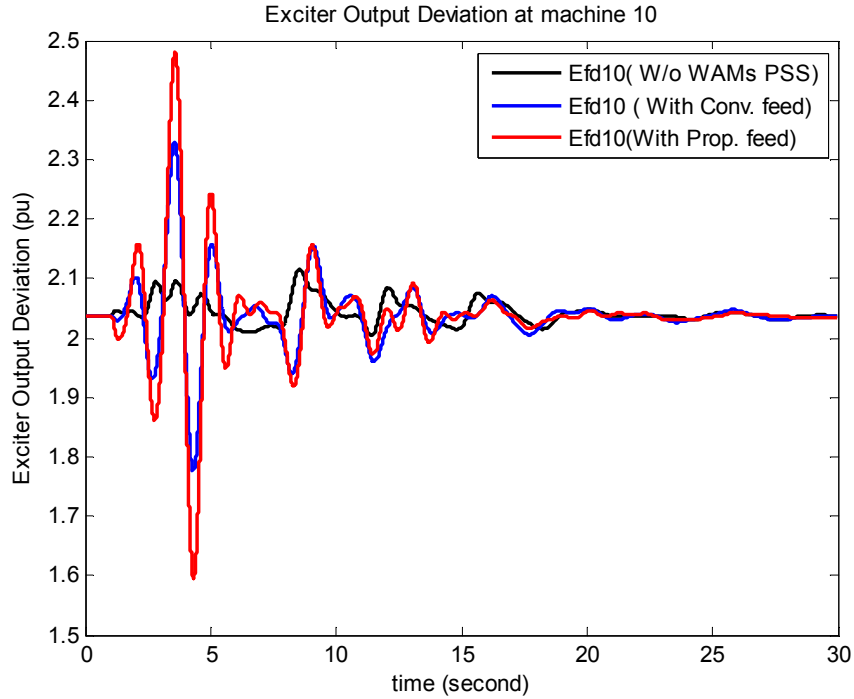


Figure. 4.11 Exciter output during fault scenario

Table 4.7 show that the CCT for each faulted bus with controller is larger than that without controller. Fig 4.10 shows that the system performance has been improved by the proposed WAM based PSS from that by conventional WAM based PSS in a 3-phase fault scenario at bus 5 with clearing time 0.06s. Fig. 4.11 depicts the exciter outputs during fault scenario. Corresponding to the system performance in fig. 4.10, the exciter adjustment with the proposed feedback WAM based PSS is larger than that with the conventional one.

4.2.2 Case 4

The system operating point considered in case 4 is the adjusted day time operating point of the IEEJ West 10-machine system. The inter-area modes of the system without PSS in case 4 are shown in Table 4.8.

Mode of concern: The mode of concern is mode 1 in Table 4.8, the inter-area mode between groups of machines (G10,G9,G7,G8,G6) \leftrightarrow (G1,G2).

Controller location: The maximum controllability for the inter-area mode 1 in Table 4.8 is corresponding to u_{10} . Then, the location for the WAM based PSS output is at AVR's input of machine G_{10} .

Feedback signal selection and parameters tuning

The Y_{fb} corresponding to $[\Delta\omega_{10}, \Delta\omega_1]$ shows that it has the maximum value of the feedback index. The best $\{N\}$ is found to be $\{N_0\}$. The optimal weighting feedback selection process has resulted in the weighting vector (normalized) for feedback signal as follows:

$$\{N_0\} = \{2, 6, 8\} \Rightarrow Y_{fb} = [0.576 \quad -0.818][\Delta\omega_{10} \quad \Delta\omega_1]^T$$

Initial parameters: $T_1=1.053$; $T_2=0.198$; $T_w=10$; $K_{stab}=0.001$;

Tuned parameters: $T_1=2$; $T_2=0.235$; $T_w=10$; $K_{stab}=0.178$;

The controller configuration is shown in the figure 4.12.

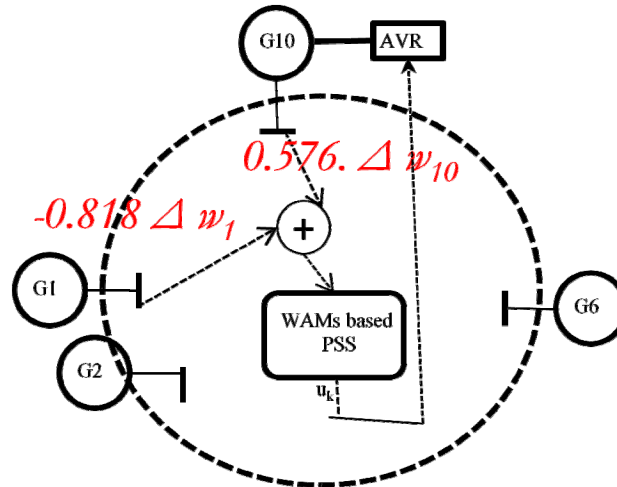


Figure. 4.12 The controller configuration in case 3

To evaluate the proposed feedback signal, the same method of parameter tuning is also done with conventional feedback.

Conventional feedback:

$$Y_{fb} = [0.707 \quad -0.707][\Delta\omega_{10} \quad \Delta\omega_1]^T$$

Initial parameters: $T_1=1.054$; $T_2=0.198$; $T_w=10$; $K_{stab}=0.001$;

Tuned parameters: $T_1=2$; $T_2=0.233$; $T_w=10$; $K_{stab}=0.093$;

Table 4.8 Affected Modes by WAM based PSS

| Modes | Without WAM PSS | | WAM PSS - Conventional | | Dominant Participation (>10%) |
|----------|-----------------|----------|------------------------|----------|---------------------------------------|
| | Eig.Real | Eig.Imag | Eig.Real | Eig.Imag | |
| 1 | -0.068 | ±2.203 | -0.154 | ±2.156 | G10,G9,G7,G8,G6 ◇ G1,G2 |
| 2 | -0.104 | ±1.219 | -0.086 | ±1.204 | G1, G2, G3...G9,G10 |
| 3 | -0.182 | ±4.726 | -0.247 | ±4.775 | G7,G8 ◇ G4,G10,G3,G5 |
| 4 | -0.158 | ±3.364 | -0.266 | ±3.375 | G10,G9,◇G5,G6,G4 |
| 6 | -0.265 | ±6.565 | -0.259 | ±6.681 | G4◇G6 |
| 8 | -0.219 | ±5.643 | -0.229 | ±5.663 | G9◇G7,G8 |

Table 4.9 Affected Modes by WAM based PSS

| Modes | WAM PSS -Initial | | WAM PSS-Final | | Dominant Participation (>10%) |
|----------|------------------|----------|---------------|----------|---------------------------------------|
| | Eig.Real | Eig.Imag | Eig.Real | Eig.Imag | |
| 1 | -0.192 | ±2.207 | -0.203 | ±2.125 | G10,G9,G7,G8,G6 ◇ G1,G2 |
| 2 | -0.104 | ±1.188 | -0.100 | ±1.186 | G1, G2, G3...G9,G10 |
| 3 | -0.200 | ±4.793 | -0.307 | ±4.822 | G7,G8 ◇ G4,G10,G3,G5 |
| 4 | -0.227 | ±3.434 | -0.308 | ±3.379 | G10,G9,◇G5,G6,G4 |
| 6 | -0.253 | ±6.665 | -0.253 | ±6.666 | G4◇G6 |
| 8 | -0.216 | ±5.660 | -0.206 | ±5.510 | G9◇G7,G8 |

By proposed method, the eigenvalue of mode of concern is improved from -0.068 ± 2.203 to -0.203 ± 2.125 . The mode's damping ratio is increased as three times, from 0.031 to 0.095. Besides, other inter-area modes, mode 3 and 4, are also improved. Their damping ratio are up to almost 2 times. Other modes are affected insignificantly by the controller.

The eigenvalues in Table 4.9 also confirm the goodness of the proposed feedback selection and the proposed iterative design, as mentioned in case 3.

Hence, similar to case 3, the proposed feedback signal in combination with eigenvalue control can damp out inter-area modes, especially the dominant inter-area mode without affecting other modes much.

Time domain simulation

Table 4.10 CCT in corresponding to faulted buses

| Faulted bus (FB) | 2 | 5 | 7 | 8 |
|-------------------------------|-------|-------|-------|-------|
| CCT (s) without WAM PSS | 0.042 | 0.07 | 0.043 | 0.070 |
| CCT (s) with proposed WAM PSS | 0.048 | 0.017 | 0.050 | 0.075 |

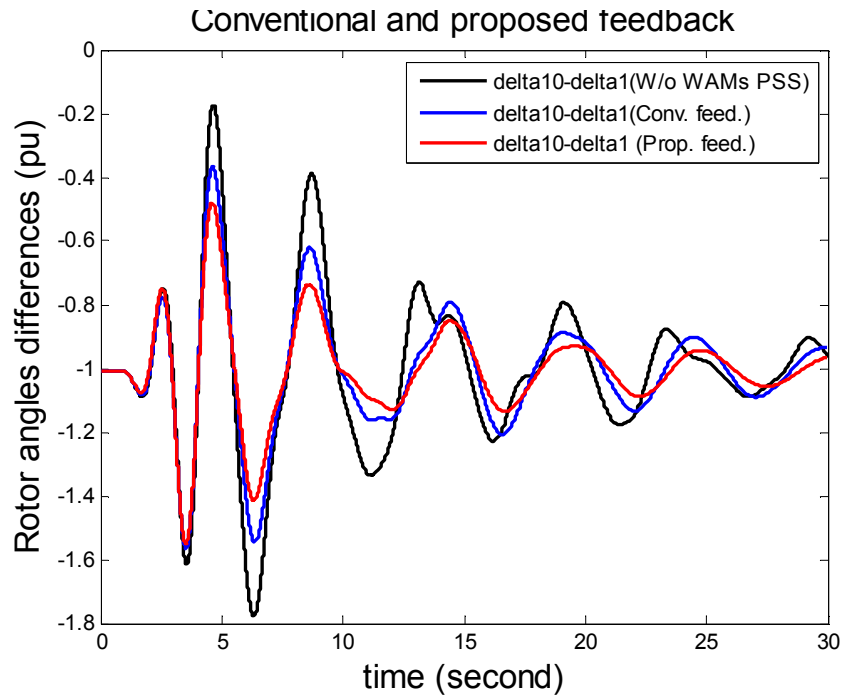


Figure. 4.13 Deviations of angular differences between machine 10 and 1

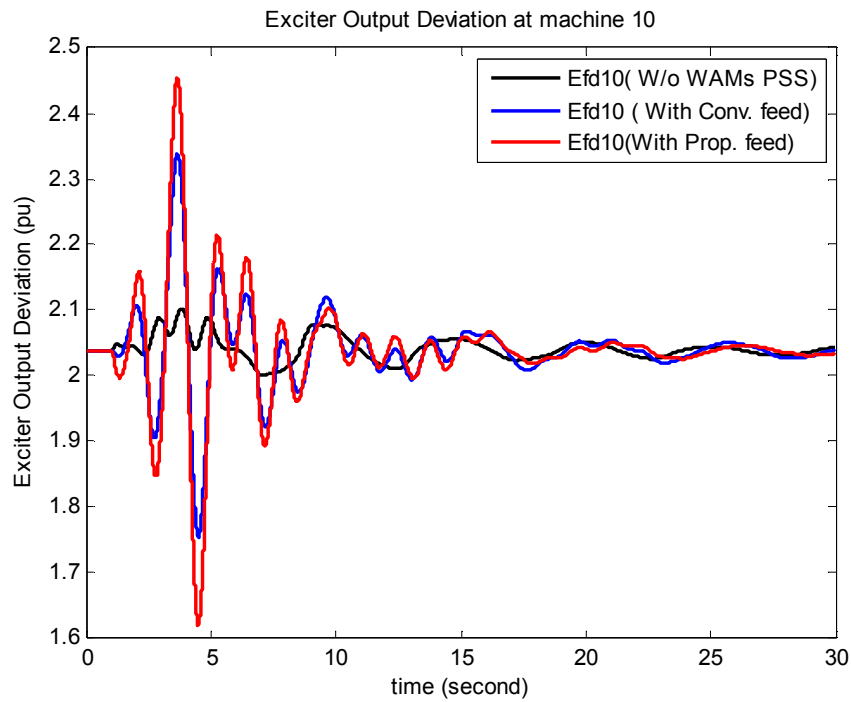


Figure. 4.14 Exciter output during fault scenario

Table 4.10 shows that the CCT for each faulted bus with controller is larger than that without controller. Fig. 4.13 shows that the system performance has been improved by the proposed WAM based PSS from that by conventional WAM based PSS in a 3-phase fault scenario at bus 5 with clearing time of 0.06s. Similar to previous cases, fig 4.14 shows that the exciter adjustments are also in corresponding with the system performance.

4.3 TIME DELAY AND MEASUREMENT ERROR CONSIDERATION

4.3.1 Impact of delay time on controller designed without time delay consideration

Proposed feedback and conventional feedback comparison under delay time

In each figures 4.15 or 4.16, system behaviors under conventional controller and proposed controller is compared. Fig. 4.15 is corresponding to case 1 for adjusted operating points, and Fig. 4.16 is corresponding to case 2 for daytime operating points of IEEJ East 10-machine system. In each case, $T_{in}=0.15s$ and $T_{out}=0.1s$.

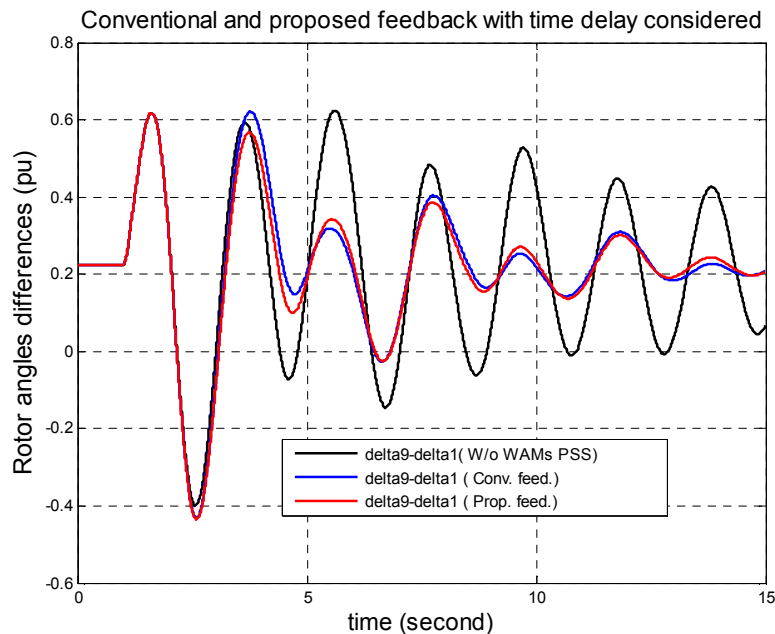


Figure 4.15 Proposed and conventional feedback considering time delay _Case 1

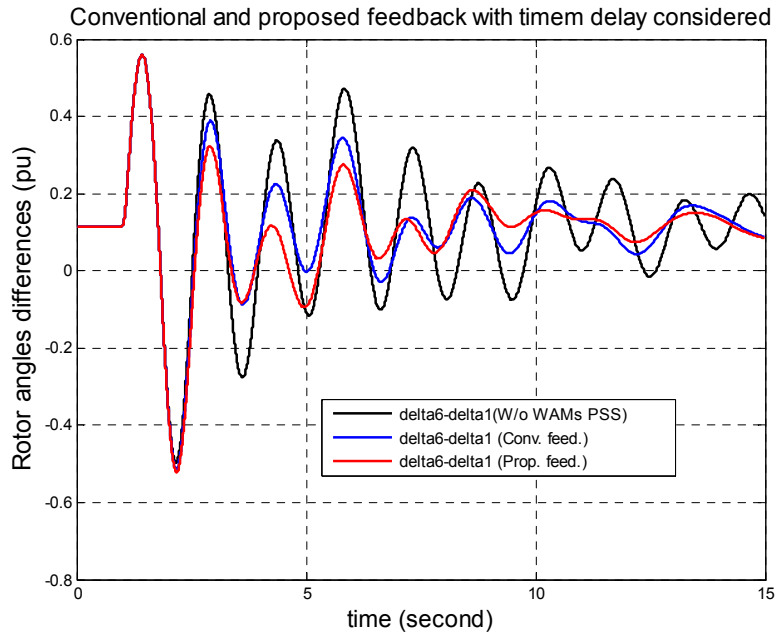


Figure 4.16 Proposed and conventional feedback considering time delay _Case 2

Figures 4.17 and 4.18 show system behaviors under conventional controller and proposed feedback for daytime and adjusted operating point of the IEEJ West 10-machine system.

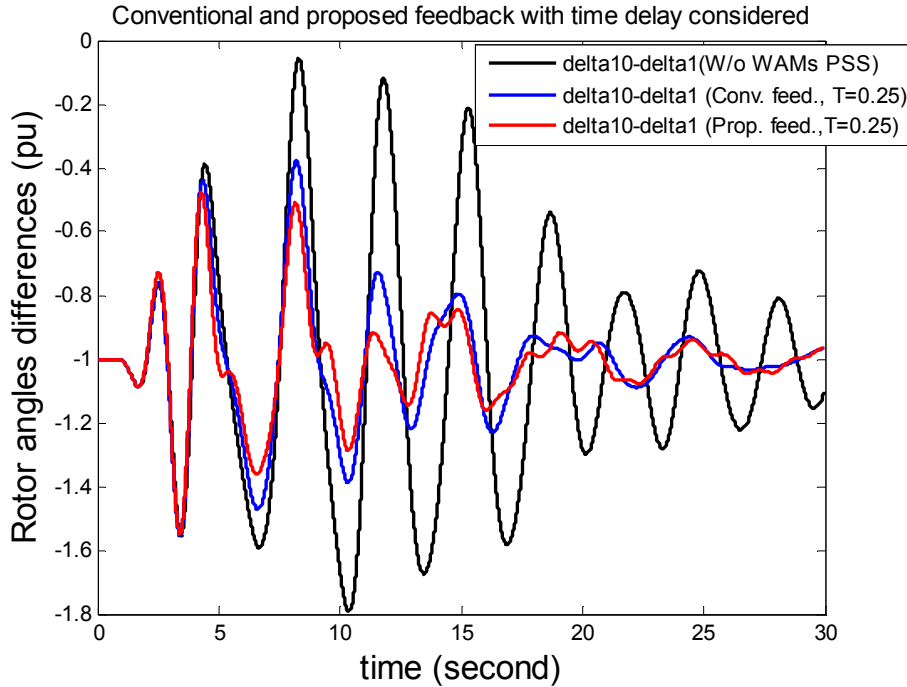


Figure 4.17 Proposed and conventional feedback considering time delay _Case 3

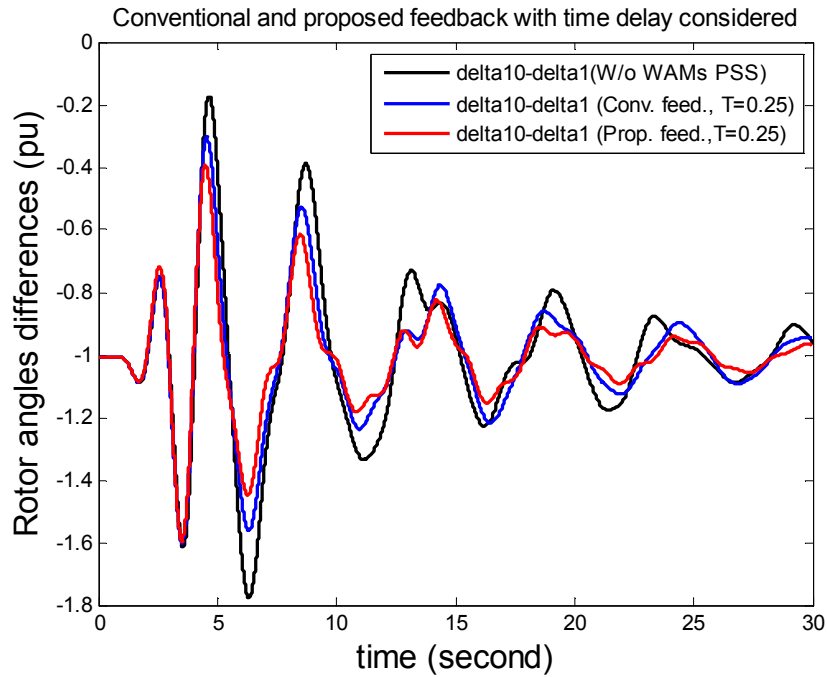


Figure 4.18 Proposed and conventional feedback considering time delay _Case 4

Figures 4.5, 4.16, 4.17 and 4.18 show that, with time delay added, the proposed feedback controller still keep the advantage of damping the dominant inter-area mode, in comparison with the conventional one.

Impact of various delay time on effectiveness of proposed controller

In each figures 4.19 and 4.20, impact of various delay time on the proposed controller performance for IEEJ East 10-machine system are shown. The assumed delay time are shown in Table 2.

Table 4.11 Assumed delay time

| T_{in} | T_{out} | $T = T_{in} + T_{out}$ |
|----------|-----------|------------------------|
| 0 | 0 | 0 |
| 0.05 | 0.1 | 0.15 |
| 0.1 | 0.15 | 0.25 |
| 0.15 | 0.2 | 0.35 |

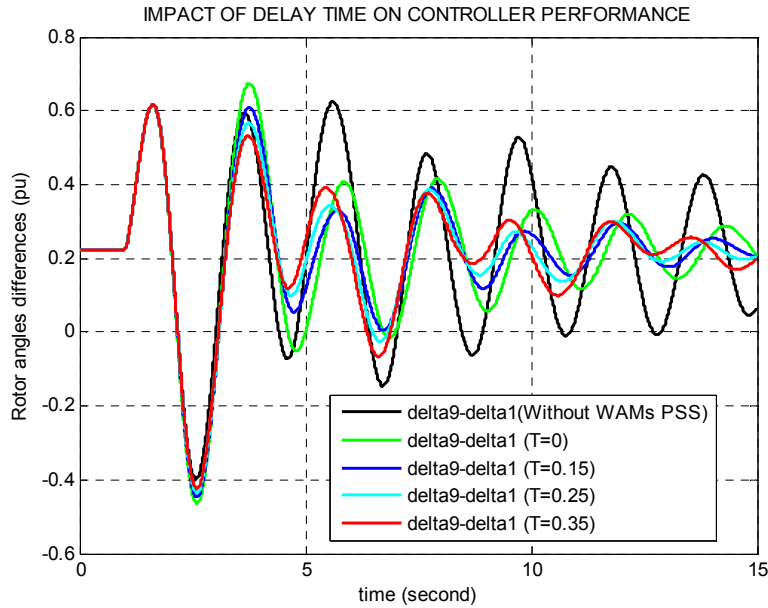


Figure 4.19 Impact of time delay on East 10-machine system_Case 1

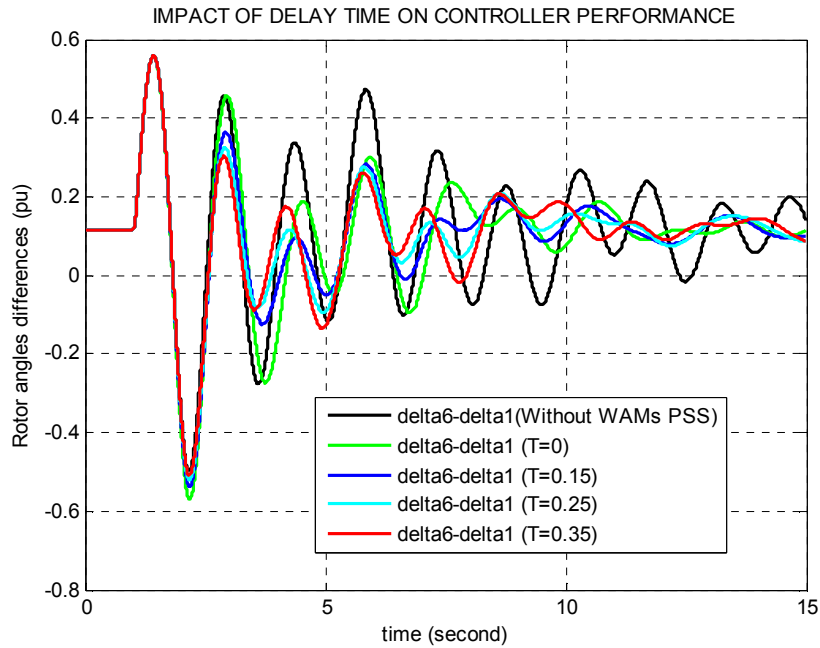


Figure 4.20 Impact of time delay on East 10-machine system_Case 2

Based on figures 4.19 and 4.20, it is seen that delay time does not have a bad impact on the system performance. As explained in subsection 3.7.2, if $e^{-\alpha_d T}$ is large enough ($\gg 1$) and $\beta_d T$ is small enough, time delay may improve a mode in wide-area damping control. However, the possibility that it destabilized that mode is larger. The reason is that the real part α_d of the

dominant inter-area mode is very near to zero, or even positive, then $e^{-\alpha_d T}$ is likely near to or less than 1.

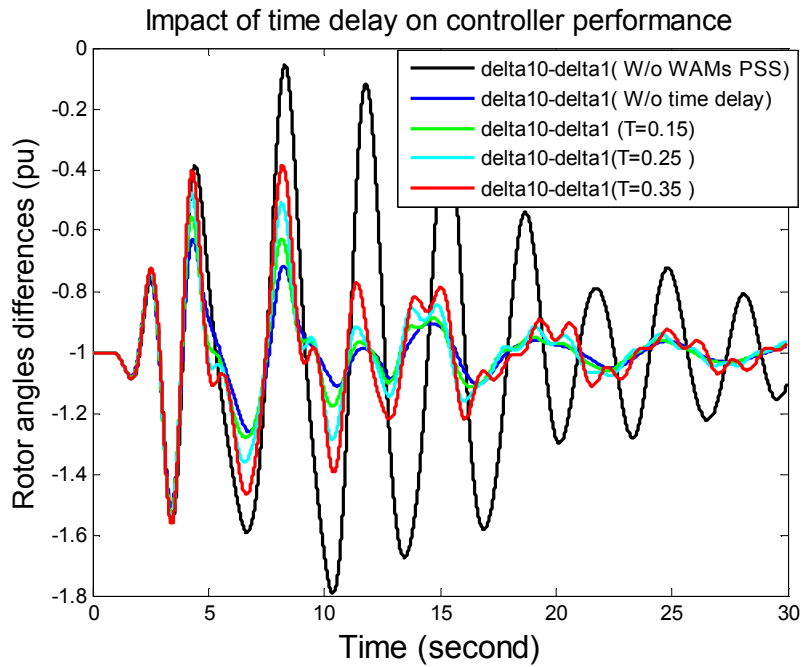


Figure 4.21 Impact of time delay on West 10-machine system_Case 3

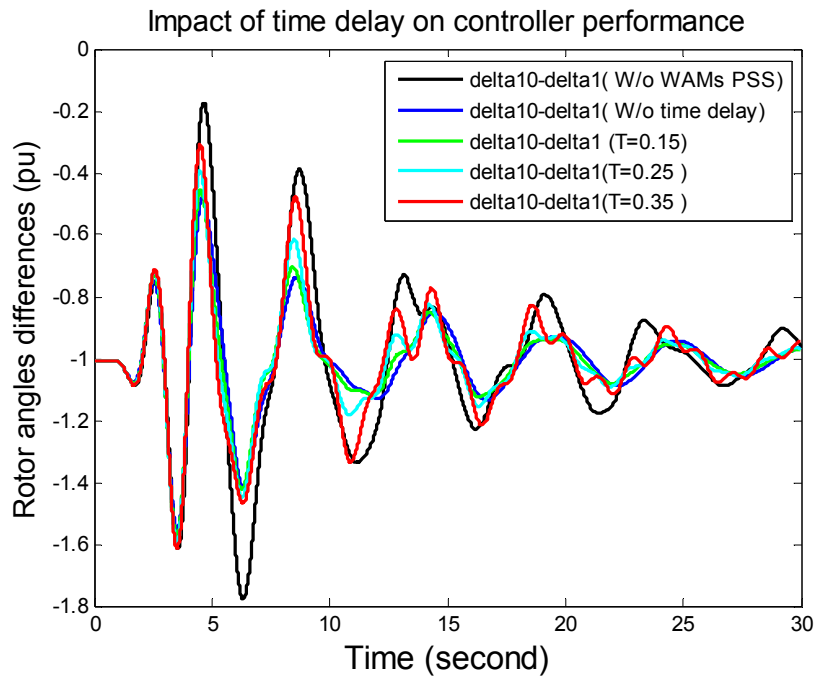


Figure 4.22 Impact of time delay on West 10-machine system_Case 4

In contrast with IEEJ East system cases, IEEJ West system cases show the more frequent phenomena. Delay time has destabilized the dominant inter-area mode in case 3 and case 4 for IEEJ West 10-machine system, as shown in fig. 4.21 and 4.22.

This subsection shows controller performances under time delay. The delay time was not considered in the design process.

In the next subsection, the delay time will be taken into account in the design process. A setting delay time of 0.25s is assumed in the design process and the controller performances are investigated for East 10-machine system.

4.3.2 Implementation of design process with time delay

This section describes the result of design procedure in which time delay is taken into account.

As shown in table 4.12, time delay for a WAM based PSS can be listed as $T=0.15$, 0.25 or 0.35 s.

To consider impact of time delay, a **setting delay time $T=0.25$** is taken into account in the process of eigenanalysis for tuning PSS's parameter.

The result of eigenvalues and tuned parameters are different when time delay is not taken into account in the PSS model, as follows:

Adjusted operating point of IEEJ East 10-machine system

PSS Configuration

Table 4.12 PSS configuration with and without considering time delay

| | Not consider T | Consider T=0.25 |
|------------------------|---|---|
| Measurements | $[\Delta\omega_9 \quad \Delta\omega_1]^T$ | $[\Delta\omega_9 \quad \Delta\omega_1]^T$ |
| Feedback $Y_{fb} =$ | $[0.76 \quad -0.65]$ $[\Delta\omega_9 \quad \Delta\omega_1]^T$ | $[0.76 \quad -0.65]$ $[\Delta\omega_9 \quad \Delta\omega_1]^T$ |
| Output | AVR9 | AVR9 |

The result of PSS configuration is determined based on eigenanalysis of open-loop system and moving direction of eigenvalue by PSS. The moving direction of eigenvalue by PSS is not affected by time delay. Therefore, PSS configuration is not changed when time delay is considered.

PSS parameter

Table 4.13 PSS's parameters with and without considering time delay

| Parameters | Not consider T | Consider |
|------------|----------------|--------------|
| T_w | 15 | 15 |
| T_1 | 0.1 | 0.1 |
| T_2 | 0.48 | 0.337 |
| K_{stab} | 80 | 80 |

By delay time $T=0.25$, the design procedure resulted in a different PSS 's parameters. T_2 changed from 0.48 to 0.337.

Eigenvalue result

Table 4.14 Eigenvalue result with setting DT =0, actual DT=0

| Modes | Without | | With WAM | | Dominant |
|-------|-------------|--------------|---------------|-------------------------------|-------------------------------------|
| | <i>Real</i> | <i>Imag.</i> | <i>Real</i> | <i>Imag.</i> | |
| 1 | -0.167 | ± 4.435 | -0.165 | ± 4.436 | $G_6 \diamond G_{1,2}$ |
| 2 | -0.071 | ± 3.084 | -0.164 | ± 2.962 | $G_{1,2,3,4,5} \diamond G_{8,9,10}$ |

Table 4.15 Eigenvalue result with setting DT =0, actual DT=0.25

| Modes | Without | | With WAM based PSS | | Dominant Participation |
|-------|-------------|--------------|--------------------|-------------------------------|-------------------------------------|
| | <i>Real</i> | <i>Imag.</i> | <i>Real</i> | <i>Imag.</i> | |
| 1 | -0.167 | ± 4.435 | -0.165 | ± 4.433 | $G_6 \diamond G_{1,2}$ |
| 2 | -0.071 | ± 3.084 | -0.217 | ± 3.078 | $G_{1,2,3,4,5} \diamond G_{8,9,10}$ |

Table 4.16 Eigenvalue result with setting DT =0.25s, actual DT= 0.25s

| Modes | Without | | With WAM based PSS | | Dominant Participation |
|-------|-------------|--------------|--------------------|---------------|-----------------------------------|
| | <i>Real</i> | <i>Imag.</i> | <i>Real</i> | <i>Imag.</i> | |
| 1 | -0.167 | ±4.435 | -0.164 | ±4.433 | $G_6 \angle G_{1,2}$ |
| 2 | -0.071 | ±3.084 | -0.425 | ±2.467 | $G_{1,2,3,4,5} \angle G_{8,9,10}$ |

With time delay impact and changing of PSS parameter, the eigenvalue result also changed, as shown in table 4.16. The ratio damping is improved to 14.7% from original value of 2.3%.

Eigenvalue result with setting TD=0, actual TD=0.25 (table 4.15) is better than that with setting TD=0, actual TD=0.0 (table 4.14). Hence, it confirmed the time domain result showed in fig. 4.16 that for this operating point, time delay has a good impact on the no-setting delay time-controller's performance.

Time domain simulation

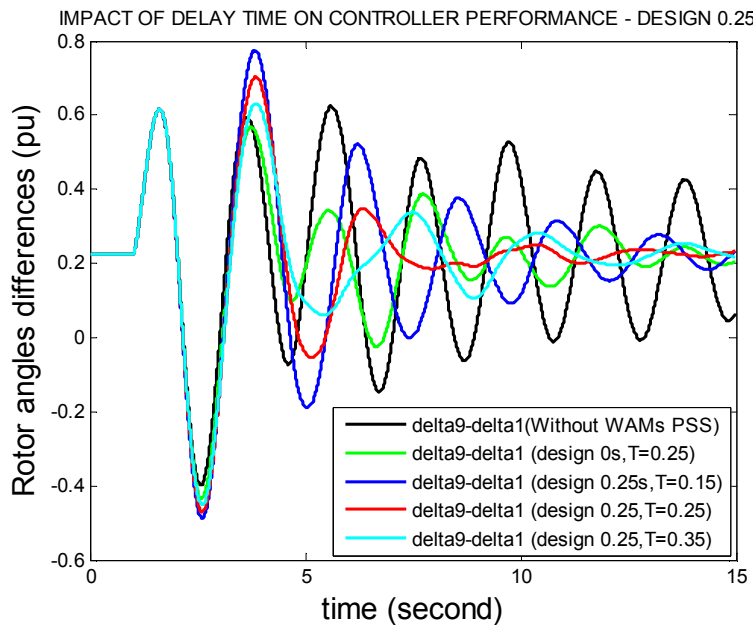


Figure 4.23 Impact of various time delay on controller performance - time delay setting =0.25s

On fig. 4.23, the red plot shows performance of designed WAM based PSS when T=0.25 matching to the setting delay time in design process. It is better than that of no-setting delay time-controller (green plot).

When the actual time delay does not match to the setting delay time, the performances of designed controller are shown by blue plot and cyan plot for actual $T=0.15$ and 0.35 , respectively. In these cases, performances of controller are not good as the matching case, but still improve system behavior.

Comparison between proposed and conventional controllers in various delay time are shown in figures 4.24, 4.25 and 4.26. It is can be seen that performance of proposed controller is better than that of conventional controller.

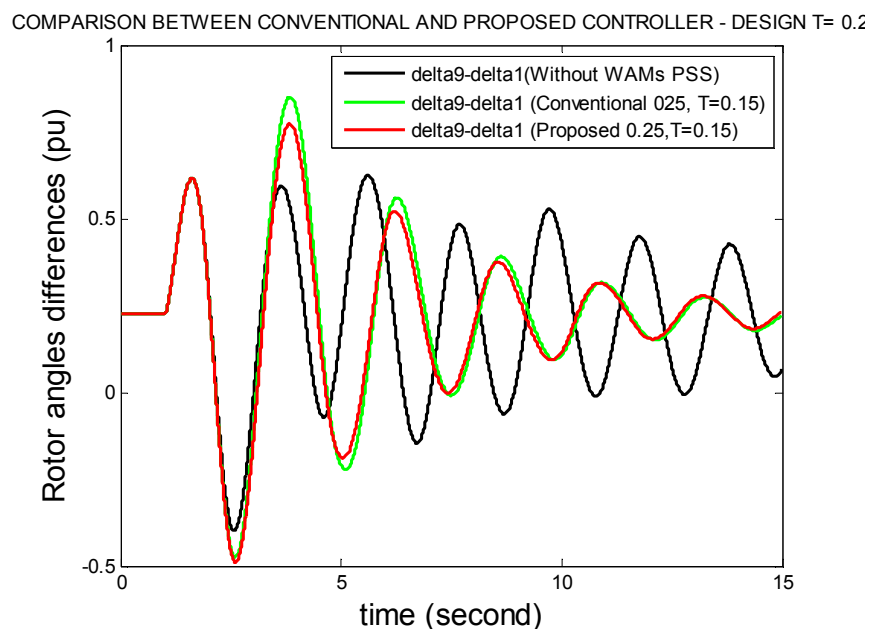


Figure 4.24 Performance of conventional and proposed controller with actual time delay $T=0.15$ s

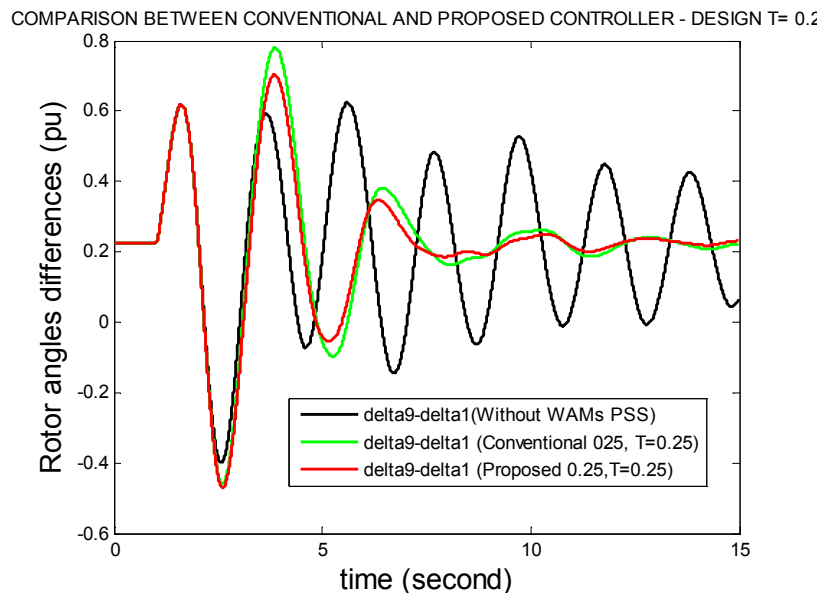


Figure 4.25 Performance of conventional and proposed controller with actual time delay T=0.25s

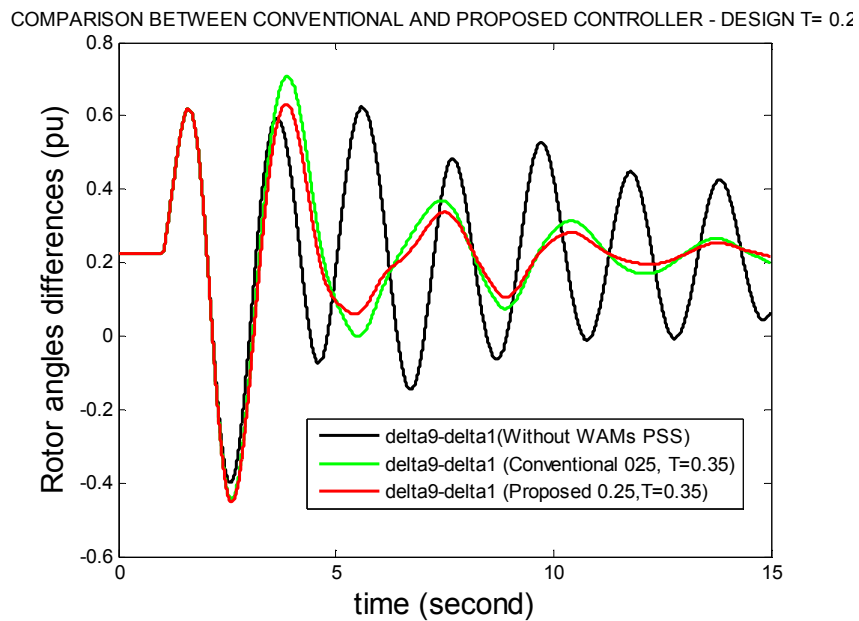


Figure 4.26 Performance of conventional and proposed controller with actual time delay T=0.35s

Daytime operating point of IEEJ East 10-machine system

PSS Configuration

Table 4.17 PSS configuration with and without considering time delay

| | Not consider T | Consider T=0.25 |
|--------------|---------------------------------------|---------------------------------------|
| Measurements | $[\Delta\omega_6 \ \Delta\omega_1]^T$ | $[\Delta\omega_6 \ \Delta\omega_1]^T$ |
| Feedback | [0.77 - 0.637] | [0.76 - 0.65] |
| Output | AVR6 | AVR6 |

Similar to case of adjusted operating point, PSS configuration is not changed when time delay is considered in the design process.

PSS parameters

Table 4.18 PSS's parameters with and without considering time delay

| Parameters | Not consider T | Consider T=0.25 |
|------------|----------------|-----------------|
| T_w | 15 | 15 |
| T_1 | 0.1 | 0.1 |
| T_2 | 0.325 | 0.253 |
| K_{stab} | 100 | 100 |

By setting delay time T=0.25, the design procedure resulted in a different PSS's parameters. T2 changed from 0.325 to 0.253.

Eigenvalue results

Table 4.19 Eigenvalue result with setting DT=0, actual DT=0

| Modes | Without WAM PSS | | With WAM PSS | | Dominant |
|-------|-----------------|--------------|---------------|-------------------------------|-------------------------------------|
| | <i>Real</i> | <i>Imag.</i> | <i>Real</i> | <i>Imag.</i> | |
| 1 | -0.142 | ± 4.259 | -0.328 | ± 4.033 | $G_6 \diamond G_{1,2}$ |
| 2 | -0.199 | ± 2.310 | -0.259 | ± 2.421 | $G_{1,2,3,4,5} \diamond G_{8,9,10}$ |
| 3 | -0.193 | ± 1.664 | -0.135 | ± 1.670 | All machines |

Table 4.20 Eigenvalue result with setting DT=0, actual DT=0.25

| Modes | Without WAM PSS | | With WAM PSS | | Dominant |
|-------|-----------------|--------------|---------------|-------------------------------|----------------------------|
| | <i>Real</i> | <i>Imag.</i> | <i>Real</i> | <i>Imag.</i> | |
| 1 | -0.142 | ± 4.259 | -0.378 | ± 4.356 | $G_6 \diamond G_{1,2}$ |
| 2 | -0.199 | ± 2.310 | -0.139 | ± 2.419 | $G_{1,2,3,4,5} \diamond G$ |
| 3 | -0.193 | ± 1.664 | -0.116 | ± 1.650 | All |

Table 4.21 Eigenvalue result with setting DT=0.25, actual DT=0.25

| Modes | Without WAM PSS | | With WAM PSS | | Dominant Participation |
|-------|-----------------|--------------|---------------|-------------------------------|-------------------------------------|
| | <i>Real</i> | <i>Imag.</i> | <i>Real</i> | <i>Imag.</i> | |
| 1 | -0.142 | ± 4.259 | -0.536 | ± 4.267 | $G_6 \diamond G_{1,2}$ |
| 2 | -0.199 | ± 2.310 | -0.214 | ± 2.455 | $G_{1,2,3,4,5} \diamond G_{8,9,10}$ |
| 3 | -0.193 | ± 1.664 | -0.134 | ± 1.664 | All machines |

With time delay impact and changing of PSS parameter, the eigenvalue result also changed, as shown in table 10. The ratio damping is improved to 12.5% from original value of 3.3%.

Time domain simulation

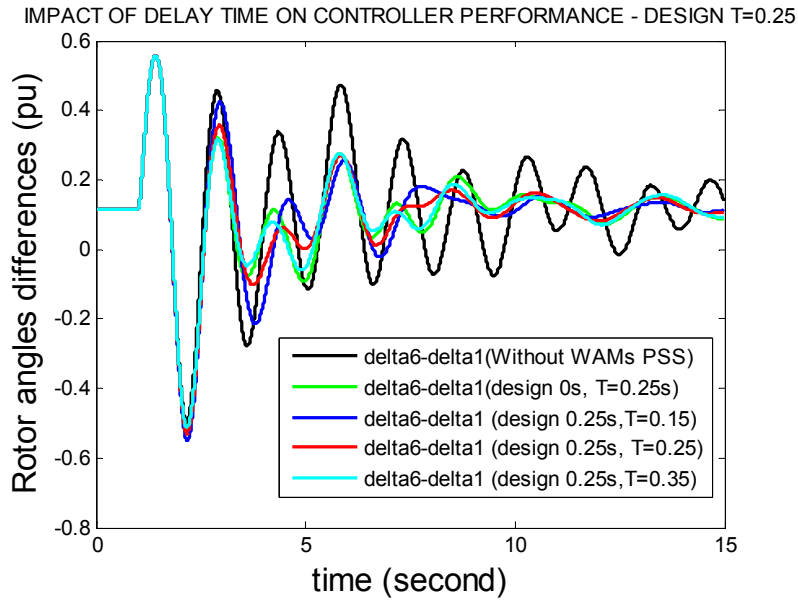


Figure 4.27 Impact of various time delay on controller performance - time delay setting =0.25s

On fig. 4.27, the red plot shows performance of designed WAM based PSS when T=0.25 matching to the setting delay time in design process. Similar to the case of adjusted operating point, it is better than that of no-setting delay time-controller (green plot).

When the actual time delay does not match to the setting delay time, the performances of designed controller are shown by blue plot and cyan plot for actual T=0.15 and 0.35, respectively. In these cases, performances of controller are worse than matching case, but still improve system behavior.

Comparison between proposed and conventional controllers in various delay time are shown in figures 4.28, 4.29 and 4.30. Similarly, it is can be seen that performance of proposed feedback controller is slightly better than that of conventional one.

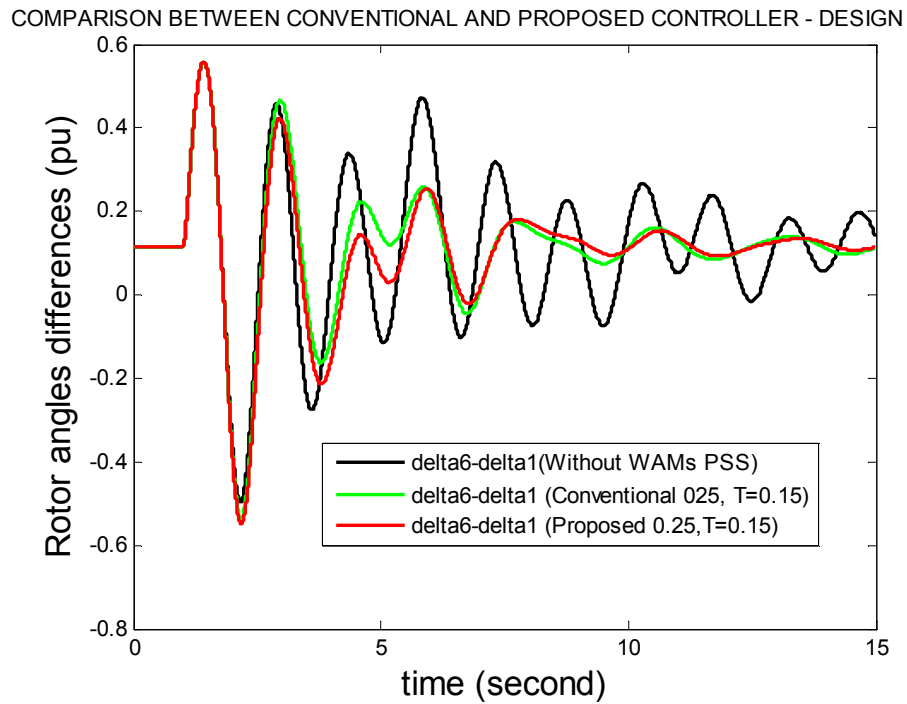


Figure 4.28 Performance of conventional and proposed controller with actual time delay $T=0.15s$

COMPARISON BETWEEN CONVENTIONAL AND PROPOSED CONTROLLER - DESIGN T=

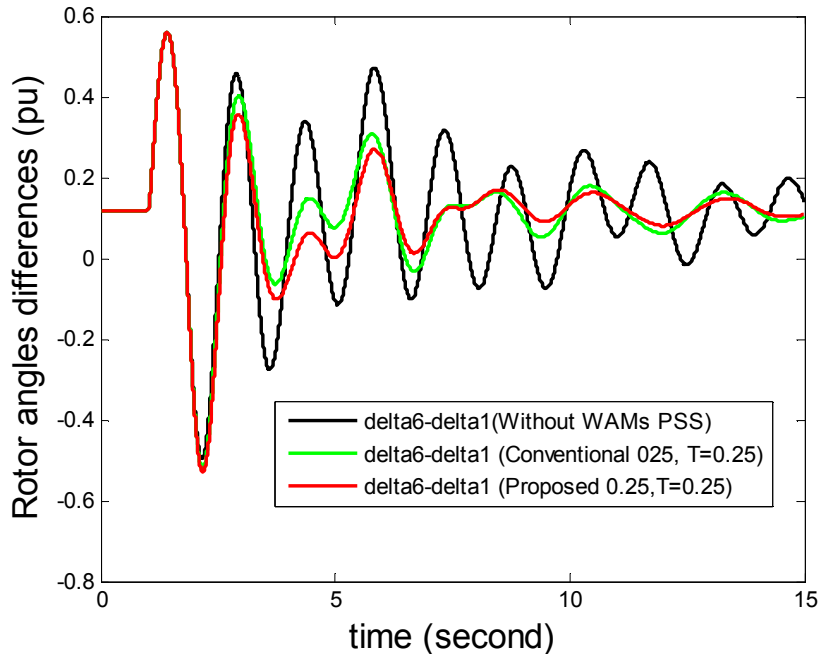


Figure 4.29 Performance of conventional and proposed controller with actual time delay T=0.25s

COMPARISON BETWEEN CONVENTIONAL AND PROPOSED CONTROLLER - DESIGN T= 0.2

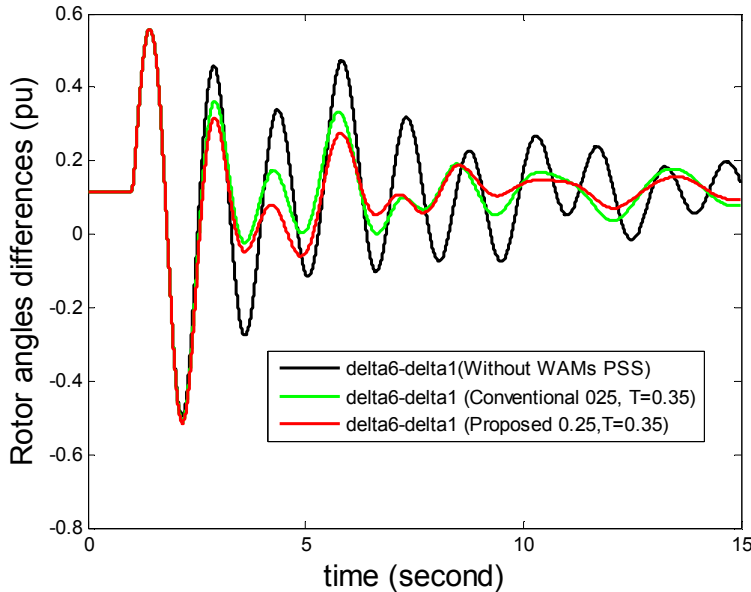


Figure 4.30 Performance of conventional and proposed controller with actual time delay T=0.35s

Conclusion for time delay consideration

A setting delay time of 0.25s, which is mean value of actual delay time, has been used into the design procedure. Then we got some conclusions, as follows:

- If the actual delay time is very close to the setting delay time, designed controller can provide the largest damping to mode of concern, as calculated and compared in eigenanalysis.

- If the actual time is more different from the setting delay time, the performance of controller is not good as that of the matching case. However, it still provides good damping to the mode of concern.

- The performance of proposed controller is always better than that of conventional controller when delay time varies from 0.15s - 0.35s.

4.3.3 Impact of time delay and measurement error on controller performance

As mentioned in subsection 3.7.4, a measurement error of $\pm 5\%$ should be considered to evaluate the controller performance. There are 4 critical cases of Y_{fb} subjected to error values of measurements. Consequently, in this section, time domain simulations of four test cases under time delay and measurement error are described. In each test case, the controller performances corresponding to 4 critical cases of Y_{fb} are compared with that of non-measurement error case.

Based on system performances of 4 tested cases, it can be seen that the impact of measurement error is insignificant. In cases 1,3 and 4, system performance with and without measurement error are not much different. In case 2, system performance with measurement errors [+5% -5%] (pink plot of fig. 4.32) is different from that without error (red plot of fig. 4.32), but it is an improvement.

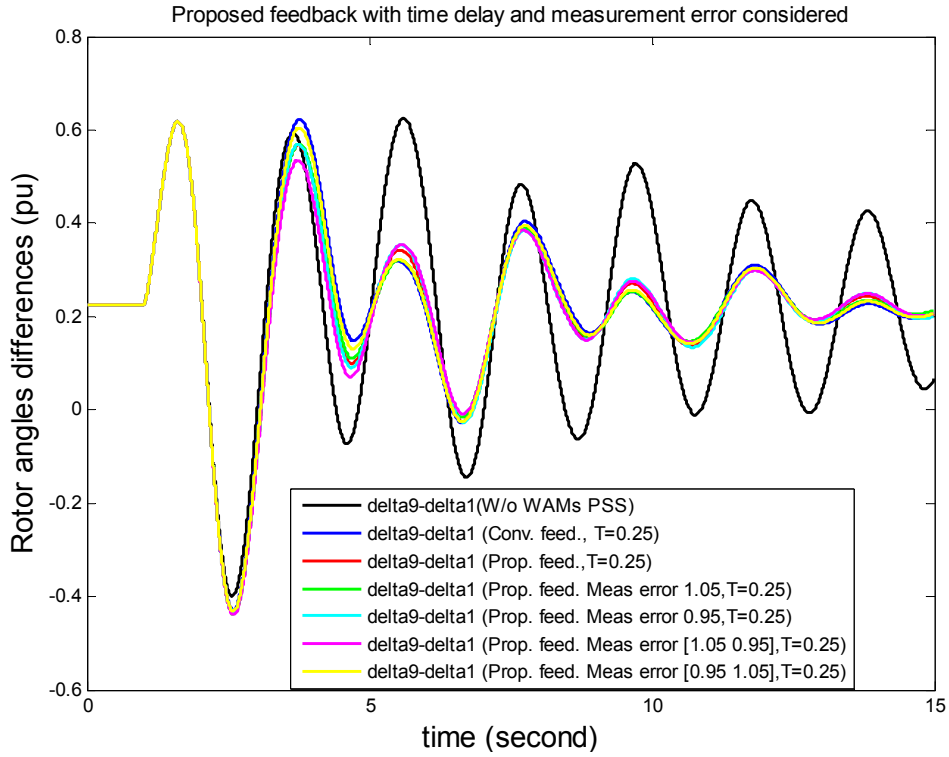


Figure 4.31 System performance with time delay and measurement error _Case 1

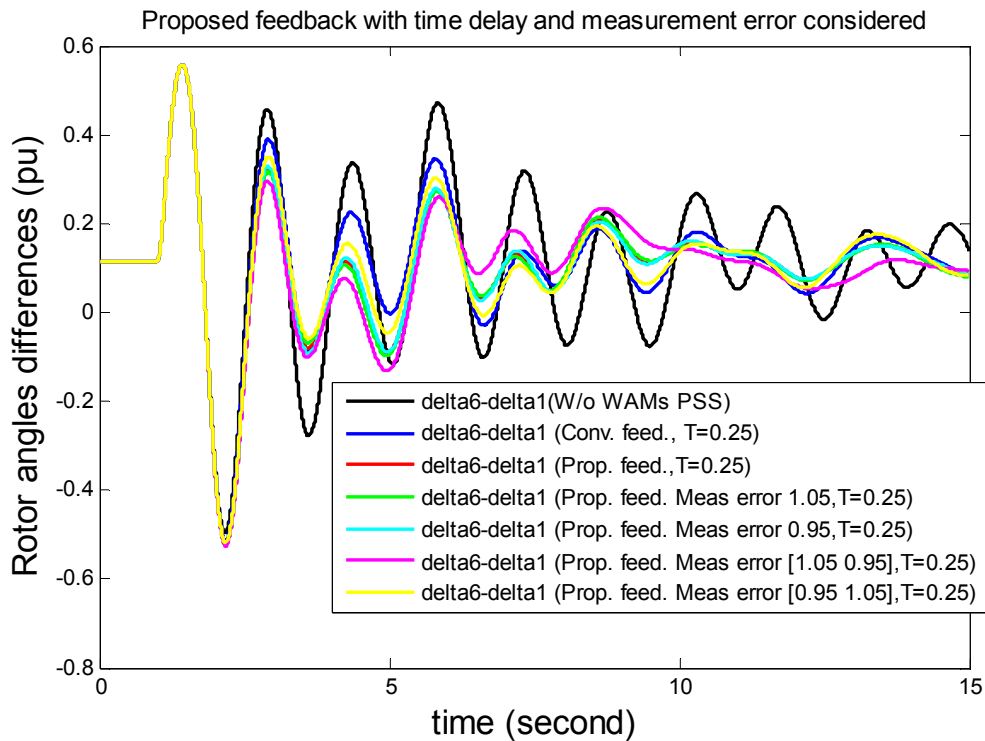


Figure 4.32 System performance with time delay and measurement error _Case 2

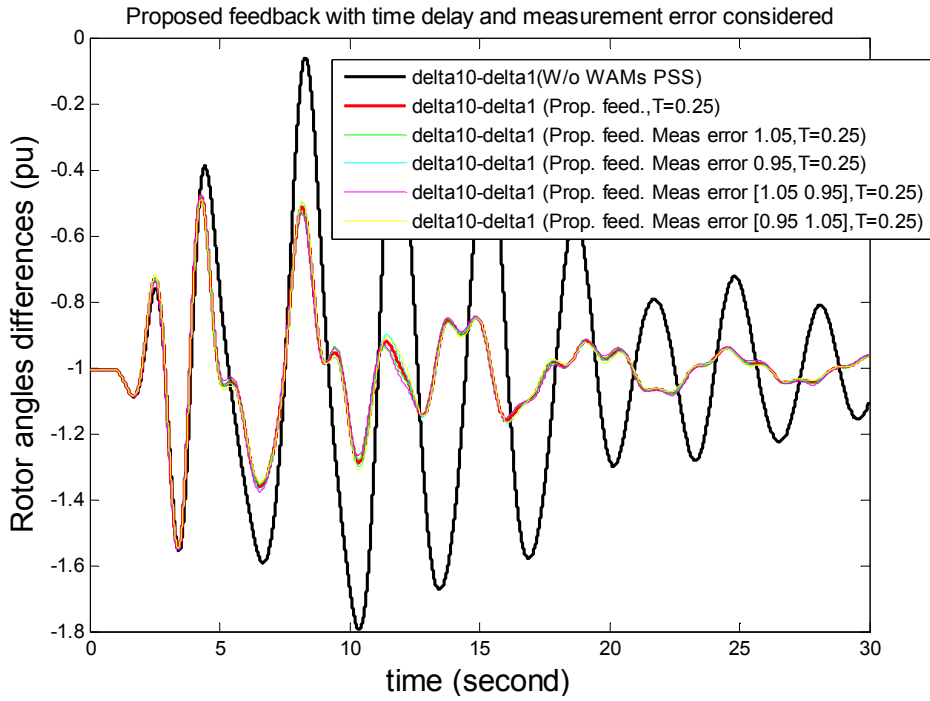


Figure 4.33 System performance with time delay and measurement error _Case 3

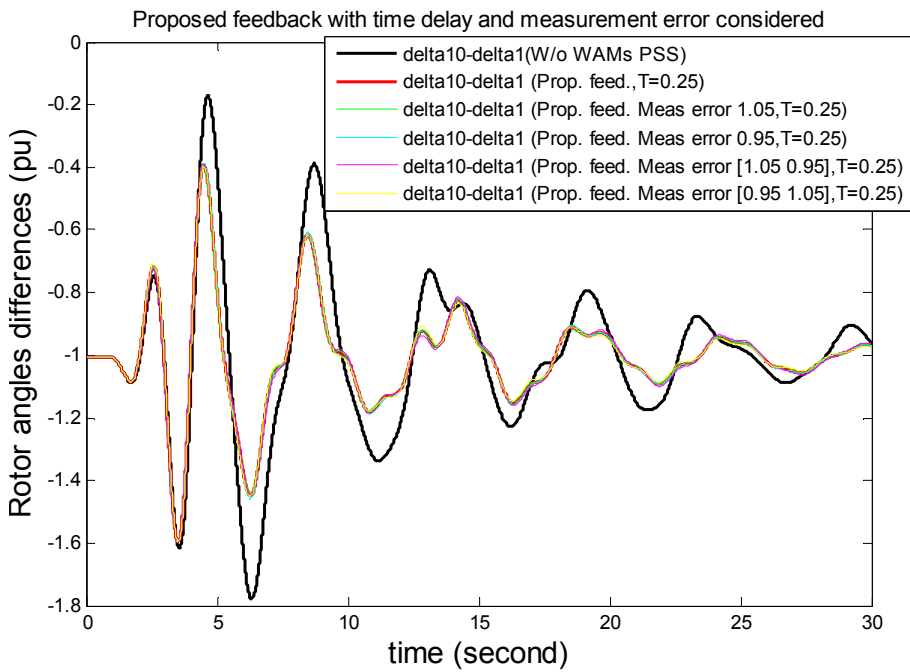


Figure 4.34 System performance with time delay and measurement error _Case 4

CHAPTER 5. CONCLUSION AND FUTURE WORK

This dissertation has proposed a design strategy for the WAM based controller with PSS form, in which the PSS parameters are tuned iteratively to minimize the real part of eigenvalue of the dominant inter-area mode, following an appropriate selection feedback signal.

In section 3.4, the optimal feedback signals are selected by maximizing the residue of the mode of concern for the formed feedback signal while minimizing that of other modes. By additionally considering residue of modes other than concern mode, the proposed feedback signal can support controller to improve the mode of concern while having not much impact on other modes. In section 3.5, an iterative design is proposed to remove modes improved by controller out of set of modes whose residues need to be minimized. By iterative design, controller can provide good damping to modes other than concern mode.

The proposed design strategy is appropriate for the concept of an adaptive controller, in which the controller configuration and parameters are changed subject to the system operating changes. The issue of power system identification is not considered in the dissertation. Instead, the system dynamic is assumed to be captured well by PMU and SCADA/EMS system, then eigenanalysis is used in the dissertation to analyze oscillations and their features. The total computational time for calculating feedback weighting vector and controller parameters is less than 5 minutes, therefore the time interval for changing controller configuration and parameters can be chosen by 15 minutes or 20 minutes. Effectiveness of designed controller may not be ensured for a larger time interval. Since the weighting vector for feedback signal and tuning parameters are calculated based on system linearization, the precise system identification and modeling are required. The research in this dissertation did not consider error or noise in the power system identification, because that the proposed design framework is used for an adaptive WAM based PSS with the time interval for re-identifying the system is not long.

This dissertation does not propose a new method of tuning controller's parameter. In the contrary, a combination method of residue based method and eigenvalue control is used for tuning controller parameter. This tuning method focuses on improving the mode of concern and does not ensure robustness stability for the power system. However, it is appropriate to the adaptive concept introduced by this dissertation.

The proposed design strategy has been tested successfully with two operating points of the IEEJ East 10-machine system and two operating points of IEEJ West 10-machine system. The results show that for each system operating point, the appropriate inputs and output for the controller are different. Furthermore, the proposed feedback selection in combination with the optimization tuning process can improve the dominant inter-area mode while not affect much the others.

Although the proposed method of feedback signal selection is general and can be applied with any number and type of participating measurements, just two participating measurements which are rotor speed angles are used in case studies and good results are obtained. In the future, effectiveness of various number as well as type of participating measurement on the proposed method will be studied. Also, more complex test systems with high number of operating points will be taken into account to verify the robustness of the proposed approach. The current test systems, IEEJ East and West 10-machine systems just has one dominant inter-area mode in each considered operating point so that only one WAM based PSS is needed. In the future, if the considered system has more than one dominant inter-area mode, multiple WAM based PSSs or multi-input multi-output WAM based PSS need to be developed.

In section 3.7, the time delay of feedback signal which is introduced by communication transmission and measurement error are considered. Case studies in section 4.3 have shown that effectiveness of proposed feedback signal is always better than that of conventional feedback signal, regardless to the time delay. A delay time of 0.25s has been chosen for consideration in design process. The result shows that if actual delay time is match to the setting delay time, the controller performance is the best. In case of actual delay time varies from setting delay time, the controller performance still provides good damping to inter-area oscillation. Besides, impact of measurement error is insignificant.

The work how to identify the change of the system operating conditions for reconfiguration of the controller is also out of scope of this dissertation. These issues will be considered in the future work.

Parameters of generator, transformer and transmission line used for test cases in the dissertation can be found at <http://www2.iee.or.jp/~pes/model/english/kikan/East10/east10.html>

(East system) and <http://www2.iee.or.jp/~pes/model/english/kikan/West10/west10.html> (West system).

LIST OF PUBLICATION

1. Ngoc Huynh Tran, Yokoyama Akihiko “Development of Wide-Area Measurement Based Adaptive Controller Design for Power System Damping ,” submitted to IEEJ Trans. Power and Energy
2. Ngoc Huynh Tran, Yokoyama Akihiko “Feedback Selection for Wide-Area Measurements Controller Design to Damp Inter-Area Mode,” CIGRE XIII Symposium of specialists in electric operational and expansion planning, May 2014, Iguacu, Brazil
3. Ngoc Huynh Tran, Yokoyama Akihiko “An Iterative Method of Feedback Selection and Control Parameter Tuning for Design of Wide-area Measurements Based Controller to Damp Inter-Area Mode”, ICEE 2014, June 2014 , Jeju, Korean
4. Ngoc Huynh Tran, Yokoyama Akihiko “Wide-Area Measurements Controller Design Based on Adaptive Concept for Damping Inter-Area Mode”, Power Systems Computation Conference 2014, August 2014 , Wroclaw, Poland
5. Ngoc Huynh Tran, Yokoyama Akihiko, Yasuyuki Tada “Observer and Controller Selection of Wide-Area Measurements Controller Based on Approximation of Multi-Modal Decomposition for Power System Stability Improvement,” 25th Annual Conference of Power & Energy Society, I.E.E. of Japan, August 2013, Niigata, Japan
6. Ngoc Huynh Tran, Yokoyama Akihiko “Feedback Selection and Eigenvalue Control for Wide-Area Measurements Controller Design to Damp Inter-Area Mode,” I.E.E. of Japan National Convention, 2014, Ehime, Japan
7. Ngoc Huynh Tran, Yokoyama Akihiko, "A Proposed Feedback Selection in Combination with Iterative Parameter Tuning for Wide-Area Measurements Damping Controller Design", 26th Annual Conference of Power & Energy Society, I.E.E. of Japan, 2014, Kyoto, Japan

REFERENCES

- [1] M.Zima, M. Larsson, P. Korba, C. Rehtanz, and G. Andersson, "Design aspect for wide area monitoring and control systems," *Proceedings of the IEEE*, Vol. 93 Issue 5, May 2005
- [2] D. Kosterev, C. Taylor, and W. Mittelstadt, "Model validation for August 10, 1996 WSCC system outage," *IEEE Trans. Power Syst.*, vol. 14, no. 3, pp.967–979, August 1999.
- [3] G. Ledwich and E. Palmer, "Modal estimates from normal operation of power systems," *IEEE Power Eng. Soc. Winter Meeting*, pp. 1527–1531, 2000.
- [4] I. Kamwa, R. Grondin, and Y. Hebert, "Wide-Area Measurement based stabilizing control of large power systems - A decentralized/hierarchical approach," *IEEE Trans. Power Syst.*, vol. 16, no. 1, pp. 136–153, 2001.
- [5] M. Larsson and D. Laila, "Monitoring of inter-area oscillations under ambient conditions using subspace identification," *IEEE PES General Meeting*, 2009.
- [6] L. Peng, W. Xiaochen, L. Chao, S. Jinghai, H. Jiong, H. Jingbo, Z. Yong, and X. Aidong, "Implementation of CSG's wide-area damping control system: Overview and experience," *IEEE/PES Power Systems Conference and Exposition*, 2009.
- [7] J. Turunen, M. Larsson, P. Korba, J. Jyrinsalo, and L. Haarla, "Experiences and future plans in monitoring the inter-area power oscillation damping," *IEEE PES General Meeting - Conversion and Delivery of Electrical Energy in the 21st century*, 2008.
- [8] J. Chow, J. Sanchez-Gasca, H. Ren, and S. Wang, "Power system damping controller design using multiple input signals," *IEEE Control Syst. Mag.*, pp.82–90, August 2000.
- [9] I. Kamwa, A. Heniche, G. Trudel, M. Dobrescu, R. Grondin, and D. Lefebvre, "Assessing the technical value of FACTS-based wide-area damping control loops," *IEEE Power Eng. Soc. General Meeting*, 2005.
- [10] N. R. Chaudhuri, A. Domahidi, B. Chaudhuri, R. Majumder, P. Korba, S. Ray and K. Uhlen, "Power Oscillation Damping Control Using Wide-Area Signals : A Case Study on Nordic Equivalent System," *Transmission and Distribution Conference and Exposition*, 2010 IEEE PES

- [11] J. Ma, T. Wang, J.S. Thorp, Z.Wang, Q. Yang, A.G. Phadke, "WAM Based damping control of Inter-area Oscillation employing Energy Storage System," *Advances in. Electrical and Computer Engineering*, Vol 12, No. 2, 2012
- [12] D. Trudnowski and J. Pierre, *Inter-area Oscillations in Power Systems: A Nonlinear and Nonstationary Perspective*, ser. Power Electronics and Power Systems, A. Messina, Ed. Springer, 2009
- [13] H. Beides and G. Heydt, "Dynamic state estimation of power system harmonics using Kalman filter methodology," *IEEE Trans. Power Delivery*, vol. 6, no. 4, pp. 1663–1670, October 1991.
- [14] A. Routray, A. Pradhan, and K. Rao, "A novel kalman filter for frequency estimation of distorted signals in power systems," *IEEE Trans. Instrm meas*, vol. 51, no. 3, pp. 469–479, June 2002.
- [15] F. Chowdhury, J. Christensen, and J. Aravena, "Power system fault detection and state estimation using kalman filter with hypodissertation testing," *IEEE Trans. Power Delivery*, vol. 6, no. 3, pp. 1025–1030, July 1991.
- [16] G. Rogers, *Power System Oscillations*. Kluwer Academic Publishers Group, 2000.
- [17] A. Heniche and I. Kamwa, "Assessment of two methods to select wide-area signals for power system damping control," *IEEE Trans. Power Syst.*, vol. 23,no. 2, pp. 572–581, May 2008.
- [18] N.Modi, M. Lloyd and T.K. Saha, "Wide-Area Signal Selection for Power System Damping Controller," *Universities Power Engineering Conference (AUPEC) 21st Australasian*, 2011
- [19] Prabha Kundur, *Power System Stability and Control*, McGraw-Hill, 1994.
- [20] M. Klein, L. Le, G. Rogers, S. Farrokhpay, and N. Balu, "H1 damping controller design in large power systems," *IEEE Trans. Power Syst.*, vol. 10, no. 1,pp. 158–166, February 1995.
- [21] Y. Sekine, A. Yokoyama and K. Komai, "Eigenvalue Control of Midterm Stability of Power System (Concept of Eigenvalue Control and its Application)," *Proceedings of the 9th PSCC*, August/September, 1987, Lisbon, Portugal, pp.885-891.

[22] L. D. Philipp, Ausif Mahmood, B. L. Philipp, "An improved refinable rational approximation to the ideal time delay," IEEE Trans. Circuits and Systems, vol. 46, pp. 637-640, May 1999.

[23] P.M. Anderson & A.A. Fouad, *Power System Control and Stability*, 2nd edition, IEEE Press.

[24] Y. Sekine, 電力系統過渡解析論, Jan 1984, the Tokyo University.

[25]<http://www2.iese.or.jp/~pes/model/english/kikan/East10/east10.html>.

<http://www2.iese.or.jp/~pes/model/english/kikan/West10/West10.html>

[26] P. Korba, M. Larsson, and C. Rehtanz, "Detection of oscillations in power systems using Kalman filtering techniques," in Proc. IEEE Control Applications Conf., 2003.

[27] Ngoc Huynh Tran, A. Yokoyama, " Wide-Area Measurements Controller Design Based on Adaptive Concept for Damping Inter-Area Mode", 18th PSCC, August 2014

[28] Edwin K.P. Chong and Stanislaw H.Zak, *An Introduction to Optimization*, Third Edition, NewYork: Willey, 2008, p. 440.

[29] L.Rouco and F.L. Pagola, "Eigenvalue Sensitivities for Design of Power System Damping Controllers, " in 40th Proc. IEEE on Decision and Control, Orlando, USA, Nov. 2001

[30] Hongxia Wu, Konstantinos S. Tsakalis and G. T. Heydt, "Evaluation of Time Delay Effects to Wide-Area Power System Stabilizer Design," IEEE Trans. on Power Syst., Vol. 19, No. 4, pp 1935-1941, Nov. 2004

[31] Biju Naduvathuparambil, Matthew C. Valenti, and Ali Feliachi, "Communication Delays in Wide-area Measurement Systems," Proceedings of the Thirty-Fourth Southeastern Symposium on System Theory, pp.118- 122, 2002